SOIL BIOCHEMISTRY

Nirupama Tyagi
Dr. Shivani

Soil Biochemistry

Soil Biochemistry

Nirupama Tyagi
Dr. Shivani

BLACK PRINTS
NEW DELHI

Soil Biochemistry

Nirupama Tyagi & Dr. Shivani

This edition published by BLACK PRINTS INDIA INC.,
Murari Lal Street, Ansari Road, Daryaganj, New Delhi-110002

Edition: 2022

ISBN: 978-93-82036-56-2

Editorial Office: 116-A, South Anarkali, Delhi-110051.
Ph.: 011-22415687

Sales & Marketing: 4378/4-B, Murari Lal Street, Ansari Road, Daryaganj, New Delhi-110002.
Ph.: +91-11-23281685, 41043100 Fax: +91-11-23270680

Production: A 2/21, Site-IV, Sahibabad Industrial Area
Ghaziabad, U.P. (NCR)
e-mail: blackprintsindia@gmail.com

CONTENTS

CHAPTER 1

AN OVERVIEW OF PHYSIOLOGY AND BIOCHEMISTRY: STRONGLY AFFECTED BY SOIL TETRACYCLINE

Dr. Shivani, Assistant Professor, Department of Agriculture and Environmental Sciences
Shobhit University, Gangoh, Uttar Pradesh, India
Email Id- shivani@shobhituniversity.ac.in

ABSTRACT:

A brand-new class of environmental pollutant is antibiotics. They are being used more often in systems for raising farm animals, and they may build up in crops, reducing nutritional value and plant development rate. This study's objective was to ascertain how tetracycline affected the physiological and biochemical characteristics of pea seedlings. The 24-hour presence of TC in the soil did not cause any noticeable alterations in the seedlings. However, the seedling appearance and metabolic activities were dramatically impacted after five days of soil TC activity. A 38% decrease in chlorophyll caused leaves to lose their green color. Shoots of pea that had been cultivated for 120 hours in either perlite with 250 mg of TC or perlite with no TC control plants were used to isolate the total protein. Proteins from non-TC shoots had 326 spots on their 2D electrophoretic maps, but TC-treated seedling shoot proteins had only 316 spots. 26 proteins' identities were discovered. The majority of proteins' intensity increased. Diphosphate kinase, superoxide dismutase peroxiredoxin, and glutathione S-transferees were significantly affected by this.

KEYWORDS:

Antibiotics, Metabolic Activities, Physiological, Tetracycline.

INTRODUCTION

Significant quantities of pollutants, such as heavy metals, aromatic hydrocarbons, solvents, plant protection agents, and medications both veterinary and human are continuously leaking into ecosystems and agrocenoses from the techno sphere. Approximately 100,000 tons of antibiotics are thought to be generated globally, according to. According to a data released by the European Medicines Agency 8,935.5 tons of antibiotics were used in 2014 throughout 29 EU member states, with 581.3 tones going to Poland. Tetracycline which has a cheap cost of manufacture, low toxicity, and a broad range of bacteria impacted was the most widely used antibacterial medicine in the EU member states in 2014. Tetracycline-related antibiotics in bacteria are thought to primarily target the ribosomal acceptor of aminoacyl-tRNA.

Tetracycline's are poorly absorbed in animal gastrointestinal tracts, and the majority of them escape metabolic alterations and are eliminated in the form of faces and urine where they finally end up in the fields. Tetracycline, ox tetracycline, and chlortetracycline are all present in manure in amounts of 46 mg per kilogram me, 29 mg per kilogram me, and 23 mg per kilogram me, respectively. However, swine slurry contains up to 139.4 mg per kg of chlortetracycline, 354.0 mg per kg of ox tetracycline, and 98.2 mg per kg of tetracycline, respectively. Tetracycline spreads in the environment due to the ineffectiveness of wastewater tetracycline removal. Tetracycline also has a lengthy metabolic half-life, which may be anywhere between 55 and 105 days. It is widely known that the absorption and toxicity of antibiotics cause different cultivable plant species to grow and develop more slowly [1], [2]. Our earlier research has also shown that tetracycline is taken up by pea, transported to the plant's above-ground regions, and then stored in leaves. Numerous defensive systems have been established by plants to shield cells from harm brought on by external stressors. Catalase and peroxidases are only

two of the ant oxidative enzymes that have been found. It has been shown, among other things, that peas, lentils, and soybeans may affect their oxidative stress enzyme activity when exposed to certain antibiotics. In addition to existing in many enzymes of a single type, the majority of enzymes implicated in plant detoxification are also present in numerous isoforms. The acerbate-glutathione cycle or superoxide dismutase, the only plant enzymes capable of oxidizing oxygen, are crucial mechanisms for removing ROS. It is well accepted that some proteins have physiological roles in plant tolerance to stresses such salt, heat, and drought. On the other hand, there is little information available about how plant proteomes react to soil antibiotics. The purpose of this work was to identify proteins that respond to soil contamination in substantially different ways and to characterize the changes in intracellular protein concentrations of those proteins.

Resources and Procedures

In seed germination pea seeds. Cysterici from Poznaska Hoopla Rollin in Tule, Poland, germinated. Seven-day-old seedlings were transplanted into pots that held three seedlings each and 200 cc of perlite size 2–6 mm, Agro Perlite, Poland. The cultivation was done for the next seven days with 12 hours of light, at 23°C and 16°C during the day and night, respectively. 8 Klux of light were being emitted. Tetracycline Sigma-Aldrich aqueous solutions at concentrations of 0, 0.5, 5, 10, 50, and 250 mg L-1 of the substrate were applied to pots containing 14-day-old plants that were 10 to 11 cm tall. Distilled water was used to irrigate the control seedlings. 15 cc of either TC solution or water were poured into the pot once. After 24 hours and 120 hours after the administration of tetracycline, samples of the seedlings' above-ground sections were taken for analysis. After 24 hours, 48 hours, and 72 hours of TC growth, plants that had been grown for 120 hours received 15 cc of distilled water to hydrate them. Following the studies, the Warmed and Maury University in Olsztyn's Waste Treatment and Disposal Department collected the contaminated soil. A Minolta SPAD-502 chlorophyll meter was used to assess the greenness of the leaves. On the other hand, dihydric and acerbate peroxidase showed a three-fold decrease in accumulation. The oxygen-evolving enhancer protein 2, chloroplast rib nucleoprotein or ATP synthase CF1 peroxiredoxin and ABA-responsive protein were among the 26 proteins found by the MALDI TOF/TOF MS technique that were present as isoforms. This phenomenon, which is often seen in 2D electrophoresis and is caused by the presence of different isoforms or degradation in the protein extracts, may possibly be connected to allelic polymorphism [3], [4].

Particular focus was placed on the proteins that were directly linked to stress when it came to the discovered proteins. Diphosphate kinase is thought to play an important part in plants' ability to withstand stress. According to a study by the increased expression of the genes for oxidative stress enzymes such as peroxidase, glutathione transferees, thioredoxin reductase, peroxiredoxin, and protective genes encoding a number of heat-shock proteins is correlated with the overexpression of the diphosphate kinase gene. The expression of this protein was unquestionably greater in TC-growing seedlings than in control seedlings. Under the action of tetracycline, it was shown that superoxide dismutase glutathione transferees, and peroxiredoxin accumulated more. Peroxiredoxin has been identified as an ant oxidative enzyme linked to salt stress and it is likely responsible for the substrate's resistance to stress brought on by antibiotics. It's noteworthy to note that our research showed that tetracycline had a negative impact on the acerbate peroxidase accumulation. In plants exposed to stress brought on by heat stress cold temperatures or stress brought on by the presence of sparfloxacin an increase in accumulation of enzyme proteins important for ant oxidative responses, including acerbate peroxidase, has previously been observed. Other antibiotics may cause similar patterns of metabolic alterations in plants, often with additional problems. For example, sulfamethazine's impact on plants causes mitochondrial dysfunction. Under the influence of tetracycline, the accumulation of

HSP 70 in pea shoots decreased by 1.5 times. When under salt, heat, or drought stress, HSP 70 proteins build up. On the other hand, pea shoots have less HSP 70 in them. During osmotic stress and sparfloxacin treatment, a significant drop in HSP 70 was observed. The proteolysis of damaged, misfiled, and oxidized proteins is regulated by the proteasome 26 protein complex, which comprises subunit. Tetracycline-induced protein damage may be indicated by an increase in the concentration of this protein and the ATP-dependent Clap protease under its control. So far, it has been shown that barley accumulates more of the ATP-dependent Clap protease, which breaks down damaged proteins, during droughts. The loss of the leaves' green tint under the effect of TC obviously had an impact on photosynthesis. Tetracycline-treated samples showed a considerable difference from the control sample in the amount of protein buildup linked to photosynthesis. Additionally, a protein was discovered that was only present in the shoots that had been exposed to TC. For the thermo tolerant Medic ago sativa L. plant, an increase in the accumulation of fructose diphosphate aldoses and a few proteins connected to photosynthesis. Suffering the effects of heat exhaustion. In addition, the HCF136 protein, a photosystem II stability/assembly component, almost quadrupled in concentration.

Fluorescence and Absorption Spectra:

The scientists' analysis of chlorophyll absorption and fluorescence spectra was prompted by variations in photosynthetic proteins and leaf color. The absorption spectra of chlorophyll a from the leaves of pea seedlings are shown the addition of tetracycline to the substrate for 24 hours and 120 hours. For all antibiotic concentrations used, the tests were performed. No alterations in the absorption spectra for any of the applied concentrations were seen 24 hours after the addition of TC to the substrate. The smallest variations are discernible at perlite concentrations as low as 0.5 mg L-1. In comparison to the control sample, a reduction in chlorophyll an absorption of 0.07, 0.13, 0.27, and 0.39 was seen with an increase in TC content. The leaves grown with 250 TC mg L-1 of perlite showed the highest reduction in the chlorophyll an absorption band. The leaves' chlorophyll concentration varied from 1.16 104 to 0.73 104 M, or from 1.7 mg per g of fresh weight to 1.06 mg per g of fresh weight. The amount of chlorophyll in the leaves reduced by 37%, leaving just 63% of chlorophyll a, after the pea had grown for 120 hours on a substrate with 250 TC mg L1 [5], [6].

For the control sample as well as all of the administered tetracycline concentrations, fluorescence spectra were analyzed. The fluorescence spectra for the chlorophyll in the pea leaves without TC and with 250 TC mg L1 of the substrate. No variations in the location of the spectrum maximum were seen for any of the applied concentrations 24 hours after the addition of TC to the substrate as compared to the control. For 250 TC mg L1, there was a 2 nm shift towards shorter waves in the maxima of the chlorophyll a fluorescence band after 120 hours. The band with shorter wavelengths was affected by the shift. Additionally, for the seedlings exposed to the highest dose of tetracycline, a 20 percent drop in fluorescence emission was seen 120 hours after the antibiotic was added to the substrate as compared to the control. Chlorophyll a, a band with a wavelength of 665 nm, was the only absorption spectrum that was examined. Shorter waves include the tetracycline spectrum, which superimposes on the chlorophyll spectrum, which is why this band was chosen. Chlorophyll concentration under the effect of tetracycline is thought to diminish after 120 hours based on clearly discernible changes in chlorophyll an absorption spectra. Lead exposure resulted in lower chlorophyll concentrations for Pharsalus mango L. and Lens culinary L. Pharsalus vulgaris L. instance of salt stress. Or a lack of moisture for Matric aria chamomile L. In order to comprehend the fundamental processes of photosynthesis and the impacts of stress on photochemistry, chlorophyll fluorescence has been employed as a potent, nondestructive, and trustworthy instrument in plant physiology. A new product has formed when the maximum of the fluorescence spectrum shifts by 2 nm 120 hours after the administration of TC. Furthermore,

no research on the impacts of stress to yet has shown alterations in the location of the fluorescence maximum. Free radicals produced by TC's impact on the plant are likely to cause chlorophyll degradation and shift the fluorescence maximum. According to Saleh et al. free radicals trigger peroxidation, which leads to the deterioration of chlorophyll pigment. This explains why the roots included reactive oxygen species, close, and dead cells [7], [8].

Callused, and Reactive Oxygen Species:

Non-fluorescent dichlorodihydrofluorescein dictate, which readily entered the cells, was used to identify reactive oxygen species. Inside the cells, this substance is broken down to a highly fluorescent dichlorofluorescein, which forms a link with ROS and can be seen under a microscope. The photos show a full set of images overlaid on one another from different specimen layers and 7. When tetracycline was applied to seedlings for 24 hours at a dose of 30 mg per kilogram me of soil weight, there were changes in the ROS content of the apical zone of the roots compared to the control sample. ROS was created as a consequence of TC. Tetracycline-treated roots had increased fluorescence intensities, and the apical zone of the roots showed signs of shrinking. Fewer free radical-containing cells could be found in control seedlings than in seedlings that had been exposed to the antibiotic's effects. Using presidium iodide, dead cells were found in the tissues of the pea. Only a compromised cell membrane allows presidium iodide to get through, staining nucleic acids and resulting in red fluorescence. In comparison to the roots of seedlings treated to tetracycline, less stained cell nuclei were seen in control seedlings. Additionally, dead cells were found in the root hairs themselves as well as in the apical and root hair zones of the roots. The rhizodermis cells delaminate in the apical zone of the roots exposed to tetracycline.

The roots and leaves were stained with aniline blue to check for close layers. The apical zone of the roots and the root hair zone both displayed fluorescence that indicated the existence of close layers in the tissues. The findings show that tissues exposed to TC's activity have a greater close content. The parenchyma and, to a lesser degree, the vascular bundles of the leaves exhibit high luminosity in the leaves. Different types of environmental stressors, such as strong light, high or low temperature, salt, drought, nutritional inadequacy, and pathogen assault, cause plants to produce ROS. Pharmaceutical and personal care product contamination of agricultural soils causes plants to produce too much ROS, which in turn encourages cell membrane impairments and lipid peroxidation, indicating the presence of oxidative stress. Arabidopsis thaliana exposed to biphenyl a showed increased ROS generation, which disrupted the stromal and thylakoid system. To prevent ROS from damaging cells and to guarantee that signal functions are carried out as intended, the ROS level must be tightly controlled. Plants have evolved effective antioxidant machinery to maintain their survival. The primary detoxification technique is the elimination of surplus free radicals. Nobody and C. Guaiacum peroxidase is one of the most significant ant oxidative enzymes in plant cells, according to H. Foyer [9], [10].

Activity of Guaiacum Peroxidase:

The activity of the oxidative stress POX enzyme was assessed by measuring the rise in absorbance in both the roots of pea seedlings exposed to TC and the above-ground sections of the pea plant. Tests were performed both immediately after the antibiotic administration and five days afterwards. Both 24 and 120 hours following the administration of TC, the tests showed an increase in guaiacum peroxidase activity in comparison to the control seedlings. Both the roots and the above-ground portions of the seedlings showed an increase in the enzyme's activity. The smallest increase in POX activity was seen in the seedling shoots 24 hours after tetracycline was added to the substrate under the impact of the lowest antibiotic concentration used. When tetracycline was applied to the pea plant's above-ground portion at a dosage of 250 mg per L of perlite, POX activity was shown to rise by nearly double. In a

dosage of 0.5 mg L-1 of perlite for the roots, no change in POX activity was seen 24 hours after the application of tetracycline. The amount of action rose when the antibiotic dosage was raised. In regard to the following concentrations, a rise of 17%, 44%, 44%, and 42% was seen for 5, 10, 50, and 250 mg L1 perlite, respectively. The evidence supports the theory that antibiotic soil contaminants increase POX activity in plant tissues. One of the key elements of the secretive of plants under environmental stress is known. Peroxidases have a variety of crucial functions in plant metabolism. They have a role in stress reactions, detoxication processes, and the control of plant growth and development. A stress-related enzyme is guaiacum peroxidase, an enzyme linked to crucial biosynthesis and defense against biotic and abiotic environmental threats. Any time ROS buildup takes place, POD manifests in plant tissues. POD scavenges ROS; nevertheless, it also increases their synthesis [58]. POD plays a significant role in the process of toxin deactivation. According to Agostino et al. peroxidases may break down the pesticide 2, 4-dichlorophenol. Peroxidases' capacity to oxidase diclofenac has also been shown. According to the dosage and exposure period, POD activity increases in roots and leaves when pharmaceutical and personal care chemicals contaminate agricultural soils. The aforementioned research and our own findings amply demonstrate that POD may be important in the transformation of drugs in plants [11], [12].

CONCLUSION

Tetracycline treatment of pea seedlings up to 250 mg L-1 applied to the growth substrate did not cause any deteriorative changes to be noticeable within 24 hours. Pea leaves lost 38% of their chlorophyll after five days of TC activity, which caused them to turn brown. Additionally, the proteome of plants exposed to antibiotics had 10 fewer proteins than the proteome of control plants. On the other side, tetracycline activity led to an increase in the number of certain proteins. Diphosphate kinase, superoxide dismutase peroxiredoxin, glutathione S-transferee, and a photosynthesis-related protein called photosystem II stability/assembly factor HCF136 were the main ones. A dramatic rise in the number of free radicals, the amount of close that was deposited, and the appearance of masses of dead cells were all noted at the highest concentration. As a result, it was discovered that environmental tetracycline can affect a plant's proteome, ability to respond to oxidative stress, and photosynthetic system.

REFERENCES:

[1] David White, “The physiology and biochemistry of prokaryotes,” *Gen. Pharmacol. Vasc. Syst.*, 1996, doi: 10.1016/0306-3623(96)90070-1.

[2] P. Bosc Author, W. K. Smith, and P. C. Miller, “Division of Comparative Physiology and Biochemistry, Society for Integrative and Comparative Biology,” *Source Physiol. Zool.*, 1973.

[3] J. P. Morton, D. A. Doran, and D. P. M. MacLaren, “Common student misconceptions in exercise physiology and biochemistry,” *Am. J. Physiol. - Adv. Physiol. Educ.*, 2008, doi: 10.1152/advan.00095.2007.

[4] E. M. Yahia, *Postharvest physiology and biochemistry of fruits and vegetables*. 2018. doi: 10.1016/C2016-0-04653-3.

[5] K. Hartfelder *et al.*, “Standard methods for physiology and biochemistry research in Apis mellifera,” *Journal of Apicultural Research*. 2013. doi: 10.3896/IBRA.1.52.1.06.

[6] K. R. Dahlberg and J. L. V Etten, “Physiology and Biochemistry of Fungal Sporulation,” *Annu. Rev. Phytopathol.*, 1982, doi: 10.1146/annurev.py.20.090182.001433.

[7] R. K. Sairam, D. Kumutha, K. Ezhilmathi, P. S. Deshmukh, and G. C. Srivastava, "Physiology and biochemistry of waterlogging tolerance in plants," *Biologia Plantarum*. 2008. doi: 10.1007/s10535-008-0084-6.

[8] R. H. Adrien, "Reviews of Physiology, Biochemistry and Pharmacology," *Anticancer Res.*, 2016, doi: 10.1016/0014-5793(80)81245-2.

[9] C. P. Mangum and P. W. Hochachka, "New directions in comparative physiology and biochemistry: Mechanisms, adaptations, and evolution," *Physiological Zoology*. 1998. doi: 10.1086/515953.

[10] H. Subramanyam, S. Krishnamurthy, and H. A. B. Parpia, "Physiology and biochemistry of mango fruit," *Adv. Food Res.*, 1975, doi: 10.1016/S0065-2628(08)60092-0.

[11] K. Rajkumar, K. Prakash, K. Saniya, K. S. Sailesh, and P. Vegi, "OSPE in Anatomy, Physiology and Biochemistry Practical Examinations: Perception of MBBS students," *Indian J. Clin. Anat. Physiol.*, 2016, doi: 10.5958/2394-2126.2016.00111.0.

[12] D. J. Wright and R. N. Perry, "Physiology and biochemistry.," in *Entomopathogenic nematology*, 2002. doi: 10.1079/9780851995670.0145.

CHAPTER 2

EXPLORING THE METHODS OF IMPROVING SOIL PRODUCTIVITY

Dr. Shivani, Assistant Professor, Department of Agriculture and Environmental Sciences
Shobhit University, Gangoh, Uttar Pradesh, India
Email Id- shivani@shobhituniversity.ac.in

ABSTRACT:

In this 5-year study, the impact of fresh and composted paper sludge application frequency on soil characteristics, silage corn and barley yields, and nitrogen uptake was assessed by contrasting one application with repeated applications. The treatments were FDS and CDS at a rate of 40 Mg ha1 on a wet basis with or without decreased N fertilizer on maize, a control with neither amendment nor N fertilizer, and the recommended N rates for maize and barley. Regardless of the frequency of application, the FDS or CDS applications considerably increased the percentage of bigger macro aggregates in the soil as well as the mean-weight diameter of aggregates. In comparison to the control and the recommended N fertilizer treatment, single or three-year additions of FDS or CDS caused, on average, an increase of 25 to 31% of the soil C and N contents. The FDS or CDS with or without additional N fertilizer decreased silage maize and N uptake in the first year of its application compared to the control, most likely because N was immobilized. The yields of silage corn were raised in the years that followed, nevertheless, either with a single treatment or with repeated applications of FDS or CDS. Results indicate that single treatments of FDS and CDS had benefits on soil characteristics and crop yields that were comparable to those of triple applications and persisted for a few years after the last application.

KEYWORDS:

Amendment, CDS, Contrasting, Fertilizer.

INTRODUCTION

Since 1997, new methods in the paper mill industry have been developed for recycling used papers, and as a result, deinking paper sludge's have been generated due to environmental concerns related to waste management. According to N'Dayegamiye those paper sludge's are removed over the course of two phases. The primary sludge is created by first separating the fine debris from the mixture in a sedimentation basin. The secondary sludge is then created by extraction in a second basin where the water-soluble fibers are broken down by microorganisms. In the second basin, mineral fertilizers are typically added to promote the development and activity of microorganisms. High C/N ratios in the primary paper sludge's from the de-inking paper mill plant cause N immobilization and lower crop yields. When primary and secondary de-inking paper sludge's are combined, the resulting mixed paper sludge's have lower C/N ratios, which makes the mixture more desirable as an organic fertilizer for use in agriculture. From such combined paper sludge's, composts are also created. Despite the fact that paper sludge's and their composts are widely accessible, their use in agriculture is still limited because of the high cost of both their application to the soils and their purchase. However, under intensive cropping systems that leave little in the way of organic residues on the soil, the utilization of these organic materials may be able to maintain crop yields and soil productivity [1], [2]. The use of paper sludge as a source of organic matter and plant nutrients to enhance soil structure is highly desirable to sustain soil productivity especially in rotation systems with minimal carbon input. The distribution of their organic carbon among the labile and stable carbon pools may determine how the soil's structure is improved and its carbon

content rises after the application of paper sludge's. Both the quantity and the quality of the organic wastes have an impact on the soil aggregation and C accumulation rate. The rates at which soil microorganisms digest organic wastes and, consequently, their ability to activate soil micro flora and create humid compounds, are related to those impacts. The intermediate products that occur during decomposition, such as polysaccharides, microbial products, together with phenolic and humid chemicals, are what cause soil aggregation. Paper sludge is a lignin-rich organic substance that resists mineralization and, as a result, helps to increase the amount of organic matter in the solid. Due to their high mineralization capacity, as demonstrated by Darkish et al. paper sludge's may also have a longer-lasting impact on soil structure and fertility than other animal manures, which often only produce short-term improvements. Applications of paper sludge's and vegetable residues with high nitrogen contents and C: N ratios of 12–25 have demonstrated a net N mineralization, which has helped to improve the nutrition and yields of wheat and maize. As a result of N immobilization by soil microorganisms during their decomposition, mixed de-inking paper sludge's often have low N content and high C: N ratios, which may hinder crop development, yields, and N nutrition. To meet the N requirements of the crop, N fertilizer should be added to their applications to the soil. The enhancement of the soil's physical and biological qualities, as shown by N'Dayegamiye may also have an impact on crop production increases and N uptake after the application of paper sludge's. Increased gas exchanges and higher water penetration and retention in the upper horizons are advantages for soils with improved soil structure. Additionally, the different macrospores between soil aggregates act as habitats for soil microorganisms, boosting soil biological and enzyme activity and, as a result, the availability and mineralization of nitrogen and phosphorus. Crop yields gradually increase as a result of improvements in soil qualities brought about by the addition of organic wastes [3], [4].

Frequent application to agricultural soils of new paper sludge's with low C/N ratios and high N contents was advised in order to promote aggregate stability, raise soil C content, and maintain soil microbial growth and activity. Reported that cull potato compost and beef calf manure had lingering effects on the physical qualities of the soil and came to the conclusion that frequent additions of these materials may not be necessary. There is limited evidence available for paper sludge's with low N contents and high C/N ratios regarding their immediate and long-term effects on crop yields and N uptake, as well as their long-term impact on soil properties. It is crucial to determine their long-term impacts on soil qualities and crop yields because it might not be possible to apply paper sludge's and their composts on a regular basis. In a clay loam under a low C input rotation system, the aim of this study was to assess the impact of one or three subsequent applications of FDS and CDS on soil aggregate stability and density, soil total N and C contents. On silage corn and barley yields as well as N nutrition, their immediate and long-term effects were evaluated.

Resources and Techniques:

The Le Bras clay loam was the subject of this study, which was carried out between 2000 and 2004 at the IRDA research station in Saint-Lambert-de-Luzon, Québec, Canada. In the A horizon , there were 330 g of sand, 470 g of silt, and 200 g of clay per kilogram me of soil. The soil's original C and N levels were 16.5 g C kg-1 and 1.4 g total N kg-1, respectively, and its initial pH was 6.2. The soil's accessible P, K, Ca, and Mg concentrations were 50, 103, 1195, and 98 mg kg-1, respectively. Mixed de-inking paper sludge's were gathered from the Canadian paper recycling facility Standalone in Quebec. Primary and secondary paper sludge's were combined at a ratio of 1.5:1. From Les Composts du Québec Inc. FDS that had been composted for more than six months was collected. A few characteristics of composted and fresh paper sludge's. With six treatments as the main plot and application frequency as the subplot, the experimental design was split-plot. With or without reduced N fertilizer, the

recommended N fertilizer rate for maize, and an unaltered, unfertilized control were among the treatments. Three copies of each treatment were performed. On plots of 10 m by 12 m, three replicates of each of the six treatments were erected. The plots were divided to evaluate the effects of a single application of FDS and CDS in 2000 and their triple applications in 2000, 2001, and 2002 on maize yields and N uptake in the second and third years of the experiment. The 12-m long by 5-m broad subplots were each. FDS and CDS were manually applied on a wet basis at a rate of 40 Mg ha-1. Ammonium N fertilizer in the amount of 160 kg N per hectare was broadcast sprayed. In the plots that received single, double, or triple treatments of FDS and CDS together with additional N fertilizer, 120 kg N ha-1 of ammonium nitrate was added as N fertilizer in 2000, 2001, and 2002. To make sure that these two important elements wouldn't be a growth constraint for maize, 60 kg P205 ha-1 and 100 kg K2O ha-1 were applied to all the plots, including the control.

FDS and CDS applications were ceased in 2003 and 2004 in order to evaluate their lasting impact on crop yields and N uptake. In 2003, all the plots received 120 kg N ha-1, 60 kg P205 ha-1, and 100 kg K2O ha-1 for silage corn, while in 2004, all the plots received 60 kg N ha-1, 60 kg P205, and 80 kg K2O ha-1 for barley. For silage corn and 90 kg for barley, the full N fertilizer rate treatment applied 160 kg N ha-1 and 90 kg N ha-1, respectively. By disc harrowing in the 0–15 cm soil layer, the organic wastes and mineral fertilizer were absorbed into the soil. Silage corn was grown from 2000 to 2003, followed by barley in 2004. All plots were planted with silage corn from 2000 to 2003 at a rate of 89000 plants per hectare. 160 kg ha-1 of barley seed was sown. As it is customary in the area, all plots had their silage corn and barley leftovers removed after each harvest [5], [6].

Analytical Techniques:

At the moment of application, the FDS and CDS were sub-sampled, and they were maintained at 4 °C until analysis. For the purpose of determining dry matter, samples were dried at 7 o C. Prior to chemical analysis, the dry samples were then crushed to pass through a 0.25-mm sieve. A dried sample was placed in a 1:1 solution of FDS or CDS and water to assess the ph. Dry combustion was used to measure the amounts of organic C and total N using an LECO C-N 1000 analyzer. In contrast, B, Cu, Fe, MN, Zn, Mo, Cr, and Co were extracted by dry aching at 4 5 0 °C for 3 h, followed by ash treatment with Hall. Phosphorus, K, Ca, and Mg were removed by digestion in H2SO4 and H2SeO3 with addition of H2SO4 for 1 h at 4 0 °C. Through the use of an inductively plasma optical emission spectrometer, the various elements present in the extracts were identified. At the start of the experiment in 2000 and in 2004 after the harvest of the barley, soil samples were taken from a depth of 0 to 20 cm. In order to evaluate the pH, texture, and P, K, Ca, and Mg contents of each experimental unit's soil, six randomly selected soil cores were obtained with a 2-cm diameter stainless auger, bulked to create a composite sample, sieved at 2-mm in the field, and air dried. To calculate the soil's C and N contents, air-dried subsamples were powdered to a thickness of around 0.5 mm.

After five years of the experiment, soil samples were taken in the autumn of 2004 to evaluate its physical characteristics [7] [8]. To calculate bulk density, two intact soil cores of 6.5-cm height and 6.5-cm diameter were taken from each plot. In order to evaluate the water-stable aggregates in each plot, one intact soil block weighing about 600 g was dug up to a depth of 0–20 cm. The soil blocks were sieved in the field at an 8-mm mesh size and stored at 4 °C until analysis. In a soil to water solution, the pH of the soil was tested. On an inductively coupled plasma optical emission spectrometer, extractable P, K, Ca, and Mg were determined in a Melic III solution. Using a Lecco C-N 1000 analyzer, dry combustion was used to measure the C and N contents of the soil. The entire carbon content was believed to be organic carbon because the soil at the experimental site was supposed to be no limestone. According to Foley and Cooper band the C content on an area basis was calculated using soil layers of 10-cm and the measured

bulk density for each soil layer. Using the wet-sieving technique, water-stable macro aggregates were identified. A succession of sieves was placed on top of 40 grimes of air-dried soil, which was then shook for 10 minutes while the sieves were submerged in water. The soil fractions recovered on each sieve were dried at a temperature of 6 5 C for 24 hours, sand content was adjusted, and the percentage of dry soil as a whole was calculated. The calculation of aggregate mean weight diameter followed Haynes and Bearer's guidelines. The cylinder method was used to calculate the bulk density of soil [9], [10].

DISCUSSION

In late October, the two innermost rows of each plot's silage corn were harvested. For the purpose of calculating dry matter, whole maize plants were cut at the soil's surface, diced, and weighed. A 600-g to 800-g subsample was then dried at 0° C before being reweighed. To calculate the dry matter grain yield, barley grain was collected, measured, and a subsample was dried at 60 °C and weighed. Total N content was analyzed on an Automated Technician Auto analyzer, and the N content of maize tissues and barley grain was evaluated by digestion in H_2SO_4 and H_2SeO_3 with the addition of H_2SO_4 for 1 h at 4 0 0 C. The sum of the tissue N concentration and the dry matter yield was used to calculate the N uptake by the silage grains of maize and barley. The SAS GLM algorithm was used to do a two-way analysis of variance on data pertaining to crop yields, N uptake, mean-weight diameter of stable aggregates, density, total N and C content, and C per hectare. The contrast analysis was performed to examine the variance in means.

Stability of soil aggregates:

When compared to the unaltered, unfertilized control, the application of FDS, CDS, or N fertilizer considerably enhanced soil macro aggregates and the mean-weight diameter of aggregates. Similar to this study, Cantigny et al. and Bipfubusa et al. found that applying paper sludge's quickly boosted the proportions and stability of soil macro aggregates. The application of FDS or CDS resulted in the formation of larger macro aggregates compared to the control, most likely as a result of an increase in organic binding agents, such as polysaccharides, microbial products, phenolic substances, and humid substances. Surprisingly, N fertilizer increased, in comparison to the control, both the fraction of soil macro aggregates and the mean-weight diameter of aggregates. Organic binding agents and rapidly assailable N from fertilizer may encourage the growth and activity of soil microbes, such as fungi, which help to create and stabilize soil aggregates in part. The findings of Lynch and Bragg Bipfubusa et al. And Nyiraneza et al indicating NPK fertilizer considerably reduced soil macro aggregates do not agree with our conclusion. Nyiraneza et al. have shown that, particularly in low residue organic systems, only long-term N fertilizer applications diminish soil macro aggregates and the MWD of water-stable aggregates. In comparison to their single addition, three subsequent applications of FDS and CDS did not significantly alter either the percentage of soil macro aggregates or the mean-weight diameter of aggregates. This shows that the development and stability of soil macro aggregates were significantly influenced by paper sludge's and their composts.

A well-structured soil can ensure good yields through improved air and water infiltration, nutrient cycling and availability to crops, and soil protection against credibility. Therefore, residual effects of these organic wastes on soil stable macro aggregates are of considerable interest. In crop rotation systems with poor residue return to the soil, such as silage corn and cereal with exported residues, improvement of soil macro aggregation with the addition of FDS or CDS is particularly crucial. Generally speaking, the de-inking paper sludge's employed in this work and other paper sludge's contain high levels of lignin-related compounds which are known to have a long-lasting effect on soil physical qualities such aggregate stability. When

compared to the control, the organic material applications had no discernible impact on the soil bulk density in the 0–10 cm soil layer. When compared to the soils that received FDS or CDS applications, the soil bulk density in the 10–20 cm soil layer was higher in the control and complete N fertilizer treatments. The decreased organic matter input in the control and N fertilizer treatments in comparison to treatments that contained FDS or CDS may be the cause of this outcome. Due to soil dilution, Foley and Cooper band and Shepherd et al. Both documented a decrease in soil bulk density after the addition of organic materials. Following the addition of FDS or CDS to the soil, a rise in macro aggregates may also be linked to a decrease in soil bulk density.

Nitrogen and Carbon Contents:

In comparison to the complete N fertilizer treatment and the control, FDS or CDS applications alone or with supplemental N fertilizer resulted in increased total N and C contents, C/N ratios, and C content on a hectare basis in both soil layers. Only the C contents and C/N in the 10–20 cm soil layer were significantly affected by FDS and CDS treatment frequency. In comparison to their single application in 2000, the three-year treatments of FDS and CDS in 2000, 2001, and 2002 resulted in a larger soil C rise in the 10–20 cm soil layer. This increase in soil C content is most likely the result of three separate applications of FDS and CDS, which add more C than a single application would have, as well as slower C degradation in this soil layer than in the top layer. In comparison to the control and the full N fertilizer treatment, single or triple applications of FDS and CDS caused an average 25% increase in the soil C content in the 0–10–cm layer. For single and triple applications, this increase was 25% and 31%, respectively, in the 10–20 cm depth range. Despite the fact that the overall amount of C applied with FDS was larger than with CDS, there was no difference between the two in terms of C accumulation in the two soil layers. When compared to the unfertilized FDS and CDS treatment, the soil C content significantly decreased in both soil layers after a five-year application of N fertilizer at a rate of 160 kg N ha-1.

According to reports by Darkish et al. And Marvel results generally indicated that applications of FDS or CDS may contribute to C accumulation and a subsequent enhancement of soil fertility and structure. Although it may not be expected in coarse textured soils with low ability to protect newly added C from mineralization the high accumulation of C in this clay loam following FDS or CDS applications may be due to the C protection from decomposition through aggregation and association with silt and clay particles. The high amount of FDS and CDS in stable C with low decomposition rate may also be responsible for the C accumulation in that soil. Due to their high lignin content paper sludge's are resistant to mineralization and help to increase soil carbon content.

Yields of maize and barley and nitrate uptake:

Results from 2000 indicated that, as compared to the unaltered, unfertilized control, FDS and CDS applications with or without N fertilizer lowered silage corn yields and N uptake. This is in line with earlier research' findings that crop yields and N uptake decreased after organic wastes were applied during the first growing seasons. Silage maize yields and N uptake achieved in 2001 and 2002 under FDS or CDS conditions without supplemental mineral N were likewise lower than yields and N uptake observed under conditions involving N fertilizer application, FDS or CDS combined with reduced N rates, and both. Combining the relatively high C: N ratios with the low total N levels in fresh sludge's and composted sludge's may have caused N to become immobilized, reducing its availability to silage corn. Based on reports by Whitehead et al. and Seneviratne for organic materials with such C: N ratios and N concentrations less than 15 g kg-1, net N immobilization by soil micro flora was anticipated.

N'Dayegamiye et al discovered that treatments of those organic materials alone at rates of 30 to 90 Mg ha-1 produced high grain maize yields and N uptake, in contrast, employing paper sludge's with low C: N ratios and high N levels. However, N'Dayegamiye demonstrated that their application to the soil yielded maize maximum yields only when N fertilizer was added at decreased rates, while apparent N recoveries ranged from 10 to 25% depending on the types of paper sludge's. In this study, silage corn yields and N uptake were high when FDS or CDS were applied with a decreased rate of N fertilizer and were comparable to those seen when a whole rate of N fertilizer was used for silage corn. The improved soil aggregation and more nutrients in the FDS and CDS, which may improve plant nutrition, may both contribute to the increased silage maize yields and N uptake in the presence of FDS or CDS combined with less N fertilizer. Numerous research has confirmed the synergy between organic matter amendments and N fertilizers that was discovered in this study. This synergy is attributed to the enhancement of soil characteristics and increased availability of N in fertilizers, both of which promote crop development and N nutrition. According to Barker N should be added to composts with stable N and fresh organic materials with high C: N ratios before application to prevent N immobilization and the associated decline in crop production. Nitrogen fertilizer, which is widely available and satisfies crop demands, also encourages the decomposition of organic matter.

FDS was shown to have higher silage corn yields and N uptake in 2001 and 2002 than CDS. That might be accounted for by the fresh materials' larger initial N content when compared to composts, as well as the fact that the CDS includes stable N that is less accessible to crops. In 2003 and 2004, FDS and CDS applications were halted in order to evaluate the residual effects on silage corn and barley yields and N uptake. To maintain crop yields throughout the course of these two years, all plots with FDS or CDS received lower N rates for corn in 2003 and 60 kg ha-1 for barley in 2004. For barley and maize, the soils with FDS or CDS were compared to those that received the full rate of N fertilizer and 160 kg N ha-1, respectively. Silage maize yields and N uptake attained in 2003 with the prescribed N fertilizer treatment were comparable to those attained with soils previously amended with FDS or CDS at a decreased N rate. In contrast to the required N fertilizer rate of 90 kg N ha-1, soils that received FDS or CDS with a decreased N rate produced higher yields of barley in 2004. The increase in soil productivity and characteristics could account for the high crop yields observed two years following the end of FDS and CDS applications. The effect of FDS and CDS application frequency on crop yields and N uptake was not statistically significant, which suggests that the residual effect was also caused by improvements in soil properties that have a positive impact on plant root development and nutrient absorption. This is an intriguing outcome because it is impractical to apply FDS or CDS on a regular basis due to the high costs of transporting and applying these organic wastes. The lack of significance of the FDS and CDS application frequency is also in line with earlier research that demonstrated the long-lasting effects of fresh and composted manure applications on crop yields and soil characteristics. The high crop yields found in soils treated with the FDS or CDS may be a result of the long-lasting changes made to the soil structure by those organic components.

Finality:

Under silage corn and barley rotation, the application of fresh and composted paper sludge's enhanced soil macro aggregates and the MWD of soil water-stable aggregates, decreased soil density, and increased soil total N and C contents. When applied repeatedly to a clay loam, N fertilizer alone improved the amount of water-stable macro aggregates in the soil but tended to deplete its C and N content when compared to the unfertilized control. Our findings demonstrated that, except in the first year of their application, the paper sludge additions produced good silage corn yields and N uptake when paired with reduced N fertilizer. This was

true even though the paper sludge's used had low N contents and high C: N ratios. Additionally, the residual impacts of fresh and composted paper sludge's on soil production persisted for a few years after they were stopped. This discovery is intriguing because FDS and CDS applications on a frequent basis could be expensive. This study demonstrated that the FDS and CDS's capacity to improve soil physical qualities was the primary driver of their favorable effects on agriculture [11], [12].

CONCLUSION

Under silage corn and barley rotation, the application of fresh and composted paper sludge's enhanced soil macro aggregates and the MWD of soil water-stable aggregates, decreased soil density, and increased soil total N and C contents. When applied repeatedly to a clay loam, N fertilizer alone improved the amount of water-stable macro aggregates in the soil but tended to deplete its C and N content when compared to the unfertilized control. Our findings demonstrated that, except in the first year of their application, the paper sludge additions produced good silage corn yields and N uptake when paired with reduced N fertilizer 120 kg N ha1. This was true even though the paper sludge's used had low N contents and high C: N ratios. Additionally, the residual impacts of fresh and composted paper sludge's on soil production persisted for a few years after they were stopped. This discovery is intriguing because FDS and CDS applications on a frequent basis could be expensive. This study demonstrated that the FDS and CDS's capacity to improve soil physical qualities was the primary driver of their favorable effects on agriculture.

REFERENCES:

[1] A. Al-Haboby *et al.*, "The role of agriculture for economic development and gender in iraq: a computable general equilibrium model approach," *J. Dev. Areas*, 2016, doi: 10.1353/jda.2016.0094.

[2] L. Poorter *et al.*, "Erratum to: Biodiversity and climate determine the functioning of Neotropical forests (Global Ecology and Biogeography, (2017), 26, 12, (1423-1434), 10.1111/geb.12668)," *Global Ecology and Biogeography*. 2018. doi: 10.1111/geb.12721.

[3] E. Stockdale, B. Griffiths, P. Hargreaves, J. Elphinstone, and A. Bhogal, "Developing a practical and relevant soil health toolkit for UK agriculture," in *International Fertiliser Society Conference in Cambridge, UK, on 7th December 2018.* , 2018.

[4] A. Tiwari and V. Jain, "A Review on E-Health Agricultural Monitoring System through WSN," *Int. Res. J. Eng. Technol.*, 2008.

[5] R. Amalia, "Pengaruh Kepribadian, Gaya Hidup Dan Konsep Diri Terhadap Keputusan Pembelian Online Di Kota Makassar," *Skripsi*, 2017.

[6] M. K. M. 1998 Tuti Meihartati, S.ST., "Faktor Ibu Yang Berhubungan Dengan Kejadian Bayi Berat Lahir Rendah Di Rsud Andi Abdurrahman Noor Tanah Bumbu 2015," *PLoS Negl. Trop. Dis.*, 2017.

[7] J. R. Rizkinannisa, "Pengaruh Coping Stress Terhadap Burnout Anggota Polisi Resorg Malang," *PLoS Negl. Trop. Dis.*, 2017.

[8] M. S. Memon *et al.*, "The effects of tillage and straw incorporation on soil organic carbon status, rice crop productivity, and sustainability in the rice-wheat cropping system of Eastern China," *Sustain.*, 2018, doi: 10.3390/su10040961.

[9] E. G. Murrell, C. R. Hanson, and E. Mcullen, "European corn borer oviposition response to soil fertilization practices and arbuscular mycorrhizal colonization of corn," *Ecosphere*, 2015, doi: 10.1890/ES14-00501.1.

[10] J. Sanou, B. A. Bationo, S. Barry, L. D. Nabie, J. Bayala, and R. Zougmore, "Combining soil fertilization, cropping systems and improved varieties to minimize climate risks on farming productivity in northern region of Burkina faso," *Agric. Food Secur.*, 2016, doi: 10.1186/s40066-016-0067-3.

[11] K. Bachteler, M. Riedel, N. Merkt, B. Ullrich, M. Erhardt, and J. Wünsche, "Effect of soil fertilization on the incidence of berry shrivel and the quality of resulting wine," *Vitis - J. Grapevine Res.*, 2013.

[12] C. Graciano, J. F. Goya, J. L. Frangi, and J. J. Guiamet, "Fertilization with phosphorus increases soil nitrogen absorption in young plants of Eucalyptus grandis," *For. Ecol. Manage.*, 2006, doi: 10.1016/j.foreco.2006.09.005.

CHAPTER 3

AN OVERVIEW ON CREATING FREE THZ PAPER OPTICS

Dr. Shivani, Assistant Professor, Department of Agriculture and Environmental Sciences
Shobhit University, Gangoh, Uttar Pradesh, India
Email Id- shivani@shobhituniversity.ac.in

ABSTRACT:

For the effective development of THz techniques, diffractive optical elements must be designed. Here, we take a look at paper structures and examine both their benefits and drawbacks for quick prototyping. It is illustrated how material characteristics like refractive index and absorption coefficient can be used when creating diffractive optical elements. We examine how the efficiency of the structure is impacted by phase step mismatch, real structure attenuation, and uneven illumination. All of these characteristics cause the diffraction efficiency to worsen, but they don't seem to have as much of an impact as the shadow effect that quickly varying zones introduce. Diffractive components are perfect for potential applications since they may be built in very excellent accordance with experimental findings. Paper optics are more commonly used for quick prototyping, however by enclosing them with water-resistant foil, their performance can be improved.

KEYWORDS:

Attenuation, Diffractive Optical, Prototyping, Quick Prototyping.

INTRODUCTION

THz radiation's increasing efficiency in emission is creating new opportunities for security noninvasive testing material identification and medical diagnosis testing, among other applications. THz waves provide promise for finding metal objects concealed behind things, much like when white-up or brown-up occurs during a helicopter's landing. We can use beam shaping to create the desired intensity pattern and elements gathering and focusing the beam to greatly increase the amount of radiation impinging on the detector's surface and ensure a larger signal and therefore more effective detection in order to effectively use and transform the THz radiation. Furthermore, in the case of a matrix of detectors, such optics can dramatically reduce optical cross-talk. THz beam mirrors can reflect radiation and are wavelength agnostic, however system setup is difficult and components are fairly pricey, especially when they have more intricate designs. Different shapes with complicated shapes are available for diffractive elements; they can be easily created using various 3D printing processes, laser cutting, or even milling, but only for axially symmetrical structures. Such components have a strong wavelength dependence, although careful design can overcome this limitation [1], [2].

Resources for THz:

Due to the rapid advancement of THz technology, it is essential to discover novel materials that will make it simple to manufacture optical components. What kind of substance should be used to create diffractive objects for THz waves? The ideal material should have good optical characteristics, be reasonably priced, and be simple to process. Attenuation coefficient must be low in order to avoid the structure from absorbing the majority of the incoming energy while yet producing a significant signal. In the whole THz region being employed, the refractive index should be more or less constant. There are numerous materials that meet these specifications. Teflon, TPX, Zone, TOPAS, polytetrafluoroethylene, and high-density polyethylene are the materials that are most frequently utilized to create THz components. High-resistivity silicon is an additional material, but other materials, such as conductive

polymers metal natural stone and met materials can also be employed to make THz beam shaping objects. It should be noted that diffractive optical elements are being produced using more and more 3D printed materials, such as polyamide 12 or other polymers. Another effort involves employing paper to shape THz beams. Finding a material with a refractive index between 1.4 and 1.7 for a specific design frequency is the optimum answer. It arises from the fact that we will experience large Fresnel losses for higher difference of refractive index between air and employed material, and using some antireflection coatings is therefore advised. However, while hemispherical lenses are often employed, it is nearly impossible to make an effective antireflection coating due to the lens's multiple points of illumination. When the refractive index is excessively low, the structure thickens and dramatically increases attenuation as well as the independent shadow effect. Also, to be noted is the fact that not all materials are suitable for outdoor use. Paper constructions are used here mostly for quick prototyping, although we can cover them with foil to protect them from moisture or rain.

Creating DOEs:

An analogy to the diffractive grating can be used to explain how diffractive optical elements work. A portion of the incident light in these structures is unaltered and propagates after the item in the same manner, while some of the energy is diverted and creates diffraction orders. Diffractive lenses do not have 100% efficiency directed into one specific order, in contrast to refractive lenses, which collect almost 100% of the incident light in the focal spot. By adjusting grating characteristics like the fill factor or the thickness/transparency of the structure, we can change the efficiency in different orders for diffraction gratings depending on the structure. Changes in amplitude or phase can be introduced by diffractive optical components. The former will reduce the radiation that is incident, whilst the latter might theoretically have an efficiency of up to 100%. The fill factor, as applied to the binary diffraction grating, is simply the percentage of the diffraction grating's period that is filled by the grating material. However, for more complex constructions, the fill factor is not as easy to read because the form, transparency, height, or width of the intended zones are all changing in different ways.

It should be noted that rapid changes in fill factor typically cause efficiency to decline by only a small percentage. The shadow impact is much more severe and can significantly reduce efficiency, especially for Kino form structures. Here, we focused our research on paper structures because they are simple to make, very economical, and quick to manufacture. Two techniques stand out as being worthwhile to discuss. One of these is laser cutting which enables the creation of binary structures or, eventually, multistep phase structures. The laser cutting kerf, or gap created by the finite laser spot size, sets a restriction on the smallest feature. The second technique is 3D printing using paper cutting. The main disadvantage of this manufacturing approach is the requirement for a thin substrate, which must be avoided in order to eliminate local zero thickness and ensure optimum structural stability. A traditional Kino form is a phase diffractive object that continuously modifies the incident light's phase between 0 and 2. Imagine cutting a thick, refractive element into layers that range in phase from zero to a maximum of two, then removing all the pieces to introduce a shift of exactly two [3], [4]. In contrast, a high order Kino form is an optical structure made of zones similar to those in typical Kino form but having thickness corresponding to the phase shift of the multiplicity of 2, and therefore having also different widths. In this way, we will obtain a structure that is thin, has the same shape as a refractive one, but is formed with steps having some maximal height. Such a structure has greater optical performance than traditional Fresnel lenses and does not exhibit first-order Kino form-like chromatic aberration. Therefore, we are able to work in the broadband range even when utilizing diffractive optics.

Refractive Index Effect on Designed Structure:

Refractive index is crucial for effective design. When specifying structure parameters in optics, the refractive index of the material that is frequency-dependent is typically employed; however, one can also use the dielectric constant of the material.

DISCUSSION

As was already noted, it is crucial to understand the optical characteristics used to construct the structure, such as the material's absorption coefficient and refractive index. Time Domain Spectroscopy can be used to precisely determine both of these values for a variety of frequencies. While the absorption coefficient informs us of the losses the structure introduces, it is necessary to define the refractive index in order to match the suitable height of the step. We can select the material with the least attenuation, but we are unable to eliminate the impact of varied absorption brought on by various construction thicknesses. Similar to the case of uneven lighting, we can model the outcome but cannot alter it. Due to the wide variety of papers on the market, it is possible to select the best one in terms of stiffness, as well as other important criteria, as well as characteristics like the absorption coefficient and refractive index. The values of the samples' refractive indices and absorption coefficients for the frequency corresponding to the design wavelength were calculated after some of the samples listed in were analyzed. Each paper's name, thickness, absorption coefficient, and refractive index are listed. The final column displays the difference in refractive indices of the paper with and without glue, expressed as a percentage, demonstrating that adding glue just marginally alters the properties of the paper [5], [6].

The initial calculation of material-specific characteristics, such as the refractive index and absorption coefficient, is necessary for an effective numerical simulation that is consistent with experimental findings. Therefore, using a Rearview TPS Spectra 3000 spectrometer, various paper samples were examined. For the usable portion of the THz frequency range, paper material parameters might be determined using a THz optical setup in transmission mode. Measurements were made in a humidity-controlled setting. Over a few years, the ageing of the paper has little effect on the measurements. The aforementioned green paper was initially verified in 2011 and as of right now, the old and new green papers share the same optical characteristics. Refractive index and absorption coefficient curves for green paper are both spherical. If we presume that paper isn't water-resistant, we may picture encasing these structures in foil and sealing them inside. So, we looked at how adding the foil affected the refractive index and absorption coefficient values. All values varied by less than 0.6%, and neither the curve's form nor its trend changed. Since foil is nearly transparent to THz radiation, the thickness of the paper sample with additional foil layers increases while the attenuation essentially stays the same, which accounts for the majority of the change in refractive indices. For a design wavelength of 1 mm, there is no discernible difference in the absorption coefficient. Refractive index and absorption coefficient variations were gathered, and we calculated one value for each parameter with its error, which is displayed.

The first group of papers are made from Xerox white paper with a paper substance of 80 and were created using the 3D printing technique. They are already attached because of the production process; however, samples' various paper layer orientations modify the attenuation coefficient. The values of the refractive indices are almost unchanged. In this orientation, paper sheets are glued and sliced in a 3D printing process in a way that shouldn't cause birefringence. The remaining samples were examined in two alternative stacking arrangements: without and with adhesive bonding between the layers of paper. We provided brief descriptions of the optical characteristics of many papers in Table 1 and will provide further information about them here. Papers 3D orient have already been described. Commercially accessible white paper

comes in 80-gram mage and is made by Lyreco. Fedrigoni produces glossy Siri Pearl paper in the color Ice White with a gram mage of 300. Black Bruno paper weighs 320 grimes per square meter and is produced by Famine in the color Nero. Grey is a 350-g/m2-weight cardboard folder made by Hamelin Top 2000 in the color White. Crossed notebook squared paper is produced in White by Basic. Argo Wiggins offers Green is Curious Metallic paper in Jaspers color and 300. Further testing was done on green paper for various foil kinds that could be used to seal the paper hermetically and counteract the effects of humidity. As we can see, measurements over the entire TDS frequency range are given in Figure 1, with green paper indicating the most comparable values of the two examined parameters.

Absorption coefficients for various samples of green paper with foil start to diverge at higher frequencies. The best measurements are made for lower frequencies since it is crucial to keep in mind that the absorption curve becomes noisier as the frequency increases. For frequencies greater than 0.7 THz, it is theoretically possible to detect the absorption coefficient and refractive index, however it is important to remember that these measurements will only be amplitude structures due to the large attenuation. While it is recommended to use different materials for phase structures at higher frequencies, paper seems to work well at lower frequencies. Therefore, we choose to utilize 0.3 THz, which corresponds to the DWL = 1 mm, due to the increased attenuation of paper for higher frequencies. As we had previously shown, such radiation can be used in THz scanning, but eventually using construction from polyamide.

To prevent undesirable effects brought on by fictitious air layers between paper layers, we must ensure proper manufacturing in case of geometry and gluing for paper constructions made up of more than one layer. As can be observed, the two tested configurations differ significantly for black paper. This impact may be seen in Figure 3's curves for the refractive index and the absorption coefficient in the form of successive peaks that arise for multiplicities of the first frequency. The following frequencies have characteristic peaks: 0.21, 0.44, 0.68, and 0.91 THz. It is clear that structures without adhesive bonding behave as Fairy-Perot resonators, reflecting resonant frequencies, whereas this effect is lost in glued structures. Since we don't know whether the attenuated frequencies are attenuated or reflected back from the paper sample, more measurements should be taken. However, since we wish to avoid this impact, we won't continue with these concerns [7], [8].

Exemplary Design:

One of the tested papers was used to create a steroidal lens to show how useful it is for building diffractive structures. The optical setup utilized in the experiment was the subject of the simulations, which are displayed. The steroidal lens creates a ring with a predetermined diameter in the focal plane rather than focusing light in a single focal point like a conventional lens. We made the structure simply by using laser cutting, therefore we employed a binary phase element that has a corrective structure for the divergent wave front that results from the pinhole. Such a structure ought to refocus the incident light into the focal plane's light ring. Unfortunately, it is nearly hard to design perfect Kino forms that would solely introduce well-adjusted phase change without any attenuation in the real world. The planned structure was therefore converted into a binary structure using paper as a material to simplify manufacturing. Another issue is that no manufactured binary constructions can be made to appear to be "hanging in the air"; instead, they all include extra supporting bars or substrate layers. Bright patches around the ring indicate that these reinforcements introduce some distortions in the resulting energy distributions, but they do so more subtly than an additional layer of material would. In order to run simulations for a toroid diffractive lens with extra reinforcements, the constructed structure was scanned.

Simulations:

On matrices with sampling, simulations were carried out using the modified convolution approach. The construction that was put to the test was built for mm wavelength, or THz frequency. A diverging wave with a diameter of 2.5 mm lighted the intended lens, which had a focal length of mm. The wave that resulted from the pinhole being 300 mm in front of the structure lighted the majority of it very equally. Here, we wish to simulate real-world situations that are typically present in experimental settings in order to demonstrate how manufacturing issues can affect the results that are achieved. Depict the ideal and scanned diffractive element input data that were prepared for simulations. While the second structure is a scanned image of an actual, produced product, the first structure is an ideal depiction of a constructed diffractive lens-like structure. The difference between those two structures is the presence of suspending bars, which are necessary to maintain the cohesiveness of various phase-changing regions. For these two objects, three simulations were performed: one taking into account the potential for manufacturing not-exact phase step height, another assuming the attenuation of the paper-based elements, and a third considering that the beam illuminating the structure has a Gaussian-like intensity shape with different diameters.

The first set of simulations examined the impact of phase change mismatch. By altering the phase delay that the phase object introduced, this was accomplished. This simulation allows examining the impact of manufacturing process precision or rather it's imprecision on the obtained efficiency because in the real scenario added phase delay corresponds to the thickness of the product. In this case, we assume that the entire structure has a constant amplitude, and we only analyse the variable value of the phase step value that corresponds to the height of the phase step producing the phase shift. The intensity distributions of the simulated structures. Then, for the constructed structure, we assume a uniform amplitude across the entire structure with a variable phase step value. The structure with supporting bars was designed, built using laser cutting, and then scanned to run simulations to confirm its accuracy. Intensity distributions for the scanned structure for various phase delays and they match the distribution predicted for the ideal structure [9], [10].

Results reveal that the uniform intensity distribution inside the circle changes due to the phase mismatch, and depending on the phase mismatch, we can see bright or dark spots in the middle, which are not present for the perfect toroid lens. Since this effect is essentially unobservable in simulation results for the scanned object, it is possible to conclude that tiny phase delay mismatching is not essential for the diffractive lens to operate well. The simulation findings for the scanned object also show that greater energy is concentrated at specific locations on the ring. The presence of suspending bars is what causes those defects. The second simulation was performed to find out how the output focal curve of the diffractive lens was impacted by the attenuation and absorption of paper. Under the premise of structural homogeneity, this was accomplished by altering the attenuation of the structure in areas where phase was changed. Compared to places that simply had air, these regions had a lesser amplitude. These intensity distributions have a constant form, making it difficult to distinguish between them. The generated intensity distributions in the scanned structure simulation are likewise extremely comparable.

We carried out the quantitative comparison because there are no discernible differences between the simulation results for various attenuations of the structure material. As can be shown, attenuation has little to no impact on how a lens functions. However, as can be seen from the integral values, it introduces changes in the volume of focused light. We calculated the total intensity of all pixels that made up the focus curve for each intensity distribution and then normalized it to the value of the ideal structure without assuming attenuation which was also the maximum value in all cases. The distinction can now be readily noticed. When we

assumed that the amplitude in the paper region was equal to 0.8 rather than 1, the ideal structure contains 15% less energy in the focal plane. In comparison to a perfect lens, the total intensity in the focal plane for scanned structures shows a substantial decrease. It is mostly brought on by the intensity disturbances that supporting bars introduce. They were created as radial lines, but a random distribution of bars might easily be used in their place. The total intensity would likely decrease, but there wouldn't be the "defects" that can currently be seen as brilliant dots in the ring.

The majority of the time, we assume uniform light while designing diffractive structures. Unfortunately, it is impossible to get absolutely homogeneous illumination in practice. Although we cannot simply alter the beam's shape, we may simulate how those imperfections will affect it. To examine the impact of lighting the proposed lens with a beam size different from lens diameter, a third comparison was conducted. This was carried out in order to illuminate a beam with a Gaussian-like shape and variable waist values. Results unmistakably demonstrate that the lighting of the diffractive lens has a significant influence on the structure's operation. Lens illumination by a narrower beam does not function as intended. Only a portion of the functional region is lighted, and as a result, only a portion of it is operating. We even cannot observe the illuminating beam focusing into a circle when it has an inadequate diameter, as in Figure 10. The diffractive structure begins to function as intended as the light area grows. There is no change observable for a Gaussian beam with a waist value greater than the diameter of the lens because the structure is fully lit. When considering changing attenuation, it can be deduced that the right illumination of the structure is more important than the precise values of the structure's thickness for diffractive elements to function successfully.

Structure and Results Manufactured:

The experimental evaluation was done in accordance with the outcomes of the simulations. A straightforward arrangement based on a Scotty diode as the source and a semiconductor transistor put on stage as the mobile detector was utilized to test the construction. The THz wave front from the source was altered with a converging lens and a pinhole to ensure that the illumination of the structure was as uniform as feasible. The planned structure focused the radiation mm after the structure, correcting the beam's divergence. The experimental setup and recalculated intensity together with the registered amplitude distribution. The experimentally acquired results demonstrate that a toroid diffractive lens-like structure that has been designed and built is capable of modifying the THz wave front. We have exhibited the experimental distribution together with simulations of both the scanned structure and the ideal structure to demonstrate the good agreement between the theoretical simulation and experimental evaluation. The form produced in the experiment and the simulation for the scanned structure are nearly identical. The fact that a true focus plane was produced at the intended distance is noteworthy. For subsequent attempts at creating new optical structures for specific applications, this conformance is crucial. The experimental analysis demonstrates that it is possible to run simulations before creating the desired thing if you are aware of the materials that were utilized to build the construction. This makes it feasible to prevent the formation of numerous structures with poor parameter values, which creates new opportunities for greater control over the THz beam [11], [12].

CONCLUSION

It so happens that paper makes an excellent THz radiation material. Paper optical elements can be produced quickly and affordably using two straightforward techniques, which also enable the creation of high-quality diffractive structures. Simulations performed using a modified convolution method enable accurate radiation behavior prediction. The agreement between experimental evaluation and numerical simulations might be very well achieved. To execute

the simulations, it is necessary to be aware of the material's parameters. It has been demonstrated that structures made of several layers of paper can be created utilizing adhesive bonding without experiencing resonance effects. Although the use of glue does not always increase efficiency, it can greatly aid in the suppression of this undesirable effect when resonance frequencies are present. Additionally, to reduce their impact on the intensity distribution in the focal plane of the intended element, we advise utilizing suspension bars in arbitrary locations. Diffractive elements may be designed and produced using paper as a material quickly, and results show that these structures can successfully alter the THz wave front. Paper constructions are also inexpensive and can be utilized to create various optical components.

REFERENCES:

[1] A. Chanana, Y. Zhai, S. Baniya, C. Zhang, Z. V. Vardeny, and A. Nahata, "Colour selective control of terahertz radiation using two-dimensional hybrid organic inorganic lead-trihalide perovskites," *Nat. Commun.*, 2017, doi: 10.1038/s41467-017-01517-0.

[2] H. Li, W. Li, Y. Feng, H. Pan, and H. Zeng, "Field-free molecular orientation by femtosecond dual-color and single-cycle THz fields," *Phys. Rev. A - At. Mol. Opt. Phys.*, 2013, doi: 10.1103/PhysRevA.88.013424.

[3] Y. Zhu *et al.*, "Structural imaging of nanoscale phonon transport in ferroelectrics excited by metamaterial-enhanced terahertz fields," *Phys. Rev. Mater.*, 2017, doi: 10.1103/PhysRevMaterials.1.060601.

[4] M. Yi, K. Lee, J. Lim, Y. Hong, Y.-D. Jho, and J. Ahn, "Terahertz waves emitted from an optical fiber," *Opt. Express*, 2010, doi: 10.1364/oe.18.013693.

[5] H. R. Seren *et al.*, "Nonlinear terahertz devices utilizing semiconducting plasmonic metamaterials," *Light Sci. Appl.*, 2016, doi: 10.1038/lsa.2016.78.

[6] H. Tao *et al.*, "Flexible terahertz metamaterials: Towards a terahertz metamaterial invisible cloak," in *Technical Digest - International Electron Devices Meeting, IEDM*, 2008. doi: 10.1109/IEDM.2008.4796673.

[7] A. H. Panaretos and D. H. Werner, "Spoof plasmon radiation using sinusoidally modulated corrugated reactance surfaces," *Opt. Express*, 2016, doi: 10.1364/oe.24.002443.

[8] M. Shirao, Y. Numajiri, R. Yokoyama, N. Nishiyama, M. Asada, and S. Arai, "Preliminary experiment on direct media conversion from a 1.55μm optical signal to a sub-terahertz wave signal using photon-generated free carriers," *Jpn. J. Appl. Phys.*, 2009, doi: 10.1143/JJAP.48.090203.

[9] A. K. Majumdar, *Advanced Free Space Optics (FSO)*. 2015.

[10] S. H. Mousavi, P. T. Rakich, and Z. Wang, "Strong THz and Infrared Optical Forces on a Suspended Single-Layer Graphene Sheet," *ACS Photonics*, 2014, doi: 10.1021/ph500207y.

[11] D. Hashimshony, C. Cohen, A. Zigler, and K. Papadopoulos, "Demonstration of submillimeter radiation generation from static field by superluminous ionization front in semiconductor capacitor array," in *Ultra-Wideband Short-Pulse Electromagnetics 4*, 1998. doi: 10.1109/UWBSP.1998.818936.

[12] O. Graydon, "Ultrathin circular polarizer," *Nat. Photonics*, 2017, doi: 10.1038/nphoton.2017.134.

CHAPTER 4

FUSION OF COMPUTER AUTOMATIC TEST PAPER COMPOSITION ALGORITHM: AN OVERVIEW

Dr. Shivani, Assistant Professor, Department of Agriculture and Environmental Sciences
Shobhit University, Gangoh, Uttar Pradesh, India
Email Id- shivani@shobhituniversity.ac.in

ABSTRACT:

This work combines the hybrid fuzzy clustering algorithm to examine the computer-automated test paper composition algorithm in an effort to enhance the impact of intelligent automatic test paper creation. This study builds a hybrid fuzzy clustering algorithm-based system for automatically creating test papers on computers. In addition, the hybrid fuzzy clustering algorithm employed in this work serves as the system's fundamental algorithm, and it is improved in accordance with the demands of intelligent document writing. The required constraint parameters are also input using an intelligent algorithm in this paper, which combines the original parameters to choose the best test questions from the database and combine them into test papers. Finally, this study builds the system structure based on the specifications for the composition of intelligent test papers. The experimental research demonstrates that the hybrid fuzzy clustering algorithm-based computer automatic test paper composition system that is presented in this paper has a good test paper composition function and can effectively advance the intelligent examination mode in colleges and universities.

KEYWORDS:

Clustering, Hybrid Fuzzy, Intelligent Document Writing, Teaching Activities.

INTRODUCTION

Every year, numerous exams are held in the context of the school's teaching activities in order to quickly assess students' learning environments and the impact of teachers' instruction. This is a crucial step in the educational process that can assist teachers in developing their instructional strategies and elevating the standard of their instruction. The most challenging issue for teachers is frequently creating a test paper with thorough knowledge points and a moderate level of difficulty. Higher standards for online exams in the future are inevitable given the growth of online education. Therefore, the requirement for an effective and clever test paper composition system is important. Granular synthesis technique, priority algorithm, backtracking heuristic method, error compensation algorithm, random extraction algorithm, and genetic algorithm are often the algorithms used to solve the challenge of creating intelligent test papers. The first several algorithms take a long time and have a poor test paper composition success rate, and it is challenging to find a better solution.

Although the genetic algorithm is a global search algorithm and has some effect on increasing the success rate of test paper composition, its test paper composition efficiency and effect still need to be improved. It is easy to fall into the trap of a local optimum, leading to premature phenomena. The network teaching management system's main purpose is to allow students to study and train online, and to allow teachers to assess students by choosing test questions from the test question library [1], [2]. The implementation of online testing involves selecting test questions from a vast test bank that adhere to various instructional test standards. It is important to consider if test results accurately reflect both the students' and teachers' degree of teaching proficiency and the students' actual learning environment. Currently, backtracking heuristic

algorithms, evolutionary algorithms, and other intelligent test papers are used as part of the procedure of extracting test questions and test papers from the question bank. Only when the number of test questions is manageable and the conditions are appropriate can the method of random selection of test questions be configured to meet the needs of the user. It is impossible to create a test paper that satisfies the user's needs since it will fall into the noni deal question region and repeat the selection of questions. The algorithm for the retrospective test paper group demands several retrospective test operations in the test selection, which is no longer able to handle the test question bank's often modified questions. The network test set system's test set criteria. The genetic algorithm is capable of adaptive global optimization, intelligent search, and good convergence, but it is prone to issues like early maturity and local optimal solutions. In this study, the computer automatic test paper composition algorithm is examined using the hybrid fuzzy clustering algorithm. A computer automatic test paper composition system based on the hybrid fuzzy clustering algorithm is then built, helping to increase the effectiveness of intelligent test paper composition.

Additional Work:

The intelligent test-setting system can easily achieve semi-automation of the test, which not only helps teachers create test questions automatically but also best satisfies the various test requirements of various teachers. The moderate difficulty and more reasonable distribution of test questions offered by the genetic algorithm-based intelligent test-setting system can guarantee the fairness and rigor of the test. Teachers, students, and administrators are the minimum number of user types for the intelligent group volume system. Administrators can manage user information and basic data management of test questions. Teachers can view all of the students in their class, manage all test questions under their own subjects, add test paper requirements, create test papers for the subjects they teach, publish tests, mark subjective questions, view score analysis, etc. Basic data management of test questions includes question kinds, questions, answers, difficulty, score, and knowledge points. User management includes user name, account number, password, e-mail, class, and subjects. Typically, the intelligent group volume system performs the following tasks. User management: Login; administrators add, remove, and modify user information as well as the permissions they grant to users. Subject management: The administrator oversees each subject's subjects, including the management of the subjects' fundamental facts and the knowledge-based information they include. Test question management: control the test questions for every subject, including their entry, editing, deletion, and export. The only test questions that a teacher can operate are those for the subjects for which he is responsible. The administrator can operate all test questions. Management of test papers: Each subject's teachers' requirements are taken into account when creating test papers. Online test: Give pupils online quizzes on various subjects and display their results. Score analysis: automatically evaluate objective questions, give students a personal analysis of incorrect questions, and inform teachers of each student's and each class's overall status [3].

Intelligent test preparation is essentially a multi-constrained, objective optimization issue. According to the test conditions established by the test teacher, the computer system automatically provides the best answer for n-question combinations that adhere to these restrictions. Generally speaking, a test paper has restrictions like the overall score, test time, test paper complexity, test question type, number of questions for each question type, and distribution of knowledge points. These restrictions on the exam paper are typically determined by the kind, score, and level of difficulty, knowledge points, and other results. The genetic algorithm, as its name suggests, mimics Darwin's theory of evolution by starting with a random population and continuously combining individuals to produce the following generation. Additionally, there will be variance during this time. Finally, the survival of the fittest down

principle ensures that the best one or more people are kept. Applying it to the intelligent volume system is more appropriate. According to the test paper difficulty, test paper structure question type, amount, and score knowledge point distribution, and other test paper group factors requested by the teacher, it may intelligently construct a set of test papers that satisfy the requirements. The database and test question data table are first designed after the purpose of the intelligent test has been examined, typically in accordance with the types of test questions such as true-false, multiple-choice, fill-in-the-blank, short answer, comprehensive, etc. that will be asked. A data table is associated with each inquiry type. When the function of an intelligent test paper is realized by coding, the test questions are first chosen from the database to generate the test paper, and then the test paper is evaluated to determine if it is the best test paper. In more detail, you can first locate every test question associated with the chosen knowledge point by using that knowledge point, and then randomly combine these test questions into several test papers. Until the fitness reaches greater than 0.98 or the number of cycle's approaches 10,000, the test paper with the highest fitness in each set of test papers is chosen as the male parent and the other test papers are randomly selected as the female parent to produce the next generation [4], [5].

DISCUSSION

The main purpose of the smart component system is to evaluate student learning results. Students frequently use exams as part of the educational process to gauge their progress, and in order for these exams to be successful, high-quality test questions are frequently required. The design of the exam papers frequently calls for a high level of evaluation and professional standards from the educators. However, a lot of professors are frequently solely in charge of the teaching component. The exam papers contain little research and frequently leave out important information. If you do not understand the test papers' major topics, you will not perform well on the test. The scientific and intelligent nature of the test question bank allows us to deal with the questions on the exam paper in accordance with the syllabus and carry out the construction of the intelligent test question bank.

The composed test papers must be separated into various levels of difficulty and delivered in steps after using the intelligent group test question bank method in order to divide the test results precisely. The level of examination by the students will be impacted by the exam papers' difficulty or simplicity, even if there is no difference in the test results. Exam papers that are overly challenging and out of the scope of the students' knowledge will not be able to accurately reflect the students' level of learning. In extreme cases, students will lose faith in their ability to learn; if exam questions are too easy, all candidates can quickly correctly answer them, giving all students the same grades in a large area; it is also impossible to determine each student's individual level of learning; and this formalized exam will also negatively impact students' enthusiasm, making it difficult for them to focus and devote themselves to learning. To summarize, the ability level of the majority of middle-level students must be considered in the test question bank's design in order for most students to accept the difficulty and allow for a stepwise distribution of grades. Exams can have a certain guiding function in students' learning since, in the current educational environment, students frequently place a high value on more formal exams. Therefore, the exam questions shouldn't be memory-based because this will cause students to think rigidly and force them to study just for test scores, which is counterproductive to achieving educational goals.

The questions in the question bank have the proper symbols and wording. Exams are serious and solemn. Exam problems will help students laugh and make exams seem less serious. In order to make the test's goal and character clear, as well as to account for the syllabus' criteria, the test's composition must be properly planned. The teacher must rigorously evaluate and calculate the test paper before it is used in class, identify any hidden faults in the test questions,

and quickly correct them. Having a thorough understanding of the style, level of difficulty, and scope of each exam question is also essential in order to give students who made mistakes after the test specific coaching and instruction. Accelerate the production of test materials. The combination of cellular automata and genetic algorithm is used for intelligent test composition, and the test question query two-dimensional space uses a spatial topological structure, which better guarantees the diversity of test questions and provides conducive conditions to find the best combination of test questions. This approach addresses the drawbacks of traditional genetic algorithms, such as precociousness and slow optimization speed. The artificial fish swarm algorithm's foraging, tail-chasing, and other behaviors were enhanced in literature and used to group rolls, which produced positive results and increased the speed and quality of the rolls [6], [7].

The fuzzy similarity relationship matrix is first established as part of the matrix analysis based on the fuzzy equivalency relationship, and it is then transformed using the square approach, which involves a significant amount of work. As a result, researchers are looking into the nets method of direct clustering that starts with the fuzzy similarity matrix. The easy and logical matrix self-multiplication operation is not used in this method. In the so-called "netting method," the element symbol is filled in on the diagonal of a fixed level cut matrix. Replace 1 with, "0" with a space, and "call the node of the position in the lower left corner of the diagonal. The next step is netting, which involves drawing the warp and weft lines diagonally from the nodes. In other words, the warp and weft lines are utilized to connect the nodes, and they can be thought of as being bundled together when they pass through the same node. Thus, it is tangled. To achieve classification, the points that can be related to one another by knotting fall under the same heading. The maximum tree method can be utilized for direct classification for matrices that only contain reflexive and symmetric fuzzy similarity relations. The maximum tree approach involves creating a particular network for clustering that adheres to the graph theory idea of "tree" and has n vertices and n 1 linked edges but no loops.

Hybrid Fuzzy Clustering Algorithm-Based Computer-Automated Test Paper Composition System:

The mathematical model of test paper composition, test paper composition target constraints, test paper composition algorithm, test paper evaluation indicators, test question structure, algorithm coding method, etc. are the main theoretical foundations of the intelligent test paper composition system. The exam paper composition system's intelligence algorithm, which is also the subject of this essay, is what makes it challenging and important. The essential constraint parameters are first entered into the intelligent test paper composition module's execution process, after which the original parameters are combined to choose the most appropriate test questions from the database and combine them into test papers. Figure 1 depicts the precise steps.

Model-View-Controller is an architectural pattern for developing and building web applications. It represents the application's structure and the division of labor between its various components. We strengthen the program's scalability and maintainability and achieve the separation of the business layer and the view layer in order to increase the effectiveness of research and development. The MVC architecture is used in the system's development. Figure 2 depicts the MVC framework's fundamental structure. This study uses business activity diagrams to illustrate the work and behavior of teachers' test paper preparation and students' online test execution, combining users' requirements for an intelligent test paper composition system. The business activity diagram for the test paper composition by the teacher is shown in Figure 1. We can see how the teacher composes the exam paper by looking at the activity diagram. The system reads the test paper composition conditions to assess whether the test questions comply with the test paper composition requirements when the teacher enters the test

paper composition system and sets the test paper restrictions in accordance with the prompts. The test questions will be chosen and the test paper will be prepared if the requirements are met. If it doesn't, the process is over and the test paper composition is deemed unsuccessful. The flow of the students' online examination may be seen by looking at the activity diagram of the exam. Students log onto the system, access the exam course units using their student ID, choose the course unit, take the online exam, submit their answers, save their exam results, and finish the process activities [8], [9].

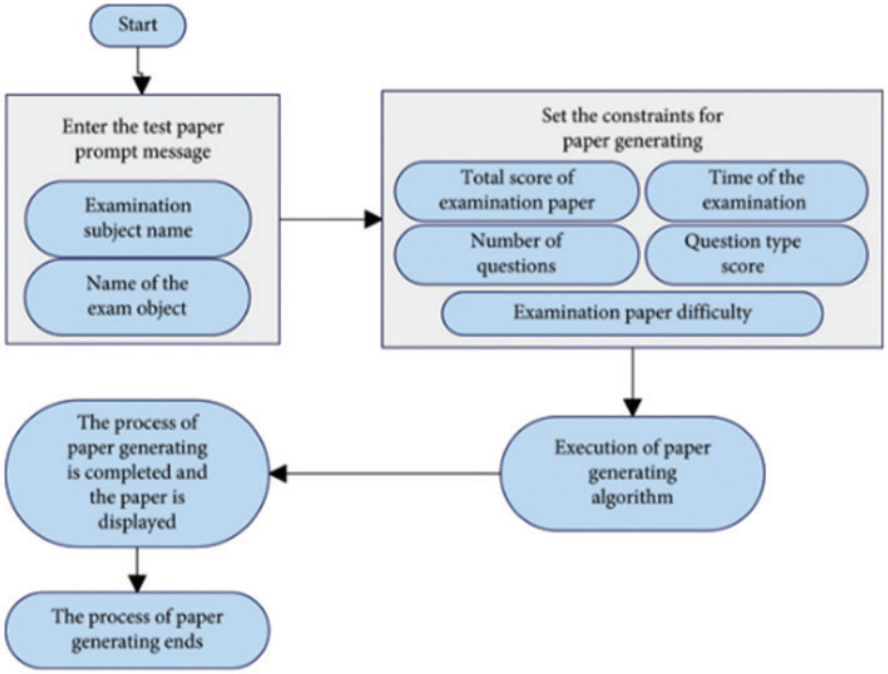

Figure1: Diagram of the Test Paper Composition System's Flow Analysis [Hindawi].

It is the flow chart for the creation of an intelligent test paper. The test paper settings are initially read by the system in order to determine the number of test questions of each different type, as shown in the flow chart for the test paper creation. The system also performs random initialization selection while initializing the selection state of each test question and setting the test question's unselected state to 0. The system then determines whether the test paper is fit for purpose after computing its fitness in this state. If the conditions are not met, the animal engages in tail-chasing, flocking, or foraging activities, and the fitness can only be recalculated if the criterion is reached. The test paper will be published if the fitness level is attained. In the event that the teacher is happy, the test paper composition process is finished; otherwise, it is repeated. The system proposed in this paper is verified for effectiveness after the system's structure has been built. As the foundational information for the database in this paper, a sizable number of test questions are collected from the internet, and the output test paper composition system's findings are then automatically checked. The outcomes of this study's examination of test paper composition and analysis of various evaluation data sets [10].

CONCLUSION

An essential component of achieving a scientific and effective management of educational administration is the study of intelligent test paper composition systems, which is a significant area of study for computer test paper composition. In order to create a test paper that satisfies the requirements, computer test paper composition involves resolving multi-objective constraints for the quality indicators that affect the test paper, such as difficulty, content, time,

score, and instructional requirements. Additionally, the intelligent test paper creation system serves as the foundation for other testing innovations such as online testing, standardization and customization of exams, and paperless testing. The intelligent test paper composition system also combines artificial intelligence technology with the expertise of human education experts in test paper composition, completes the design of the test paper content through the computer, and ensures that the test paper generated by the computer meets the expert-level standard. In this study, the hybrid fuzzy clustering algorithm is combined to research the computer-automated test paper composition method, and a hybrid fuzzy clustering algorithm-based computer-automated test paper composition system is developed. The experimental research demonstrates that the hybrid fuzzy clustering algorithm-based computer automatic test paper composition system that is presented in this paper has a good test paper composition function and can effectively advance the intelligent examination mode in colleges and universities.

REFERENCES:

[1] R. Guo, G. Lu, B. Qin, and B. Fei, "Ultrasound Imaging Technologies for Breast Cancer Detection and Management: A Review," *Ultrasound in Medicine and Biology*. 2018. doi: 10.1016/j.ultrasmedbio.2017.09.012.

[2] G. Chetty and M. Yamin, "A distributed smart fusion framework based on hard and soft sensors," *Int. J. Inf. Technol.*, 2017, doi: 10.1007/s41870-017-0008-9.

[3] R. Shortt, A. Verhallen, and P. Fisher, "Monitoring Soil Moisture to Improve Irrigation Decsions," *Factsheet*, 2011.

[4] N. Bridgford, "Darwin's Theory of Evolution," *Young Scientists Journal*. 2009.

[5] J. Dubochet, "Why is it so difficult to accept Darwin's theory of evolution?," *BioEssays*, 2011, doi: 10.1002/bies.201000142.

[6] A. H. Ibrahim and M. Baharuddin, "Criticism of Darwin's Theory of Evolution by Muslim Scholars," *Online J. Res. Islam. Stud.*, 2014.

[7] Y. Nishiyama, "The mathematics of egg shape," *Int. J. Pure Appl. Math.*, 2012.

[8] K. R. Shivanna, "Gálapagos Islands and Darwin's Theory of Evolution," *Resonance*, 2018, doi: 10.1007/s12045-018-0636-9.

[9] M. Ruse, "Charles Darwin's theory of evolution: An analysis," *J. Hist. Biol.*, 1975, doi: 10.1007/BF00130439.

[10] S. Klumpenhouwer, "Early Catholic Responses to Darwin's Theory of Evolution," *Undergraduate Academic Journal*. 2011.

CHAPTER 5

EXPLORING THE ROLS OF GANGLIOSIDE AND ITS APPLICATION

Dr. Shivani, Assistant Professor, Department of Agriculture and Environmental Sciences
Shobhit University, Gangoh, Uttar Pradesh, India
Email Id- shivani@shobhituniversity.ac.in

ABSTRACT:

Salic acid-containing glycosphingolipids are called gangliosides. They can be found in many other cell types, but they are most common on the cellular surfaces of neuronal cells, where they form a complicated pattern. A comprehensive summary of their architectures, occurrence, and metabolism is given in the publication. There is a summary of the main functional, biochemical, and path biochemical aspects. It should be emphasized that gangliosides are mostly present in the medium of cultured cells as free monomers, as monomers linked to proteins, and as oligomers in the form of micelles or vesicles. Gangliosides can aggregate into various shapes and sizes in an aqueous environment. The majority of the time, they are micelle structures between 280 and 630 kids with GM3 and GM4 also being vesicles in the case of gangliosides with tiny head groups.

KEYWORDS:

Glycosphingolipids, Gangliosides, Salic Acid, Sugar Residues.

INTRODUCTION

Glycosphingolipids, together with glycoproteins and glycosaminoglycan's, are a component of the glycocalyx that coats the surface of eukaryotic cells. Gangliosides, silica acid-containing glycosphingolipids, make up a sizeable portion of the glycan's on the surface of neuronal cells. GSLs are lipids made up of a sphenoid base, one or more sugar residues, and other components. Salic acids are nine-carbon sugars that are produced synthetically from phosphoenolpyruvate and -acetylmannosamine. They are more acidic than other carboxylic acids and negatively charged at most physiological pH levels, with a typical value of about 2.6. The German biochemist Klink gave the term ganglioside to a class of acidic GSLs that he isolated from ganglion cells and from the brains of people who had amaurotic stupidity. Sub maxillary cumin was the source of silica acid's initial isolation in 1936. Its structure was determined by various groups in the 1950s, and it was discovered to be the same as the N-acetylneuraminic acid identified by Klink and Fail lard. By Kuhn and Wigand, the initial ganglioside structure was deciphered in 1963. Brain gangliosides were given a nomenclature by Svennerholm in 1962. In the 1960s, Sendoff and others discovered the biochemical flaws behind the illnesses formerly known as amaurotic stupidity, GM1-gangliosidosis Taya-Sachs and Sendoff disease [1], [2].

Organization and terminology:

Gangliosides combine a glycan and a lipid component in their structures, and as a result, they contribute to both the cellular liposome and the glycine/Salome. The GSLs contain a wide range of carbohydrate sequences, including gangliosides. Although GSLs contain carbohydrate residues with a variety of structural, linking, and numeric configurations, only few of the so-called series with distinctive carbohydrate sequences can be discovered in closely related animals. Only a small number of the GSL series, specifically the ganglion series in adult mammals, can have silica acids connected to them within the gangliosides. The most prevalent silica acid in humans is -acetylneuraminic acid, however many other species also have high levels of -glycolylneuraminic acid. Over 50 distinct silica acids have been identified in total.

They may also be -DE acetylated, -methylated, sulfated, or changed by factorization. They may be -acetylated at positions. The glycan component of these lipids is designated by the nomenclature of GSLs. The names of the related structures are currently assigned by two ganglioside nomenclature systems. The Svennerholm short-hand nomenclature, which was initially based on the chromatographic migration order of ganglion-series gangliosides, is preferred by the majority of studies. Later, it was expanded to include different root systems. Less frequently used is the IUPAC system which is more thorough. The pianos forms of D-GA lactose Acetyl-glucosamine, or Acetylgalactosamine are attached to lactosylceramide orgalactosylceramide in a defined order and linkage, according to Svennerholm. The names reveal the series, the number of silica acids, and, indirectly, the number of uncharged carbohydrates.

Since it was once thought that this number couldn't go above 5, the name ganglioside denotes that it comprises neutral sugars from the ganglion series. The sequence Gal1-3GalNAc1-4Gal1-4GlcCer defines this series. Salic acids can be bonded to various locations within the core structures just once, twice, or several times. They are most frequently found in 2, 3- and 2, 8-linkages to other silica acids as well as to the inner or outer galactosyl residue. Position II of the gangliotetraose moiety of ganglioside GM1 has a galactosyl residue with a 3-OH-group attached. II3Neu5AcGg4Cer is the equivalent IUPAC-IUBMB short name. The ganglioside biosynthetic strategy can also be used to determine the structures of ganglion-series gangliosides. Ganglion-series GSLs of the 0-series typically have no silica acids on the GA lactose at position II, one on the a-series, two on the b-series, and three on the c-series.

Although they are both 0-series gangliosides, GM1b and GD1c have b and c in their names. Additionally, ganglioside core structures can be altered; they can be lengthened, as in GD1aGalNAc. This ganglioside is found, for instance, on spinal neurons and has been linked to several neuropathies and types of the Guillain-Barre syndrome via the development of autoantibodies. In the brains of Taya-Sachs disease patients, a modified GM2 derivative containing turbine in amide linkage to the silica acid carboxyl group has been discovered. This chemical class is made more complex by hybrid-type GSLs and gangliosides with post glycosylation modifications. Bovine brain has been found to contain lacto-ganglion hybrid-type gangliosides, for instance [3], [4].

The ganglion, gala, lacto, and neglect series includes the majority of gangliosides discovered in adult animals. A part of the gala series, ganglioside GM4 frequently contains a -hydroxyl-fatty acid within the creamed moiety. Its structural breakdown is NeuAc2, 3Gal1Cer. Additionally, gangliosides with different core structures are momentarily produced during development. One such example is the stage-specific embryonic antigen SSEA-4, a globe series ganglioside. Adult human erythrocytes adult human kidney and adult human different stem cells all contain globe-series gangliosides. For instance, mesenchymal stem cells generated from cord blood express SSEA-4 but neither SSEA-3 nor Globe-H. Invertebrates typically lack gangliosides, with the exception of echinoderms.

For instance, arthropods produce acidic GSLs with a Man1, 4Glc1, 1′Cer core that have glucuronic acid as opposed to Salic acids. There is no standard short-hand name for echinoderm gangliosides. They exhibit structural characteristics not found in mammalian gangliosides, including Salic acid residues in the oligosaccharide moieties, 2, 11-linked Salic acids, Salic acid methylation or salvation, or, for instance, a glycol inositolphosphoceramide core. Echinoderm gangliosides exhibit neurogenic and growth-inhibitory effects in cultured neurons. They are more effective than other gangliosides in this regard and increase the neurogenic effects of nerve growth factor.

DISCUSSION

The creamed portion of gangliosides contains primarily saturated fatty acids. Although they are less common in brain gangliosides -hydroxylase fatty acids are, for instance, abundant in gangliosides from the colon, liver, or kidney, as well as in GM4. For an II3Neu5AcLacCer with a sphingosine of 18 carbons and a sterol residue within the creamed section, identifiers like GM3 are used to describe the lip form of the ganglioside. Although the functional effects of the lipid component's heterogeneities are mainly unknown, they can conceal the ganglioside glycan's' receptor function by interacting with membrane cholesterol. Another illustration is the fact that only GM1 with unsaturated acyl chains is sorted from the plasma membrane to the trans-Golgi network and the ER. The creamed part of GM1 controls retrograde transport of the cholera toxin coupled to GM1. Ganglioside analysis is increasingly focusing on ganglioside profiling with regard to glycan and creamed structures.

Occurrence:

In the brain, where their incidence in the grey matter is around 5-fold higher than in the white matter, gangliosides are particularly prevalent. The values range from 2 to 14 g lipid-bound Salic acid/mg protein in adult human brain areas. Neurogenesis, synaptogenesis, synaptic transmission, and cell proliferation are all correlated with ganglioside expression in the brain. A change from the a- to b-series and an increase in the creation of complex gangliosides accompany axon genesis in cultured murine hippocampus neurons, but not dendritogenesis. The number of gangliosides is one to two orders of magnitude smaller in extra neural tissues than in the brain; nonetheless, there are still relatively high quantities of ganglion-series gangliosides in the colon, erythrocytes, liver, spleen, and testis, GM4 in the kidney, and SSEA-4 in embryonic stem cells. Cellular gangliosides create intricate, tissue- and cell-type-specific glycan patterns in part. As a result of physiological and pathological processes including cell proliferation, differentiation, viral transformation, ontogenesis, oncogenes are, embryogenesis lactation, or tumor progression these are not stable over time. Instead, they alter. The nervous system is home to gangliosides of the ganglion-series, which make up 10-12% of the lipids there. The distribution of the simple gangliosides GM3 and GD3 shifts during brain development to more sophisticated gangliosides like GD1a and GT1b. The amount of lipid-bound Salic acid fell from 1070 g/g wet weight in a 25-year-old healthy probed to 380 g/g wet weight in an elderly person. Ganglioside concentration and composition of the brain likewise alter with age. Despite this, GQ1b, GT1b, and GD1b concentrations rise with age while GM1 and GD1a concentrations decline. The composition of gangliosides changes with age in the liver as well. On the functional effects of such modifications, there are only suggestions [5], [6].

In serum, gangliosides are also present. Particularly present there are GM3, GD3, GD1a, GM2, GT1b, sialylneolactotetraosylceramide, GD1b, and GQ1b, which are carried by serum lipoproteins, mostly LDL, followed by HDL and VLDL. About 98% of these substances are delivered by serum lipoproteins. It may turn out that these assignments need to be updated in light of the identification of extracellular micro vesicles which could not be separated from lipoproteins in earlier investigations. Rat experiments revealed that the GM1 and GM3 probes had serum half-lives of 1.4 and 1.8 h following injection of Salic acid-labeled gangliosides GM3 and sphingosine-containing labelled ganglioside GM1. After three hours, the liver absorbed 75% of the GM1 probes and 38% of the GM3 probes, with less penetration occurring in the central nervous system, kidneys, and lung. The plasma membrane is where the majority of gangliosides are found intracellular. However, gangliosides can also be found in organelle membranes like those in the nucleus and mitochondria, where they play a role in Ca2+ homeostasis and GD3 regulates apoptosis, respectively. The acylation of Salic acid residues in various places can occasionally change the glycan's present in gangliosides. Gangliosides

contain acetylated Salic acids, which are thought to be oncofetal markers seen on many tumors and exist particularly in developing cells and tissues. N-glycolylneuraminic acid is another modified Salic acid. It is only present in very small concentrations in human tissues, with the exception of some tumors and fetuses. Neu5Gc, sometimes referred to as the Hanganutziu-Deicher antigen, is a part of glycoconjugates. When compared to birds and reptiles, it is largely lacking in many animals of the Deuterostome lineage, such as simians, mice, rats, cattle, pork, or lamb. Neu5Gc on glycoconjugates contributes to xenoantigenicity in pig-human xenotransplantation and in cats, Neu5Gc distinguishes the blood groups A and B 2GD3 is found in feline blood group A erythrocytes 2GD3 on blood group B, and feline blood group AB erythrocyte membranes contain.

Because of an irreversible inactivation of the CMAH gene, which codes for Cytosine monophosphate-N-acetyl-neuraminic acid hydroxylase, on chromosome 6p21.32, humans are unable to synthesize Neu5Gc. This enzyme is assumed to have lost its activity during a sialoquake in human evolution because it transforms CMPNeu5Ac to CMPNeu5Gc. Both traditional chromatographic methods and antibody staining can be used to determine Neu5Gc and Neu5Ac-containing gangliosides or, for greater sensitivity, chromatography and ESI-MS can be used. The immunochemical detection of GM3 as a biomarker of non-small-cell lung cancer is one possible use. Additionally, ganglioside lactones have been found in a variety of tissues, including the mouse brain and the human brain. Ganglioside lactones are tumor-associated antigens that are found on tumor cells like melanoma and are more immunogenic than gangliosides. Gangliosides can be Latinized in vitro and then undergo a strong negative Cotton effect in CD spectroscopy at 235 nm. Differences in time and place are also seen in the ganglioside lipid component. Gangliosides containing C20 sphingosine are only minimally present in undifferentiated neural cell cultures, but their quantity rises as cell differentiation progresses. In the cerebellum or forebrain of the rat brain, the proportion of gangliosides containing C20 sphingosine increases with age. Mice have also shown spatial differences in the sphenoid base chain length, with C20 species being specifically localized along the entorhinal-hippocampus projections whereas C18 species were extensively distributed across the frontal cortex. Human motor and sensory neurons differ in their fatty acid and sphenoid base makeup [7], [8].

Nutrition:

Gangliosides are consumed together with food because they are a part of the majority of vertebrate cell types, such as egg yolk, meat, or milk. Gangliosides, particularly GD3 and GM3, are found in milk's membrane-bound fat globules. During the first few months of life, dietary gangliosides alter the gut micro biota and guard against infections. With the help of acid-catalyzed factorization, over 80% of dietary gangliosides in newborns make it through the stomach and are then absorbed in the intestine. Ganglioside levels in serum rise as a result of dietary ganglioside ingestion. For the rapidly developing baby brain, Salic acid from gangliosides and other glycoconjugates is a crucial component in human nutrition. Nutritional Neu5Gc uptake's pathophysiological effects aren't known. Ganglioside structures and levels were formerly determined through in-depth chemical investigation, but today this is tried within lipidomics employing mass spectrometry as the key method.Chloroform-methanol extraction is typically used to separate gangliosides from tissues and bodily fluids. When modest amounts of water are present in the extraction solvent, such as when utilizing the solvent system chloroform: methanol: water: 5:1 extraction efficiency can improve. Gangliosides partition into the upper, aqueous phase when extraction is followed by a partition step like that created by Filch et al. In contrast to the majority of other lipid classes. They can then be extracted by a solid phase extraction and separated from neutral GSLs using anion exchange chromatography such as using DEAE Sephardi. Under alkaline circumstances,

changes such ganglioside factorization and O-acetylation of Salic acids are lost. These are frequently used to remove fatty acid-containing glycerophospholipids with ester linkage. Gangliosides from tissues can be identified without alkaline treatment, for instance, following a partition step after chloroform/methanol extraction in a 1:2 ratio and the requirement for information on these alterations.

Thin layer chromatography high performance liquid chromatography, and other techniques that can be connected to mass spectrometry are used to separate gangliosides based on the glycan content of those compounds. This makes it easier for mass spectrometry to identify them, and it's necessary for staining them with the appropriate lections, antibodies, or other binding proteins to characterize them. Reversed phase chromatography can further differentiate isolated ganglioside classes based on their creamed structure, albeit it is not necessary for mass spectrometric profiling. If appropriate reference chemicals are available, mass spectrometry can be used to quantify samples in addition to staining and densitometry. Comprehensive ganglioside analysis is a very difficult endeavor within lipidomics because the biosynthetic machinery causes heterogeneities in both the lipid and the glycan portion. In order to comprehend ganglioside metabolism and function lip forms become more crucial in addition to glycoforms, which are very well known through glycoprotein analysis. Different mass spectrometry ganglioside determination procedures have been developed. They heavily rely on the ionization technique known as electrospray mass spectrometry, however MALDI also plays a part. Through ascertain the analyses' spatial distribution, imaging techniques using MALDI and Secondary Ion Mass Spectrometry are available, ranging from preanalytics through bioinformatics data management. Little is known about the conformation of gangliosides in their natural, membrane-bound environments, except from their composition. Gangliosides do not have X-ray data, although isolated glycan's have been studied in a variety of ways. Compare which, for instance, demonstrates that the glucose moiety of GM3 is concealed behind phosphatidylcholine head groups, for a simulation of GM3 conformations in a bilayer [9], [10].

Biosynthesis:

The heterogeneities within the creamed portion originate from the manufacture of creamed at the endoplasmic reticulum, and the diversity of cell surface glycan's, including that of gangliosides, is created within the Golgi apparatus. The salvage processes that recycle Salic acids, sugars, fatty acids, and sphenoid bases can be separated from the de novo synthesis of gangliosides. In differentiated cells, the latter process may predominate overwhelmingly. Ceram ide is produced in the cytoplasmic leaflet of the ER membrane, where ganglioside production begins. The pyridoxal phosphate-dependent serine palmitoyltransferase catalysis the condensation of L-serine and a coenzyme A-activated fatty acid in the first step. Using L-serine radiolabelled in position 3, it is possible to track the de novo production of GSLs. For the brain's growth and neuronal lipid production, astrocytes' external supply of L-serine is crucial. According to genetically modified mice with inadequate phosphoglycerate dehydrogenase, L-serine production from D-glucose results in severely lower levels of gangliosides, abnormalities in brain morphogenesis, and significantly shorter lifespans.

The acylation of sphinganine to dihydroceramides with various chain lengths comes after the NADPH-dependent reduction of 3-ketosphinganine to sphinganine by 3-ketosphinganine reductase. N-acyltransferases from the lasso's family acrylate additional sphenoid bases during salvaging. Ceram ide synthase 1, which is expressed in the brain and necessary for the synthesis of the membrane anchor of gangliosides, is encoded by the Lass 1 gene. Cerebellar ataxia and Purkinje cell degeneration are linked to spontaneous recessive mutations in the lass1 gene in mice. Although the majority of the fatty acids in the creamed portion of brain gangliosides are nonhydroxylated, it appears that all members of the lasso's family may also transfer the

appropriate 2-hydroxy-fatty acids. The dihydroceramide denaturize des dehydrogenates dihydroceramides to creamed, and des2 hydroxylases phytoceramides. The transport protein CERT transports creamed to the Golgi apparatus, at least in part in a protein-dependent way, as creamed is the common precursor of GSLs and sphingomyelin.

General Ganglioside Formation Factors:

The transfer of nucleotide-activated monosaccharide units onto creamed and then onto GSLs with developing glycan chains is the next step in the production of GSLs. At the rate of bulk vesicle flow, glycosylation is related to exocytosis through the Golgi apparatus to the plasma membrane. Only a small number of enzymes function in a combinatorial biosynthetic pathway to produce the complex ganglioside and GSL glycoforms seen on eukaryotic cell surfaces.

In the labs of Rose man and Base, the first glycosyltransferases involved in the production of gangliosides were characterized. Ganglion-series gangliosides are divided into members of the 0-, a-, b-, and c-series depending on how many Salic acids are linked to the inner galactosyl residue. The Neu5Ac2, 8Neu5Ac sequence, which is uncommon in glycoproteins, is present in b-Series gangliosides. The same glycosyltransferases, which exhibit less selectivity than those working early in the route, can generate higher members of these various subseries.

The expression of the sialyltransferases and glycosyltransferases involved in the ganglioside biosynthesis pathway depends on the cell type and developmental stage. In the course of brain development, ganglioside pattern changes and following differentiation, differences in glycolipid composition have also been discovered across various types of neuronal cells. Additionally, ganglioside patterns differ between various cell types and alter as cells differentiate.

For instance, in mouse embryonic development, 1, 3-N-acetylglucosaminyltransferase expression is high and declines to undetectable levels in most cell types after birth. This enzyme is responsible for the synthesis of glycolipids of the lacto and neglect series. Expression is mostly seen in the spleen of adult animals and it is only found in Purkinje cells of the cerebellum.

The biosynthesis of GSLs, including gangliosides, occurs at internal membranes, from which they are exocytotically transferred to the plasma membrane. Human autosomal recessive infantile-onset symptomatic epilepsy syndrome, which is brought on by a nonsense mutation in the gene encoding GM3 synthase, is the only known disease caused by a defect in glycosyltransferase of ganglioside biosynthesis. This is true despite the fact that many human diseases are known to be caused by defects in GSL and sphingolipid degradation. It is important to note that during GSL formation, membrane-bound glycosyltransferases interact with their membrane-bound glycolipid substrates by diffusion within the two-dimensional plane of the lipid bilayer, which is a key distinction between ganglioside biosynthesis in the Golgi apparatus and degradation in the endolysosomal compartment.

As a result, reaction rates can start to follow two-dimensional enzyme kinetics and become independent of the reaction volume. As a result, kinetic constants can be normalized, for instance, in terms of the quantity of membrane protein, on lipid surface area rather than reaction volume. Because of this, transmembrane domain-deficient glycosyltransferases are significantly less active towards substrates that are coupled to membranes. The glycosidase, which are soluble enzymes, and the substrates, which are membrane-bound, are degraded in endosomes and lysosomes. This helps to explain why, in contrast to biosynthesis, the degradation of GSLs with short glycan chains requires endosome and lysosome lipid-transfer proteins. There is evidence of ganglioside creation by plasma membrane-associated glycosyltransferases in addition to ganglioside biosynthesis in the Golgi apparatus.

Series Gala:

The hexose residues are present in-numeric structure in the monoglycosylceramides glucosylceramide and galactosylceramide, which are also known as cerebrosides. Only lower creatures have Glaciers with the configuration, and mammals are highly immunogenic to them. Only ganglioside GM4 is produced from Glacier; the majority of gangliosides are biosynthesized from Ulcer. It has been found that ganglioside GM4 is a small part of human brain gangliosides and that it is localized within myelin. It can also be found in abundance in some fish species and is found, among other places, on erythrocytes, kidneys, and the gut. Glacier and sulfa tide are the members of the gala series that are most frequently discovered in oligodendrocytes, Schwann cells, kidney, testis, and gut. They appear to interact with the carbohydrate head groups of sulfa tide and Glacier on various myelin layers where they are present in large numbers in the multilamellar layers of the myelin where they are necessary for glial adhesion. Fatty acid hydroxylase-2 produces 2-hydroxy-fatty acids, which make up the largest portion of myelin lipids. Their existence in gala-series GSLs promotes interactions between the GSLs' carbohydrates.

Ulcer synthase, in contrast to Glacier synthase, seems to be unnecessary for oligodendrocytes. While creamed galactosylation catalyzed by UDP-glucose: creamed galactosyltransferase occurs at the ER membrane, the later steps of gala-series GSL biosynthesis, formation of sulfa tide digalactosylceramide and ganglioside GM4 take place in the lumen of the Golgi apparatus. Ceram ide galactosyltransferase is a type I transmembrane protein with the catalytic domain on the luminal side of the ER, in contrast to the majority glycosyltransferases in ganglioside production, which are type II transmembrane proteins. According to research done on mice and zebra fish, ST3Gal V, which also produces GM3 and GM4, can create GM4. As a result, Glacier and Lacer, the predecessors of GM4 and GM3, appear to be necessary for their development. Little is understood about how GM4 works. It exhibits immunosuppressive effects, interacts with the myelin basic protein, and protects guinea pigs from experimental allergic encephalomyelitis.

Glucosylceramide-Derived Gangliosides:

The transfer of a glucose residue from UDP glucose to creamed, which is catalyzed by UDP-glucose: creamed glucosyltransferase, is the first step in the production of the majority of gangliosides. Despite the fact that Ulcer and Glacier synthases catalyze comparable processes, their cans have different sequences. A type III transmembrane protein is known as creamed glucosyltransferase. It assembles in the cytosol as monovalent dimers or oligomers with its C-terminal catalytic domains. Glucosylceramide must cross a membrane since Ulcer and Lacer are formed on different faces of the cytoplasmic membrane and the luminal site of the Golgi membrane, respectively. Short chain Ulcer analogues are transported through the Golgi membrane via the ABC-transporters ABC-B1 and ABC-C1, which are mediated by an unidentified lipase. After the cytoplasmic lipid-transfer protein FAPP2 transports Ulcer to the ER where it may be translocated by an unidentified lipase or at the trans-Golgi transversal translocation can be carried out. The -glycosidase Gba2 can destroy a portion of the Ulcer pool when it reaches the cytosolic leaflet of the plasma membrane. The glycolipid transfer protein, GLTP, and FAPP2, which are both cytosolic Ulcer-transporters, are candidates.

Higher gangliosides undergo extra cytoplasmic glycan chain orientation during production on the luminal face of the Golgi apparatus Galactosyltransferase I converts glucosylceramide to lacer by transferring a GA lactose residue from UDP GA lactose. Step-by-step, more carbohydrate residues are added to the expanding glycan chains. The hematosides GM3, GD3, and GT3, which are salivated derivatives of Lacer, act as precursors for complex gangliosides of the 0-, a-, b-, and c-series. The presence of zero, one, two, or three Salic acid residues linked

to the position 3 of the inner galactosyl residues distinguishes these various series. Gangliosides from the 0- and c-series are only present in trace levels in mature mammalian brains, and GM1b and GD1 are only momentarily produced during chick brain biogenesis. Genetically modified mice lacking ST3Gal V have 0-series gangliosides in concentrations that are comparable to the overall ganglioside content of healthy animals. These mice are unable to produce GM3 and higher a-c series gangliosides. They exhibit altered glucose homeostasis and an accelerated insulin receptor signaling pathway, which is a crucial discovery that supports the hypothesis that GM3 or a higher ganglioside produced from it inhibits the insulin receptor in vivo [11], [12].

CONCLUSION

For instances, see. Ganglioside complete synthesis is a labor-intensive and time-consuming procedure that is often only carried out in specialized laboratories. It primarily depends on the successive glycosylation of a 3-O-protected azidosphingosine with appropriate protection and activation of the glycol donors. Trichloroacetimidates and techniques for -selective spallation processes are examples of this. Additionally, chemo enzymatic processes have been developed, wherein oligosaccharyl fluorides are coupled to native or fluorescent creamed anchors using an engineered endoglycoceramidase or wherein various glycosylation steps are catalyzed by glycosyltransferases or glycosidase. Genetically modified bacterial strains can manufacture ganglioside oligosaccharides like GM3, GM2, GM1, GD3, and GT3. Lactose can be internalized in E. coli as a precursor to be utilized as an acceptor for glycosyltransferases in the biotechnological manufacture of ganglioside head groups. The preparative manufacture of neoglycolipids with ganglioside head groups using a lung squamous-cell carcinoma line and 12-azidododecyl -lacto side as an appropriate primer is one use of the ganglioside biosynthetic machinery.

REFERENCES:

[1] T. Kolter, “Ganglioside Biochemistry,” *ISRN Biochem.*, 2012, doi: 10.5402/2012/506160.

[2] Y. H. Xu, S. Barnes, Y. Sun, and G. A. Grabowski, “Multi-system disorders of glycosphingolipid and ganglioside metabolism,” *Journal of Lipid Research*. 2010. doi: 10.1194/jlr.R003996.

[3] R. B. Chan *et al.*, “Comparative lipidomic analysis of mouse and human brain with Alzheimer disease,” *J. Biol. Chem.*, 2012, doi: 10.1074/jbc.M111.274142.

[4] A. R. Kroken, A. P. A. Karalewitz, Z. Fu, J. J. P. Kim, and J. T. Barbieri, “Novel ganglioside-mediated entry of botulinum neurotoxin serotype D into neurons,” *J. Biol. Chem.*, 2011, doi: 10.1074/jbc.M111.254086.

[5] H. Attrill, A. Imamura, R. S. Sharma, M. Kiso, P. R. Crocker, and D. M. F. Van Aalten, “Siglec-7 undergoes a major conformational change when complexed with the α(2,8)-disialylganglioside GT1b,” *J. Biol. Chem.*, 2006, doi: 10.1074/jbc.M601714200.

[6] D. E. Saslowsky *et al.*, “Ganglioside GM1-mediated Transcytosis of cholera toxin bypasses the retrograde pathway and depends on the structure of the ceramide domain,” *J. Biol. Chem.*, 2013, doi: 10.1074/jbc.M113.474957.

[7] P. M. Crespo, V. T. Demichelis, and J. L. Daniotti, “Neobiosynthesis of glycosphingolipids by plasma membrane-associated glycosyltransferases,” *J. Biol. Chem.*, 2010, doi: 10.1074/jbc.M110.123422.

[8] L. Anastasia *et al.*, "NEU3 sialidase strictly modulates GM3 levels in skeletal myoblasts C2C12 thus favoring their differentiation and protecting them from apoptosis," *J. Biol. Chem.*, 2008, doi: 10.1074/jbc.M805755200.

[9] E. Kiyokawa, T. Baba, N. Otsuka, A. Makino, S. Ohno, and T. Kobayashi, "Spatial and functional heterogeneity of sphingolipid-rich membrane domains," *J. Biol. Chem.*, 2005, doi: 10.1074/jbc.M502244200.

[10] M. Valsecchi *et al.*, "Sphingolipidomics of A2780 human ovarian carcinoma cells treated with synthetic retinoids," *J. Lipid Res.*, 2010, doi: 10.1194/jlr.M004010.

[11] G. Moussavou *et al.*, "Role of gangliosides in the differentiation of human mesenchymal-derived stem cells into osteoblasts and neuronal cells," *BMB Reports.* 2013. doi: 10.5483/BMBRep.2013.46.11.179.

[12] S. Bergante *et al.*, "Gangliosides as a potential new class of stem cell markers: The case of GD1a in human bone marrow mesenchymal stem cells," *J. Lipid Res.*, 2014, doi: 10.1194/jlr.M046672.

CHAPTER 6

EXPERIMENTAL STUDY ON NANSHA SOFT SOIL CREEP CHARACTERISTICS

Dr. Shivani, Assistant Professor, Department of Agriculture and Environmental Sciences
Shobhit University, Gangoh, Uttar Pradesh, India
Email Id- shivani@shobhituniversity.ac.in

ABSTRACT:

To better understand the creep properties of the soil in the Pearl River Delta's interaction marine and terrestrial deposits, a number of tests were run. The results of the secondary consolidation test demonstrate that the consolidation state determines the conditionality of the influence of consolidation pressure on the secondary consolidation coefficient. The value of the ratio between the coefficients of secondary consolidation and compressibility is 0.03, which is virtually constant. Shear stress, rather than the buildup of shear strain, controls the direct sheer creep failure of soil in the shear-box test. Consolidation can lessen the effects of creep, which are directly related to the drainage conditions in the triaxial creep features. Triaxial creep damage will cause a rapid increase in the strain rate in soft soil.

KEYWORDS:

Creep Properties, Consolidation, Infrastructure Building, Pearl River.

INTRODUCTION

Infrastructure building is prospering due to China's economy's rapid growth, bringing long-term settlement, long-term strength, and other difficulties into people's sights. Since soft soil is extensively dispersed throughout China and its deformation and strength depend on time, the impact of creep cannot be ignored. Investigators have conducted some theoretical and experimental studies to analyses the quantitative and qualitative aspects of creep characteristics. Taylor and Merchant examined the secondary consolidation phenomena of soft soil and hypothesized that the frictional resistance of soil particles was the primary cause of secondary consolidation settlement of soil. A good linear association was discovered between the secondary consolidation coefficient and compression index when Mersin and Godlewskicompiled the results of secondary consolidation of regularly consolidated soil obtained by predecessors. The secondary consolidation coefficient was a topic of discussion by Newland and Alley who believed that the reconsolidation pressure was more important than the consolidation pressure. Nash et al. disagreed with that point of view and reported that increased initially before decreasing as consolidation pressure mounted.

Leroueil et al. addressed a few arguments that centered on the connection between consolidation pressure and. Bulk creep is all that occurs during secondary consolidation, while triaxial creep occurs when shear creep and volume creep of the soil are coupled. Bishop and Love bury conducted experiments to examine the creep properties of undisturbed clays, and subsequent studies expanded on their findings. The characteristics of general soft soil, such as increased water content, a greater void ratio, more compressibility, lower shear strength, and higher sensitivity, are all present in interacting marine and terrestrial deposits of soft soil. However, there are some fundamental physical and mechanical characteristics that set marine soft soil apart from terrestrial soft soil due to its unique sedimentary environment and high silt concentration. In the experiments presented in this research, the creep characteristics of soft soil in interaction marine and terrestrial deposits acquired from Nansha in Guangzhou were

studied. Water contents ranged from 46% to 73%, and the void ratio was between 1.7 and 2.16. These values were highly variable and lower than those of marine soft soil. The soil samples' average liquid limit was roughly 47.8%, while their average plastic limit was about 24% [1], [2].

Secondary Consolidation Test:

After the first consolidation is finished, soft soil will continue to creep deform over time, and the effect of secondary consolidation cannot be disregarded. In this study, soft soil samples from various depths were examined, and the secondary consolidation qualities of the samples were examined using a consolidation test. The soft soil samples' water content and density were approximately and 56 percent, respectively. The undisturbed soil sample in the shear-box testing was the same size as the consolidation test sample, with a water content of 48% and a density of 1.74 g/cm3 respectively. To investigate the shear creep characteristics of soft soil in an interactive marine and terrestrial deposit, shear-box tests were carried out using a direct shear apparatus controlled by the shearing force, which was modified by a routine strain-controlled direct shear apparatus. A schematic diagram is plotted in Figure 1. The following criteria were used to determine each shear stress level that was used in the experiments: In order to define each level of shear stresses in shear creep tests, the peak strength of soil samples under various consolidation pressures is first determined by conducting consolidated-drained direct shear tests, where the loading times and the value is 46. According to the requirement that the shear deformation is less than 0.01 mm/day, the length of each stage of shear stress was determined. The peak strengths of consolidated-drained direct shear tests under various consolidation pressures are listed.

Triaxial Creep Test:

The triaxial creep mechanism differs from the secondary consolidation and shear creep mechanisms, which couple shear creep and volume creep of soil. Both the drained creep test and the untrained creep test were carried out by stress-controlled triaxial apparatus in order to conduct further research on the creep properties of soft soil in interactive marine and terrestrial deposits. The indoor temperature was kept at 24°C to eliminate the influence of temperature on the test. The specimen used in the triaxial creep test had a diameter of 39.1 mm, a height of 8 mm, a water content of 54%, and a density of 1.68 g/cm3. In those tests, soil samples were first compacted for two days under a 200-kappa confining pressure before successively applying each degree of deviatory stresses over the course of three days under various drainage circumstances. Routine triaxial equipment was used to get the peak strength of the triaxial test at a specific all-around pressure which was 210 kappa for the drained triaxial test and 100 kPa for the untrained triaxial test [3], [4].

DISCUSSION

It is not easy to distinguish between primary and secondary consolidation, and when kPa, the - curves are parallel to one another under each stage of loading, meaning that the coefficient of secondary consolidation does not change with the consolidation load and remains constant. However, the secondary consolidation coefficient varies when the consolidation load is low. These conclusions can see that when the consolidation pressure increases, the coefficient of secondary consolidation of soft soil sample No. 1 smoothly comes to an end. When the consolidation is small, the partition of primary-secondary consolidation is straightforward when the load ratio is the same, the curves are no longer parallel to each other under the condition of kPa, implying that the coefficient of secondary consolidation is not a constant and relates to t; and when the consolidation is large, the partition of primary-secondary consolidation becomes unclear. It demonstrates that as consolidation pressure increases, the coefficient of secondary consolidation first starts to rise before beginning to fall. When the kPa

is present, the coefficient of secondary consolidation, on the other hand, approaches a constant and stops fluctuating. In conclusion, the soil's ability to consolidate determines the relationship between the coefficient of secondary consolidation and consolidation pressure. The soft soil is over consolidated and the coefficient of secondary consolidation rises with the increase in consolidation pressure when the consolidation pressure is less than the reconsolidation pressure. The coefficient of secondary consolidation will decrease with an increase in consolidation pressure and eventually approach a constant value when the soft soil enters a normally consolidated state. The maximum value is reached as the consolidation pressure approaches the reconsolidation pressure. Similar phenomena are demonstrated in the results of one-dimensional consolidation tests of soft soil conducted by Nash et al. and Yu et al. And Yin et al. believe that the coefficient of secondary consolidation is related to the consolidation pressure when the consolidation pressure is less than the reconsolidation pressure. Shi et al.'s and Bertram's test results also suggested that the coefficient of secondary consolidation did not alter with the consolidation pressure. In this case, the soft soil is in the normally consolidated state and the coefficient of secondary consolidation does not depend on the consolidation pressure. This is because the sampling depth of soft soil is relatively shallow and the consolidation pressure provided by tests is greater than reconsolidation pressure.

The same load, the instantaneous deformation and shear strain rate rise as the shear stress increases. When the shear stress is low, like in the case of, the amount of immediate deformation dominates the total amount of deformation, and the value of the shear strain barely varies as the passage of time progresses. In other words, with low shear force, there is essentially little shear creep deformation. Shear strain and time have a more prominent nonlinear relationship as the shear stress increases because the shear creep deformation is more visible and includes a larger portion of displacement. The soil sample will be damaged in a very short amount of time as long as the shear stress climbs to a peak strength, and failure time gets shorter as consolidation pressure increases. It suggests that shear stress, rather than the buildup of shear strain, is what primarily controls the indirect sheer creep failure of soil. Additionally, we can conclude that = 0.60.7 based on the outcomes of shear creep experiments conducted under various consolidation pressures; this means that the consolidation effect can raise the peak strength of straight shear creep. Although the soil sample won't directly experience shear creep damage once the shear force reaches the strength of the consolidated-drained direct shear test, it will be destroyed once it does. We may observe that is larger than under the same consolidation pressure and that it gets bigger as the consolidation pressure rises.

Curves of the average shear strain rate vs time at various pressures. It is discovered that, under a specific consolidation pressure, the shear strain rate increases as the shear stress increases, and that, before the shear stress reaches the peak intensity of direct shear creep, the shear strain rate reduces over time at each level of shear stress [5], [6]. The shear strain rate initially decreases quickly at the beginning of loading and then swiftly approaches zero with the passage of time; yet, in this instance, the soil samples won't be harmed due to the high initial shear strain rate. When the shear stress reaches, the shear strain rate will quickly rise after loading and eventually cause the soil sample to fail. The failure time falls and the strain rate's falling stage shortens with a rise in consolidation pressure. It was determined that while the initial high shear strain rate did not result in soil degradation from shear creep, the final destruction of the soil would result from an increase in the shear strain rate.

Triaxial Creep:

The triaxial creep test results, where the axial strain is and is the axial strain rate. The Chen method is utilized to obtain the axial strain-time curves of loading, and show the curves of axial strain against time under various deviatory stresses, respectively. According to the results, the soil samples' axial strains and creep characteristics vary depending on the drainage

circumstances, and under the same deviatory stress, the axial strain of an untrained creep test is smaller than that of a drained creep test. Although the soil sample deforms significantly during the drained creep test, there is no failure; however, during the untrained creep test, the displacement of the soil sample rapidly rises once the deviatory stress reaches 115 kPa. In an untrained creep test, only the creep is responsible for the deformation; whereas, in a drained creep test, both the consolidation and the creep are responsible for the deformation. The soil sample won't be harmed by accelerated creep, which is always in a state of steady creep with a growing deviatory stress, within the range of a certain stress in both the drained creep and the untrained creep test. In the untrained creep test, the creep effect is very slight at lower stress levels, but it becomes increasingly noticeable as deviatory stress increases. Once deviatory stress reaches a value of 115 kPa, the soil sample will be damaged after a period of steady creep due to accelerated creep. The outcome is not unexpected because the soil sample is consolidated in the drained creep test, where shear strain and volumetric strain are present, whereas in the untrained creep test, where there is just shear strain. Due to the lack of lateral constraint and a known failure surface, triaxial untrained creep tests exhibit constant creep before rapid creep in contrast to shear creep, and the failure time is also significantly longer.

Illustrate the connections between strain rate and time under various deviatory stresses. The initial strain rate is found to be at its highest when the deviatory stress is reduced, notwithstanding the drainage condition, yet the soil sample will not be ruined. In comparison to the untrained test, the strain rate in the drained test is significantly higher. This is so because consolidation deformation, which is larger than creep deformation, is included in the deformation of drained creep along with creep deformation. we can deduce that when the soil sample is in the condition of untrained and in the drained test, which is at a state of certain deviatory stress (kPa), the decreases as the time increases; in particular, the decreases abruptly at the beginning of loading, and then the drop will slow down along with the development of time and approach zero. According the deviatory begins to decrease over time once it reaches a value of 115 kPa in the case of untrained creep. However, when 580 min, the deviatory starts to increase sharply and results in the final creep damage of the soil sample. The entire process can be broken down into three stages.

As a result, even though the triaxial creep test involves shear stress, the consolidation condition has a greater impact. The soil sample is very readily destroyed by shear creep in the untrained test when the soil sample is in the condition of drainage, when the creep effect may be disregarded. However, because the drainage condition of actual engineering always falls between the results of the drainage creep test and the results of the untrained creep test, it is required to take the effects of consolidation into account, which also makes the research more difficult. Infrastructure building is prospering due to China's economy's rapid growth, bringing long-term settlement, long-term strength, and other difficulties into people's sights. Since soft soil is extensively dispersed throughout China and its deformation and strength depend on time, the impact of creep cannot be ignored. Investigators have conducted some theoretical and experimental studies to analyses the quantitative and qualitative aspects of creep characteristics.

Taylor and Merchant examined the secondary consolidation phenomena of soft soil and hypothesized that the frictional resistance of soil particles was the primary cause of secondary consolidation settlement of soil. The secondary consolidation coefficient C a and the compression index C have a good linear connection, according to Mersin and Godlewski who summarized the results of secondary consolidation of soil that had previously been regularly consolidated. In their discussion of the impact of consolidation pressure on the secondary consolidation coefficient C a, Newland and Alley argued that C a depends only on its reconsolidation pressure and not at all on consolidation pressure. Nash et al. disagreed with

that idea, reporting that can increased initially before decreasing as consolidation pressure grew. Leroueil et al. addressed a few arguments that centered on the connection between consolidation pressure and C a. Bulk creep is all that occurs during secondary consolidation, while triaxial creep occurs when shear creep and volume creep of the soil are coupled. Bishop and Love bury conducted experiments to examine the creep properties of undisturbed clays, and subsequent studies expanded on their findings [7], [8].

The characteristics of general soft soil, such as increased water content, a greater void ratio, more compressibility, lower shear strength, and higher sensitivity, are all present in interacting marine and terrestrial deposits of soft soil. However, there are some fundamental physical and mechanical characteristics that set marine soft soil apart from terrestrial soft soil due to its unique sedimentary environment and high silt concentration. In the experiments presented in this research, the creep characteristics of soft soil in interaction marine and terrestrial deposits acquired from Nansha in Guangzhou were studied. Water contents w ranged from 46% to 73%, and the void ratio e 0 was much more variable and lower than in marine soft soil. The average plastic limit W P and liquid limit W L of the soil samples, respectively, were about 24% and 47.8%, respectively.

The primary-secondary consolidation divide is not clear and the e-let curves are parallel to one another at each stage of loading when p 50 kPa, indicating that the coefficient of secondary consolidation is independent of the consolidation load and remains constant. However, the secondary consolidation coefficient varies when the consolidation load is low. Additionally, Figure 4 demonstrates that as consolidation pressure increases, the coefficient of secondary consolidation first starts to rise before beginning to fall. The coefficient of secondary consolidation, however, approaches a constant and stops fluctuating when the p is more than 200 kPa. In conclusion, the soil's ability to consolidate determines the relationship between the coefficient of secondary consolidation and consolidation pressure. The soft soil is over consolidated and the coefficient of secondary consolidation rises with the increase in consolidation pressure when the consolidation pressure is less than the reconsolidation pressure.

The coefficient of secondary consolidation will decrease with an increase in consolidation pressure and eventually approach a constant value when the soft soil enters a normally consolidated state. The maximum value is reached as the consolidation pressure approaches the reconsolidation pressure. Similar phenomena are demonstrated in the results of one-dimensional consolidation tests of soft soil conducted by Nash et al. and Yu et al. and Yin et al. believe that the coefficient of secondary consolidation is related to the consolidation pressure when the consolidation pressure is less than the reconsolidation pressure. Shi et al.'s and Bertram’s test results also suggested that the coefficient of secondary consolidation did not alter with the consolidation pressure. In this case, the soft soil is in the normally consolidated state and the coefficient of secondary consolidation does not depend on the consolidation pressure. This is because the sampling depth of soft soil is relatively shallow and the consolidation pressure provided by tests is greater than reconsolidation pressure [9], [10].

CONCLUSION

This work employs a series of experiments to investigate the creep characteristics of soft soil in Pearl River Delta's interaction marine and terrestrial deposit. And from this, the ensuing conclusions are possible. The soil's state of consolidation affects the relationship between the coefficient of secondary consolidation and the consolidation pressure. The coefficient of secondary consolidation may only be roughly regarded as a constant when the soil is in the typical consolidation state. For the soil samples examined in this research, where the value of is 0.03, Mari’s formula is suitable. Under consolidation, shear stress rather than the buildup of

shear strain primarily controls the indirect sheer creep failure of soil, and when the shear stress is low, there is essentially no shear creep deformation. Under the same consolidation pressure, the peak strength of shear creep is 0.6–0.7 times more than the peak strength of slow shear test. In the triaxial creep tests, the axial strain of the untrained creep test is lower than that of the drained creep test because the drainage conditions affect the axial strains and creep properties of soil samples differently. The triaxial creep test is more impacted by the consolidation stage even though it relates to shear stress. The soil sample is very readily destroyed by shear creep in the untrained test when the soil sample is in the condition of drainage, when the creep effect may be disregarded. To prevent the foundation failure brought on by a fast-loading rate in the filled project, we should limit the loading rate. In some applications of practical soft soil engineering, soil creep causes the extra pore water pressure to increase and the effective pressure to fall even while the load remains constant. Therefore, while building a structure on soft soil, the earth should be treated first to increase the soil's drainage capabilities and prevent shear creep failure.

REFERENCES:

[1] Q. Luo and X. Chen, "Experimental research on creep characteristics of nansha soft soil," *Sci. World J.*, 2014, doi: 10.1155/2014/968738.

[2] D. H. Kang, T. S. Yun, Y. M. Lau, and Y. H. Wang, "DEM simulation on soil creep and associated evolution of pore characteristics," *Comput. Geotech.*, 2012, doi: 10.1016/j.compgeo.2011.09.003.

[3] M. Sun, H. Tang, M. Wang, Z. Shan, and X. Hu, "Creep behavior of slip zone soil of the Majiagou landslide in the Three Gorges area," *Environ. Earth Sci.*, 2016, doi: 10.1007/s12665-016-6002-x.

[4] Q. J. Zhou and X. P. Chen, "Experimental study on creep characteristics of soft soils," *Yantu Gongcheng Xuebao/Chinese J. Geotech. Eng.*, 2006.

[5] M. Sonoda and Y. Kurashige, "Characteristics of surface soil creep on a forest slope in Japan," *Geomorphology*, 2017, doi: 10.1016/j.geomorph.2017.03.006.

[6] L. Zou, S. Wang, and X. Lai, "Creep model for unsaturated soils in sliding zone of Qianjiangping landslide," *J. Rock Mech. Geotech. Eng.*, 2013, doi: 10.1016/j.jrmge.2013.03.001.

[7] Y. F. Wang, Z. Y. Cai, Z. G. Zhou, and Y. F. Guan, "Creep characteristics of an oozy soil under drained k0 consolidation," *Yantu Lixue/Rock Soil Mech.*, 2015, doi: 10.16285/j.rsm.2015.08.016.

[8] B. Ferdowsi, C. P. Ortiz, and D. J. Jerolmack, "Glassy dynamics of landscape evolution," *Proc. Natl. Acad. Sci. U. S. A.*, 2018, doi: 10.1073/pnas.1715250115.

[9] L. Barden, "Primary and secondary consolidation ofclayandpeat," *Geotechnique*, 1968.

[10] L. Barden, "Primary and secondary consolidation of clay and peat," *Geotechnique*, 1968, doi: 10.1680/geot.1968.18.1.1.

CHAPTER 7

EXPANDING THE SOIL CRACKS: PROGRESS IN A CHANGING ENVIRONMENT

Dr. Shivani, Assistant Professor, Department of Agriculture and Environmental Sciences
Shobhit University, Gangoh, Uttar Pradesh, India
Email Id- shivani@shobhituniversity.ac.in

ABSTRACT:

With the deep reshaping of the natural world, engineering issues that were previously avoided progressively come to the surface, with expanding soil crack under the changing environment becoming a controlling factor of expansive soil slope stability. The issue of expansive soil fracture has gradually grown in importance as research, explaining how cracks form from expansive soil's fundamental characteristics and highlighting the importance of crack control. We provide an overview of the expansive soil crack features research methodologies and findings currently available. The future focus will be on developing crack measurement and calculating methods and investigating the correlation between surface feature and crack depth through statistical analysis.

KEYWORDS:

Deep Reshaping, Montmorillonite, Slope Stability, Soil Cracks.

INTRODUCTION

Most of the clay minerals in expansive soils, including montmorillonite, are hydrophilic and have substantial swelling and shrinking properties. Expansive soil differs from regular clay in three ways: it is expansive, cracks, and over-consolidates. Over consolidation and expansion are centered in crack. Expansive soil will shrink as water content decreases, causing a crack; when the environment changes and has a drying and wetting influence, the crack will deepen. The spread of cracks will also be aided by the discharge of expansive soil over consolidated tension. The crack creates seepage, which leads to soil swelling and crack aggravation while destroying the integrity of expanding soil. Therefore, the main determinant of the stability of an expansive soil slope is fracture. Expansive soil is unsaturated soil with unique technical qualities. It has been studied for almost a century in terms of its fundamental mechanical and physical characteristics, engineering applications, and administration techniques. Unsaturated expanding soil basic theory has steadily matured; project success relied on a number of outstanding models. However, the study of the crack, which is important for expansive soil intensity, deformation, and seepage, has been slow. As a result, it is important to summarize the research output, highlight the study blind spot and difficulty, and highlight the research work that has to be done in the future.

Fundamental Qualities of Expansive Soils:

Expansive soil is a unique type of soil with over consolidation, swelling, and shrinkage features as well as cracking. Swelling and shrinkage characteristics are the main cause of the expansive soil engineering disease. Many researchers have studied expansive soil, proved the swelling and shrunk deformation to be irreversible through numerous experiments that looked at the swelling and shrinking mechanism, the influence rule of expansive soil from the drying and wetting cycles, and swelling shrinkage anisotropic [1], [2]. Putting that forward, they then explained the swelling shrinkage essence of the expansive soil using the seepage press theory in physics, chemistry, and suction potential. The expanding potential was diminished by

swelling shrinkage, according to Gong et al. People agree that the effects on swelling and shrinkage induced by initial dry density, water content, and pressure are regular [6]. Due to past upper soil erosion, deposited expansive soil has a small natural void ratio, a high degree of density, and attributes that contribute to its initial structural strength. Expansive soil cracks form as a result of the unloading effect; exterior characteristics of the naturally occurring expansive soil over consolidation include strong initial strength and low seepage character. The relationship between crack, expansion, and over consolidation is closed; a fracture obliterates the soil's integrity, causes seepage to exacerbate the expanding soil welling shrinkage, and expands the crack further.

Study on the Need for Extensive Soil Cracks:

For naturally expansive soil, damage during the soil-generation process results in soil natural cracks; changing environmental conditions give rise to dry-wet cycles, and the dry-wet cycle occurs on the soil to a certain depth; the soil also experiences frequent swelling and shrinkage, and naturally occurring cracks appear or gradually expand. As the water continues to evaporate, the soil continues to contract, increasing the measurement of secondary crack formation. The primary cause is expansive soil's high shrinkage and low seepage characteristics; the unit of soil surface layer shrinks first when soil evaporates, vertical soil shrinkage is unrestricted and occurs freely, while horizontal soil shrinkage is constrained by interacting soil inside. When the water content of the below-ground soil does not significantly change as a result of the evaporation of the above soil, the shrinkage of the upper and below-ground soil is uneven, and a soil crack develops. The crack of expansive soil is frequently caused by the uneven shrinking.

Crack Growth Progress:

When a vertical fracture forms due to an alteration in the external environment, the transformation will become apparent.

(1) A vertical crack surface forms; the area that comes into contact with the outside air is amplified; the horizontal shrinkage is plainly aggravated and the vertical shrinkage continues; the crack then expands downward until a certain equilibrium is reached. The fracture development mechanism.

(2) Although soil shrinkage occurs gradually both close to and distant from the surface of the vertical crack, inhomogeneous shrinking at the vertical crack will result in the formation of additional horizontal cracks.

(3) Widespread soil exposes the atmosphere to weather-related changes. When precipitation seeps into expansive soil, it will be loose, absorb water, and eventually saturate.

Long-term evaporation causes the surface water and free water in the soil's top layer to evaporate into the atmosphere, changing the soil's saturation level from saturated to unsaturated. Natural expanding soil seeps below, and if evaporation continues, the layer soil will shrink and split; yet, the deep soil is unaffected. Rain penetrates the soil along the fissure; if more rain falls after the fracture is created, the crack facilitates the swelling of the deeper, more expansive soil and serves as a conduit for water evaporation. Additionally, the water in soaking expanding soil rises repeatedly beneath the capillarity of the crack; the crack gradually gets deeper until it finds equilibrium. In other words, a change in weather from fine to rainy encourages the fracture to form and spread [3], [4].

DISCUSSION

Terzaghi initially focused on the impact of crack expansion on soil strength and noted that the crack is a structural characteristic of over consolidation. Kempton discovered that a fissure

would generate a concentration of stress and that the soil would be damaged once the tension reached its maximum shear strength. Researchers Yao et al. Boa and Yin et al. investigated the impact of cracks on strength, deformation, and seepage; they hypothesized that expansive soil has some strength and that cracks control not only size effects but also alteration and reduction characteristics. Numerous studies showed that existing cracks compromised the stability of the soil, reduced its strength, and reduced its capacity to slide; yet, the cracks serve as an advantageous passageway for water seepage and evaporation. When it rains, the water rushes into the cracks and allows penetration. If the water seeps into an unfavorable slope, the pressure will be increased. These two factors lessen the risk and have a significant impact on the slope's stability. Expanding soil causes cracks to form and grow; releasing the strength of expansive soil during excavation will result in the development of cracks; and changing the water content will result in the deformation and cracking of expansive soil. All of these can explain how the characteristic of a crack is a reflection of swelling and excessive consolidation, and how a crack is essential to the stability of an expansive soil slope and regulates the strength of expansive soil.

Crack Observation Measurement:

There is a fissure in the interior of the soil, which can open or close when the outside environment changes. The process of change is complicated, making it challenging to see directly or indirectly. Currently, it is impossible to accurately describe and analyses how a crack develops; however, using crack studies, statistical analysis, morphological description, and evolution of the crack have been successfully accomplished. With the aid of CT, Lu et al. investigated the expanding soil evolution that occurs often throughout cycles of drying and wetting. Based on the number of CT and the rule of volume change accumulative total, they proposed a crack damage variable. According to Yi et al. Who used fractal theory to study the fractal characteristic of expansive soil, the strength of expansive soil is correlated with the fractal number. Yuan et al. provided the simplified crack model; they used optical microscopy to analyses expansive soil and talked about whether it would be possible to quantify the fracture for grey entropy. Ma et al. used a humidity test instrument to study the cracks evolution and examined the test results. Through the use of a centrifugal model test, Chen et al. investigated the deformability and stability of expansive soil slopes, examined the mechanism of crack occurrence and development, and explored the impact of infiltration on the stability of expansive soil slopes. The mechanism of cohesive crack development was visually examined and measured by Tang and Kong. The resistivity approach was utilized by Gong et al. To examine the growth of an expanding soil crack [5], [6].

From everything mentioned previously, we can see the crack clearly by taking a picture. The operation is straightforward, but the human component is highly complicated. Human component is less important than it is for other resistivity methods, but soil properties like void ratio and water content have a significant impact. Although the device is more expensive and requires more frequent operation than the norm, measuring the dynamic crack quantitatively and without loss using CT and ultrasonic technology has a greater precision. Additionally, the success of the study is limited to laboratory testing; there is no effective obvious means of crack at spot. Particularly in the context of a changing environment, studies on the measurement of cracks, the expansion of cracks, and the evolution of strength decay are lacking.

The analysis of slope stability is where most people begin when conducting extensive soil engineering applied research. Any engineering examples of expansive soil slope instability demonstrated that instability is the result of cracking, regardless of whether surface cracks are visible or not be covered or crack too small. Therefore, the stability of an expanding soil slope will depend on the amount of soil cracking. In real-world engineering, the longitudinal fracture depth is inaccurate; the expansive soil crack depth can reach 4 meters. No matter what, the

depth of expansive soil slope eliminated must be obvious whether by replacing or adding cement-based materials to expansive soil, or by other techniques. Otherwise, there will be tremendous economic waste and strain, and the outcome of treatment cannot be guaranteed. Thus, in light of the unsaturated soil theory, several researchers investigate expansive soil cracks using fracture mechanics and linear elastic mechanics. Morris et al. established the relationship between the depth of the crack, the characteristics of the soil, and the specified suction distribution using various theories. According to field tests and elasticity theory, Lee et al. Konrad and Aydan and Zheng et al. Developed a theoretical model of cohesive soil cracking. According to Sun et al. The primary cause of cracking is suction as a result of shrinkage increasing tensile strength; they deduced the secondary crack spacing formula. Li et al.'s analysis of the effective cohesion and effective angle of internal friction led to the linear elastic theory relations. Many calculation models for crack depth have been developed and established, however they are all based on studies of expanding soil cracking mechanisms utilizing the mechanics principle. Under drying and wetting cycles, the expansive soil fracture actually widens and deepens before eventually becoming stable. The crack depth should serve as the basis for stability analysis of expanding soil slopes involved in crack depth, however no one seems to be interested in the crack depth theoretical prediction model under changing environmental conditions.

Creating a Crack Observation Method:

The strength, seepage, and deformation of expansive soil differ from integrated soil because of the fractures. When analyzing the strength, seepage, and deformation of expansive soil, we must take the germination and cracking process into account. But at the moment, we mainly introduce the crack into the computation model at random or based on assumptions. Therefore, the following will be the focus of the expansive soil study under test: observation and measurement of the crack with the process of germination study of the influence mechanization of strength, seepage and deformation of expansive soil, quantification of the crack, and so on. In light of the crack measure method, we can approach it from the following angles [6], [7].

(1) Resistivity method: measure the resistance as current passes through the soil; the test results can reveal something about the soil's structure indirectly. Resistivity is a useful tool for tracking the dynamic development of cracks up to a certain point. We can understand the influence rule regarding the water content and void ratio by repeatedly measuring the crack at various water contents and void ratios; by quantifying and tracking the crack dynamic development of lossless in the drying and wetting cycles test, we can determine the final depth of cracks.

(2) Ultrasonic technique: detect the ultrasound velocity in the soil using an ultrasonic pulse transmission technique; the various ultrasonic will reflect the soil's development state on the inside. If we define the damage variable, we may use the fracture depth measurement information to think about the outcome of macroscopic mechanics.

(3) The CT method: is comparable to ultrasonic in that both are able to assess the growth and germination of fractures in a dynamic, quantitative, and lossless manner, with adequate precision to test demand. Because the CT instrument is expensive and has a higher-than-normal operational demand, and because the growth of expansive soil cracks is constrained, we only examine the crack in a small number of cases. The main issue at hand right now is how to promote CT technology for testing and practicing engineering.

(4) Liquid flow method: create a high-velocity chemical reagent that can condense quickly from the standpoint of hydrodynamics, pour it into cracks after they have stabilized, and remove it when it has condensed. The condensed chemical will represent cracks in expansive soil at various locations, and the depth of the crack can be determined directly. The earth is not harmed when measuring cracks using this method, and we can repeat the process as necessary.

The crack depth is a dynamic process with drying and wetting cycles, therefore getting an exact reading of the crack's depth is challenging and the variance is significant. We can compute the crack depth from the obtained surface crack width by conducting a theoretical study to determine the calculation technique for fracture depth when water content, dry density, and cycle's index vary.

(6) Optical image analysis method: By using an image acquisition system that consists of a long-distance microscope, three axis displacement platforms, a CCD camera, and a video monitor, we can observe and gather images of the expansive soil crack development process. From these images, we can infer information about the crack's non-contact, continuous, and systemic microstructural changes. This technique has a wide range of applications and can be used in engineering practice; however, we must manage the image collection to prevent jamming as much as possible and make sure that the image can respond to the onset of cracks objectively [8], [9].

Cracks in Description and Statistics Techniques:

Geometric factors including the trend, dip angle, width, length, and step of the crack all have an impact on expansive soil engineering mechanics. Current crack morphology of expansive soil can only be reflected in the description and quantification of the crack; there are no pertinent reports about the quantitative description method of crack occurrence and development at this time. We should therefore focus on improving the quantitative description method of crack incidence and development in order to provide the groundwork for including crack variables into a broad soil constitutive model. There are several shortcomings in the research of the influence of expansive soil character since the fundamental idea behind the distinction between expansive soil and unsaturated soil is still in its infancy. In the future, crack quantification and its impact on strength, deformation, permeability, and stability of expansive soil, as well as analysis of quantitative research, will be crucial directions due to the constant development of unsaturated soil mechanics, test instruments, and observation methods. Additionally, it is vital to establish the occurrence of cracks and construct a mathematical and physical model through the necessary geotechnical and mechanical testing.

Results that are pertinent will advance the fundamental theory of unsaturated soil mechanics and advance the field. In order to model the soil fracture, Amara Siri et al. Employed the universal distinct element method. The software of UDEM was widely used in primary analysis, and it is fully comparable to the Fast Lagrangian Analysis of Continua with FLAC having the edge. The primary research approaches will involve UDEM analysis of soil shrinkage cracks. Furthermore, the Monte Carlo approach also known as the random simulation method has been utilized in numerous fields, including particle transport, statistical physics, reliability analysis, and military affairs, to handle a variety of problems when the subject of research involves random processes and outcomes. Since the occurrence of soil shrinkage cracks is a random process, we believe the Monte Carlo method is a good way to simulate the fracture.

Currently, the Monte Carlo approach is often used to simulate rock fracture but has not been reported to be utilized to simulate soil crack. In the future, we might consider applying the technology to research soil shrinkage fractures. Existing techniques for seeing and representing expansive soil cracks have limitations and are influenced by human factors. Studies on expansive soil cracks often focus on qualitative research; quantification studies on the crack's depth and width are rare. In addition, finite element software lacks the quantization model, which is necessary to take into account expansive soil crack strength, deformation, permeability, and stability analysis. As a result, the calculation result differs from reality observation in terms of the form, distribution, and growth of the crack in real engineering. The

expanded soil observation technique must be improved, crack quantitative indicators must be identified, and software development must be strengthened as soon as the research findings are widely applied in engineering practice [10], [11].

CONCLUSION

The key to slope stability is the nature of expansive soil cracks. Currently, a number of crack character accomplishments have been made, but the conclusions are not universally accepted. The seepage-related crack is closely spaced, and seepage has an effect on the expansive soil's strength and deformation. Therefore, develop the technique for obtaining crack character images and information processing, perform crack depth measurement and statistical analysis, investigate the relationship between depth and surface crack characteristics, and talk about the feedback mechanism of dynamic cracks description, swelling and shrinkage, and over consolidated characteristics; establish the contact about the process of crack with the expansive soil strength, deformation, penetration, and swelling shrink The focus of research on expanding soil will be on developing a constitutive model that takes cracks into account in terms of how they affect strength and deformation.

REFERENCES:

[1] J. M. Arocena and C. Opio, "Prescribed fire-induced changes in properties of sub-boreal forest soils," *Geoderma*, 2003, doi: 10.1016/S0016-7061(02)00312-9.

[2] Y. Xu, K. Wu, Z. Bai, and Z. Hu, "Theoretical analysis of the secondary development of mining-induced surface cracks in the Ordos region," *Environ. Earth Sci.*, 2017, doi: 10.1007/s12665-017-7050-6.

[3] W. Sang *et al.*, "Effect of hydrofracking fluid on colloid transport in the unsaturated zone," *Environ. Sci. Technol.*, 2014, doi: 10.1021/es501441e.

[4] L. Wu and R. Huang, "Landslide mechanism and strengthening analysis of cutting slopes in expansive soil areas in China," *Iaeg2006*, 2006.

[5] Q. X. Huang and W. Z. Zhang, "Research on downward crack closing of clay aquiclude in shallow coal seam safety mining," *J. Coal Sci. Eng.*, 2011, doi: 10.1007/s12404-011-0324-9.

[6] R. Huang, L. Wu, and R. Hu, "Mechanical analysis of cut slope failures in expansive soil areas," *Acta Geol. Sin.*, 2007.

[7] L. Z. Wu and R. Q. Huang, "Numerical simulation and optimum design of anchor frame beam strengthening expansive soil roadcut slope," *Yantu Lixue/Rock Soil Mech.*, 2006.

[8] S. L. Shen, Y. S. Xu, and L. A. Chang, "Analysis research on soil fracturing around deep mixing column," *Yantu Lixue/Rock Soil Mech.*, 2006.

[9] L. Z. Wu and R. Q. Huang, "Calculation of the internal forces and numerical simulation of the anchor frame beam strengthening expansive soil slope," *Geotech. Geol. Eng.*, 2008, doi: 10.1007/s10706-008-9184-5.

[10] F. Dang, H. Chen, W. Ding, and X. Yin, "Rock and soil damage-fracture space mechanics: The divisional damage-fracture theory," 2007. doi: 10.2991/iske.2007.263.

[11] A. J. Puppala, N. Banavathu, S. R. Qasim, R. Williammee, and N. Intharasombat, "Laboratory Investigations to Address the use of Compost Amendments to Enhance Expansive Subsoils," 2004. doi: 10.1061/40756(149)6.

CHAPTER 8

EXPLORING THE PACKAGING DESIGN: ARTIFICIAL INTELLIGENCE APPROACH

Rohit Saini, Assistant Professor, Department of Agriculture and Environmental Sciences
Shobhit University, Gangoh, Uttar Pradesh, India
Email Id- rohit.saini@shobhituniversity.ac.in

ABSTRACT:

The evolution of human life has changed dramatically over hundreds of years as a result of the development of chemistry. Chemical research has been utilized to produce a wide range of goods, including different medications and cosmetics of all kinds. Electronic component and computer software technology have advanced quickly in recent years, and the fourth round of technological revolution is now under way, which is beneficial for the growth of numerous businesses. Traditional paper-cutting and cosmetic bag design techniques should also consider the benefits of wireless communication and artificial intelligence technology, and they should work with other traditional industries to implement technological changes that will aid in the transmission of traditional craftsmanship. Due to aggressive cosmetics marketing, there are an increasing number of cosmetics on the market today, and traditional paper-cut art is an artistic design technique that is comparable to cosmetic design. After using wireless communication technology and artificial intelligence to update both businesses, both will see tremendous growth.

KEYWORDS:

Artificial Intelligence, Cosmetics, Chemistry, Computing Resources.

INTRODUCTION

One of the technologies with the most users in recent years is artificial intelligence. Alongside big data and cloud computing technology, it is present. It is among the top three high-tech innovations in terms of utility. Due to the fact that artificial intelligence relies on algorithms to work with databases and computing resources to make general judgments about things and understand potential operations and effects when artificial intelligence technology is combined with big data, cloud computing can call upon a significant amount of computing resources to process the things that need to be processed at any given time through the server group. The best server group is the supercomputer, which can assist the d Algorithms are frequently employed in conjunction with artificial intelligence. To the greatest extent possible, artificial intelligence can be completed by using various algorithms for each thing to be processed, which can also increase efficiency and accuracy. Algorithms and artificial intelligence are often ideal for diverse purposes, and different artificial intelligence algorithms also play distinct purposes. Some algorithms are good in target retrieval and are suited for querying all types of provided target ranges, while others are good at accurate analysis and are suitable for small items. Therefore, in order to get the algorithm that best suits our case and the use system, we typically need to alter it before the experiment [1], [2].

Modern cosmetics are defined as substances other than soaps applied to the human body with the intention of improving, preserving, or changing one's appearance for example, for performance or to clean, dye, rub, correct, or protect the skin, hair, nails, eyes, or teeth. The creation of cosmetics like rouge and blush, however, has been delayed in the past because the components are not readily apparent. Due to the advancement of chemistry, humans started looking into the chemical makeup of substances in modern times. Generations of cosmetics have been created and developed as a result of chemists' experiments. Therefore, less than 300

years have passed since the eighteenth century, which is the key development era for cosmetics. Furthermore, the majority of the cosmetics we use are made from foreign materials, which is another pain because of the waning national power of modern China and the stagnation of research and technology. The current domestic cosmetics also cannot be compared to the development of hundreds of years outside due to the issue of development time. It is only fair to say that we are still attempting to catch up and have the chance to reach the previous high point, if not beyond it. The ancestors' aspirations for a better life and their blessings for others and themselves are depicted in the traditional paper-cut art that has been practiced in China for thousands of years. To commemorate both New Year's Eve and the Spring Festival, paper-cutting is typically done around that time. Different paper cuts depict various human mindsets. Some people wish for a pleasant day and a good harvest in the upcoming year, while others wish for them to graduate from high school. Others wish for the happiness and prosperity of the entire family.

As a result, each person's blessing is unique, just as paper cuts vary in shape and significance. Then, a few days before New Year's Eve, paper cuts are used to write messages of hope and goodwill to one another on doors and windows. Fireworks then herald the arrival of New Year's Eve and the New Year, which represent the most basic aspirations of the time. People experience new toys today thanks to the emergence of numerous technological devices and new technologies, and they increasingly stop appreciating old art. The state has started to actively encourage and assist in reviving the traditional talents of our own country and nation; thus we should revive the craft of paper cutting. Despite the fact that the art of paper cutting is currently in decline because to its low cost of production, labor, and materials, it may still be spectacular in the future when combined with new technologies. As a result, we made the decision to integrate the art of kerygma with other cutting-edge technologies in order to promote and revive the traditional art sector. In the end, we decided to focus on cosmetics packaging as the last factor, designing the conventional paper-cut art and packaging for cosmetics to have the best possible design outcome using wireless connection and artificial intelligence technology [3], [4].

A Nuclear Adaptive Algorithm for Paper-Cut and Cosmetic Packaging Design Based on the Soft plus Function:

An amazing Chinese cultural tradition is the practice of paper cutting. Paper-cutting activities based on window decorations are carried out all throughout the country, especially as the Spring Festival draws near. This not only ensures that the paper-cutting craft is passed down through the generations but also enhances the joyful mood. Paper-cutting is primarily the practice of using scissors to cut paper into different shapes and patterns, such as the forms of flowers or Chinese characters. Paper-cutting is a cultural and creative medium that uses figurative and exaggerated techniques to convey the delights, sufferings, and joys of its audience. The look of the packaging has a big impact on how many products are sold. Consumers can form first impressions based on packaging design. According to certain studies, consumers' intention to make a purchase is significantly influenced by their initial impression. Cosmetics are a crucial good that are widely used worldwide and are a must for female consumers. Cosmetics have a sizable consumer base and must be repurchased because they are consumables, which can result in ongoing earnings for businesses. The competition in the cosmetics sector is growing as more businesses enter the sector. When there are similar results, the cosmetics package might entice customers to purchase.

It's crucial to figure out how to create cosmetic packaging with qualities that will catch consumers' attention. It is necessary and even has a significant effect on the sales of cosmetics how to allow customers to experience the effectiveness of cosmetics while also caring for the packaging and taking delight in visual and spiritual pleasure. The packaging for cosmetics must

convey the brand's effect, the product's distinctive concept, and a feeling of humane care to the user. A Nuclear Adaptive Algorithm, Section 2.3 Using the Soft plus Function as a base The kernel adaptive algorithm's anti-impulse interference performance is good thanks to the properties of the soft plus function, which can also speed up convergence. When using conventional process design, these two performances can get rid of interference signals. As a result, the soft plus-based algorithm is used in this paper. The adaptive kernel algorithm is created.

DISCUSSION

Wireless communication design research spans a broad and dynamic terrain of inquiry, invention, and optimization. It is a multidisciplinary project that brings together professionals in domains including materials science, electrical engineering, and computer science with the common goal of improving wireless communication. Designers and researchers explore a wide range of crucial topics within this broad scope, advancing us towards a more interconnected, effective, and secure wireless future. The fundamental goal of design research in wireless communication is to create the infrastructures, protocols, and technologies that drive our wireless world. This project encourages creativity and the creation of cutting-edge solutions that push the envelope of what is possible. Design research is a pioneer in turning ideas into real, high-performing systems, whether it's aiming for lightning-fast data transfer speeds, cutting latency to unnoticeable levels, or boosting the dependability of our wireless connections. The ability of design research in this area to promote ongoing wireless network performance enhancement is one of its main benefits. Researchers contribute to expanded capacity, broader coverage, and improved network stability by analyzing and optimizing many aspects of wireless networks, from the protocols regulating data transfer to the physical infrastructure supporting connectivity. Users benefit from enhanced connectivity, frictionless communication, and superior service quality all of which are crucial in our digitally interconnected society [5], [6].

Another tenet of design research in wireless communication is effective resource utilization. The wise distribution of resources including radio frequency spectrum, electricity, and network infrastructure is crucial in a time when wireless networks are subject to escalating demands. To maximize efficiency from constrained resources, design researchers dive into the complexities of resource management. This translates into an environmentally friendly and practical strategy for wireless communication, guaranteeing that our wireless ecosystems can satisfy current and future demands without placing an undue burden on resources. Design research is essential in resolving the widespread privacy and security problems that surround wireless communication. The demand for strong security procedures grows more urgent as wireless data transmission becomes more common. To strengthen the digital fortresses defending our wireless networks, researchers in this field labor ceaselessly to develop and improve encryption algorithms, authentication procedures, and threat mitigation strategies. These initiatives are essential for protecting sensitive information and promoting wireless communication trust. Design study helps to reduce the negative environmental effects of wireless communication, which are major global concerns today. To lessen the carbon footprint of wireless networks, researchers investigate eco-friendly communication protocols, low-power device designs, and energy-efficient network management techniques. This dedication to sustainability is in line with broader initiatives to lessen technology's negative environmental effects and usher in a more environmentally friendly wireless communication era.

Design research is essential in forming the interconnected ecosystems that make up the Internet of Things (Iota) and the concept of smart cities, both of which are fast taking shape. For Iota applications, researchers are investigating low-power, long-range wireless solutions. As a result of these technologies' effective data collecting, management, and analysis capabilities,

smarter, more connected cities and environments are made possible, improving the quality of life for locals. Better user experiences are one of the design research's most obvious benefits for wireless communication. Researchers improve communication services' quality by creating quicker data transfer rates, lower latency, and more dependable connections. This translates into more fluid online gaming, immersive augmented reality apps, and smoother video streaming. Design research essentially improves how users engage with wireless technology, making it more pervasive in their daily lives. Design research encourages collaboration between specialists from other domains since it is intrinsically cross-disciplinary. Researchers frequently collaborate with experts in fields like machine learning, artificial intelligence, and materials science in addition to the more conventional fields of electrical engineering and computer science. This multidisciplinary approach expands the possibilities for wireless communication and inspires original responses to challenging issues.

Our wireless world is characterized by global connectivity, and design research is essential to fostering and maintaining this connectivity. Researchers help wireless networks expand and become more widely available, closing the digital divide and giving underprivileged populations access to vital communication services. This link, made possible through design research, has broad ramifications and makes it possible for people, communities, and countries to fully participate in the digital age. Wireless communication is a lifeline in times of emergency, and design study ensures its robustness. Researchers put forth a lot of effort to strengthen wireless networks, creating infrastructures and protocols that hold up even in the face of crises and disasters. First responders and emergency management organizations can coordinate operations, save lives, and lessen the effects of disasters thanks to this resilience. Wireless communication radically alters access to education and information, and design research drives these changes. Remote learning is made possible by wireless technology, removing geographic restrictions and enhancing learning options. Additionally, it democratizes information access, enabling people to pursue knowledge, keep informed, and engage in the digital economy even in isolated or rural locations.

The research on wireless communication has a significant impact on healthcare as well. To enable virtual healthcare services, telemedicine and remote patient monitoring depend on dependable, high-quality wireless connectivity. The improvement of patient outcomes and the expansion of healthcare to underprivileged communities are all facilitated by design research in this field. Design research in wireless communication is important for extending scientific investigation beyond the immediate applications. In order to collect data for a variety of scientific fields, such as environmental monitoring, space exploration, and oceanography, wireless communication is essential. In order to facilitate ground-breaking findings and advance our understanding of the natural world, researchers create and improve wireless communication technologies. Design research in wireless communication crosses national boundaries and promotes cooperation between people, businesses, and governments on a worldwide scale.

It makes cross-border cooperation, communication, and the sharing of information easier. This connection is evidence of the transformational potential of wireless communication research, which keeps dismantling barriers and bringing people together around the world. In conclusion, wireless communication-based design research is a dynamic and diverse endeavor that influences the very structure of our digital world. Its benefits are extensive, affecting every facet of our life, from how we communicate with one another to how sustainable and resilient our technology is. To ensure that wireless communication stays a pillar of our connected society, design research pioneers' technologies that push the envelope of what is practical.

Wireless communication design research will surely advance us towards a time where communication is more effective, available, secure, and sustainable than it has ever been [7], [8].

Scope of wireless communication-based design research:

An interdisciplinary field called design research with an emphasis on wireless communication looks into, develops, and optimizes many elements of wireless communication systems and technology. Because wireless communication technology is advancing so quickly, design research in this area has a broad reach and is always changing. In the context of design research based on wireless communication, the following are some important areas: The creation and advancement of wireless network protocols and standards, including those for Wi-Fi, Bluetooth, 4G/5G/6G, and beyond, can be studied through research. Addressing concerns with data speeds, network dependability, and energy efficiency is part of this. Investigating cutting-edge antenna designs and technologies to improve the performance, range, and coverage of wireless signals. This covers beam forming techniques, phased array antennas, and MIMO Multiple Input Multiple Output systems.

Utilizing the radio frequency spectrum to its fullest potential by using strategies like dynamic spectrum allocation, cognitive radio, and spectrum sharing. Iota Connectivity: Studying low-power, long-range wireless technologies like Lora WAN, NB-Iota, and Zig bee that are appropriate for Internet of Things applications. Research on the architecture and technology for 5G and beyond wireless networks, such as network slicing, massive MIMO, and millimeter-wave communication. Development of private and secure wireless communication solutions, including encryption algorithms, authentication procedures, and threat mitigation strategies. Investigating strategies for effective resource allocation, network optimization, and administration in wireless networks to guarantee both quality of experience (DoE) and quality of service (Qu's). Energy Efficiency: Investigating methods to lower the energy consumption of wireless infrastructure and equipment, such as power-saving protocols and energy-efficient modulation algorithms. Research into GPS alternatives like Wi-Fi positioning and indoor positioning strategies, as well as methods for precise and dependable wireless localization and positioning systems, is known as wireless localization and positioning (WLP). Studying cutting-edge wireless communication techniques include underwater acoustic communication, visible light communication (VLC), and quantum communication.

Human-Computer Interaction (HCI): Examining the effects of wireless communication on user experiences and creating intuitive user interfaces for wireless hardware and software. Cross-Disciplinary Research: Working with specialists in related disciplines including artificial intelligence, materials science, and machine learning to integrate these technologies into wireless communication systems. Examining the effects of wireless communication on the environment, particularly how to manage technological trash and how much energy is used. Analyzing regulatory and policy frameworks and rules that control wireless communication and suggesting changes or adjustments to solve new problems. Infrastructure for smart cities and the internet of things: Investigating how wireless communication contributes to the creation of Iota ecosystems and smart city infrastructure. In today's linked world, design research in wireless communication is extremely important and is vital in determining the direction of communication technology. To address practical issues and promote innovation in wireless communication systems, researchers in this area work with industry stakeholders, governmental organizations, and academia.

The Benefits of Design Research for Wireless Communication:

Wireless communication-based design research has a number of important benefits that support the development of numerous businesses and the advancement of technology. The following

are a few major benefits of performing design study in this area: Technological Advancements and Innovation: Design study investigates novel wireless communication theories, concepts, and technology. Faster data rates, lower latency, and higher dependability are just a few of the cutting-edge solutions that are created as a result, pushing the envelope of what is currently achievable. Performance Enhancement of Wireless Networks: Wireless communication systems can be optimized for higher performance, more capacity, and wider coverage through study. For users, this results in better connectivity and service quality. Effective Resource Use: Research aids in the effective use of resources including power, network infrastructure, and radio frequency spectrum. For wireless networks to be able to handle the rising demand, this is essential. Design research produces more reliable security and privacy features for wireless communication networks. This is necessary to safeguard private information and guarantee wireless networks' dependability. Research is being done on energy-efficient communication protocols and hardware to lessen the carbon footprint of wireless networks. This is crucial for sustainability and minimizing technology's negative environmental effects.

Development of Wireless Technologies for Iota and Smart City Applications: Design research enables the development of wireless technologies suited for Iota and smart city applications. Cities will become more connected and smarter as a result of these technologies' effective data collection and management capabilities. Better User Experiences: Wireless communication research makes connections more dependable, transfer's data more quickly, and reduces latency, all of which improve user experiences. For applications like video streaming, online gaming, and augmented reality, this is very crucial. Collaboration across Disciplines: Research in wireless communication frequently entails cooperation with specialists from a variety of disciplines, including computer science, electronics, materials science, and more. This multidisciplinary approach promotes a wider viewpoint and supports original thinking. Global Connectivity: Design research helps wireless networks grow, bridging the digital divide and giving remote and underserved places access to communication services. Economic Growth: As a result of opening up new markets and business prospects, advances in wireless communication technology promote economic growth. This may result in the creation of jobs and a rise in global competitiveness [9], [10].

Response to emergencies and disasters: Research in wireless communication increases the dependability of networks in these situations. To coordinate efforts and save lives, this is crucial for emergency management organizations and first responders. Education and Information Access: Research-driven access to wireless communication technologies enables remote education and gives people in rural or remote places access to information and resources. Remote patient monitoring and telemedicine both heavily rely on wireless connectivity. The results of this research are better patient outcomes and access to healthcare. From environmental monitoring to space exploration, wireless communication is crucial for data collecting across a range of scientific disciplines. This area of study has led to more reliable data transmission and collecting. Global connectedness and Collaboration: Wireless communication research promotes communication and cooperation between individuals, groups, and countries, enabling global connectedness and collaboration.

CONCLUSION

After gathering information on cosmetic packaging and paper-cut art, we discovered that although established sectors are rapidly dwindling, emergent industries are growing at an exponential rate. In order to draw more attention from all spheres of society to historic industries and restore its glory, this paper primarily employs artificial intelligence technology and wireless connectivity to create paper-cut art and cosmetic packaging designs. This article primarily gathers marketing and profit statistics from traditional industries over the past few years, analyses the data, and examines both traditional marketing examples and modern

marketing perspectives. Later, create images and a packaging map that are more in line with the public's taste and are full of both conventional and cutting-edge cosmetic images using wireless connectivity and artificial intelligence technology mixed with paper-cut art and the requirements of cosmetic packaging. After the redesign is finished, we print the finished diagram using a CNC machine, change it further using cutting or other techniques as necessary, and then provide a qualified opinion to wrap up the full experimental procedure. In actuality, manual design is still quite difficult, and the needed image can only be produced automatically by a computer after which a corner is cut and adjusted to produce the template graphic. We eventually obtained the finished product after reviewing and making a few minor modifications.

REFERENCES:

[1] H. E. Nilsson *et al.*, "Printed write once and read many sensor memories in smart packaging applications," *IEEE Sens. J.*, 2011, doi: 10.1109/JSEN.2010.2095496.

[2] K. Kibaroglu, M. Sayginer, and G. M. Rebeiz, "A Low-Cost Scalable 32-Element 28-GHz Phased Array Transceiver for 5G Communication Links Based on a Beamformer Flip-Chip Unit Cell," *IEEE J. Solid-State Circuits*, 2018, doi: 10.1109/JSSC.2018.2791481.

[3] R. L. L. Li *et al.*, "Design of compact stacked-patch antennas in LTCC multilayer packaging modules for wireless applications," *IEEE Trans. Adv. Packag.*, 2004, doi: 10.1109/TADVP.2004.831866.

[4] I. Doerr *et al.*, "Parameterized models for a RF chip-to-substrate interconnect," *Proc. - Electron. Components Technol. Conf.*, 2001, doi: 10.1109/ECTC.2001.927883.

[5] J. Buckley, B. O'Flynn, J. Barton, and S. C. O'Mathuna, "A highly miniaturized wireless inertial sensor using a novel 3D flexible circuit," *Microelectron. Int.*, 2009, doi: 10.1108/13565360910981517.

[6] I. T. Nassar, T. M. Weller, and J. L. Frolik, "A compact 3-D harmonic repeater for passive wireless sensing," *IEEE Trans. Microw. Theory Tech.*, 2012, doi: 10.1109/TMTT.2012.2210440.

[7] T. Kamgaing and O. M. Ramahi, "Multiband electromagnetic-bandgap structures for applications in small form-factor multichip module packages," *IEEE Trans. Microw. Theory Tech.*, 2008, doi: 10.1109/TMTT.2008.2003525.

[8] K. Kibaroglu, M. Sayginer, and G. M. Rebeiz, "A Low-Cost Scalable 32-Element 28-GHz Phased Array Transceiver for 5G Communication Links Based on a <inline-formula> <tex-math notation="LaTeX">2×2 </tex-math> </inline-formula> Beamformer Flip-Chip Unit Cell," *IEEE J. Solid-State Circuits*, 2018, doi: 10.1109/jssc.2018.2791481.

[9] B. Abiri and A. Hajimiri, "A 69-to-79GHz CMOS multiport PA/radiator with +35.7dBm CW EIRP and integrated PLL," in *Digest of Technical Papers - IEEE International Solid-State Circuits Conference*, 2018. doi: 10.1109/ISSCC.2018.8310355.

[10] J. Liao, "Design of agricultural greenhouse environment monitoring system based on internet of things," *Nongye Gongcheng Xuebao/Transactions Chinese Soc. Agric. Eng.*, 2016, doi: 10.11975/j.issn.1002-6819.2016.11.033.

CHAPTER 9

THE ARTIFICIAL FROZEN SOIL MODEL AND CREEP CHARACTERISTICS

Rohit Saini, Assistant Professor, Department of Agriculture and Environmental Sciences
Shobhit University, Gangoh, Uttar Pradesh, India
Email Id- rohit.saini@shobhituniversity.ac.in

ABSTRACT:

The longest underground connecting channel in China built using the artificial freezing technology is used as the background for the research of the long-term stability of the large-scale freezing project. Using the MTS 370.25 mechanical testing machine, the uniaxial compressive strength test, triaxial shear test, and triaxial creep test of artificially frozen soil were performed at various temperatures. Triaxial creep tests for artificially frozen soil were performed under various loads and temperatures. A fractional-order constitutive model of frozen silt with sand was proposed in light of the results of the creep test. It is discovered that the proposed fractional-order model can accurately replicate the properties of frozen silt with sand by comparing the computed findings with the tested ones. The suggested model is more accurate and sensitive to stress than other models of creep in frozen soil. The effectiveness of the model is confirmed through simulation of the connecting channel construction and comparison with the observed data at the site, further confirming that the model has significant guiding relevance for the freezing project.

KEYWORDS:

Artificial Freezing, Compressive Strength, Constitutive Model, Creep Characteristics.

INTRODUCTION

Compound materials known as frozen soils are made up of gaseous inclusions, liquid water, solid mineral particles, and ice crystals. Because of its components and sensitivity to temperature, frozen soils' mechanical properties are more complex than those of unfrozen soils. Frozen soils exhibit nonlinear viscoelastic-plastic behavior, which is now widely acknowledged. Therefore, linear approximations cannot be employed in some projects, such as the scuppernong frozen connecting tunnel project examined in this study. The most crucial mechanical features for engineering building are the strength and creep characteristics of frozen soils. A number of experimental research on the mechanical properties of frozen soil had been undertaken to meet the demands of the application of engineering activities. According to Jess Berger frozen soil meets the Mohr-Coulomb strength requirement when subjected to modest confining pressure. An improved Hook-Brown criterion was utilized by Yang et al. To explain the nonlinear strength properties of frozen soil under low confining pressure. Triaxial strength tests of frozen sand were conducted by Lai et al. Who also suggested an elastoplastic damage constitutive model based on continuous damage theory? An elastic-plastic constitutive model of frozen soil under high confining pressure was put forth by Yak [1], [2]. In order to present an elastoplastic incremental frozen loess constitutive model in the triaxial condition, Lai et al. conducted static triaxial compression experiments of frozen loess and introduced the plastic theory. In order to examine the frozen soil constitutive model based on the Mohr-Coulomb yield criterion.

Understand and Kayli used a differential creep test to investigate the effects of stress, temperature, and soil structure on the creep rate of frozen soil in their study on the creep mechanical properties of frozen soil. Valor et al. pointed out that creep is brought on by the

formation and growth of micro cracks and other faults in soil, using sand as an example. Sun et al. presented a straightforward and practical creep constitutive relation for frozen soil based on the element model. Li et al. developed a nonlinear creep damage coupled constitutive model of artificially frozen clay and frozen sand under unloading state and complex stress path circumstances based on numerous uniaxial and triaxial creep tests of artificially frozen soil. The effects of temperature, particle rearrangement, and particle contact surface features on creep were investigated by Bai et al. In order to create a suitable mechanical model, Chen and Qian researched the creep process and uniaxial compression test of artificial frozen soil. By examining the results of creep tests conducted on frozen soil at various temperatures, established a creep model of frozen soil with temperature acting as an independent variable. Through the frozen soil creep test, Aaronson and spring man were able to determine the creep model of rich ice-frozen soil at a temperature near to 0°C. Wang et al.'s description of the one-dimensional accelerated creep stage of frozen soil in the Nishihara model utilized the non-Newtonian viscous element as opposed to the Newtonian viscous element. The stress level is a significant element determining the strength and deformation of frozen soil, according to numerous studies on the creep of frozen soil. The geotechnical constitutive model's use is crucial. Using the constitutive model as a foundation, Yuan et al. proposed various works that should be taken into consideration in engineering applications. Triaxial creep tests were performed by Mange ET along warm frozen silts, and based on the results, a fractional-order rheological element model was developed.

Most of this research demonstrate that the creep curves under various stress levels only take into account primary and secondary creep stages and neglect the impact of temperature effect. According to the test results in this study, when the stress level surpasses the stress threshold, the creep curves may be characterized by three distinct stages, and the influence of temperature effect will be present in the properties of frozen soil and constitutive model. In this study, triaxial creep experiments for artificially frozen soil were conducted under various pressures and temperatures. A fractional-order constitutive model of frozen silt with sand was proposed in light of the results of the creep test. The suggested model is more accurate and sensitive to stress than other models of creep in frozen soil. The proposed fractional-order model can simulate the properties of frozen silt with sand very well and has a great engineering value and realistic significance, according to test data of frozen soils at various temperatures and test conditions used to validate the proposed model [3], [4].

Background Information and Test Strategy:

The Fuzhou Zip-Wu Interval's connecting tunnel is China's longest subway connecting passage built using the freezing method. This connecting passage's centerline is 6.4 meters from the closest pile foundation of the flyover pier, and its center distance is 66 meters. The strata are strengthened using the artificial freezing technique, and the construction is done by subsurface excavation. Figure 1 depicts a portion of the connecting passage's frozen curtain. The effective frozen curtain thickness is 2.0 m, and the average temperature of the frozen earth is less than 10°C. The construction risk level for this connecting tunnel is grade I since it is the longest in China to be built using the freezing method, and because of its complex placement. This freezing engineering differs from ordinary freezing engineering in that it has a long freezing duration, a big freezing volume, a lengthy excavation and building period, a complicated surrounding environment, and high deformation control needs. This project cannot be fully accommodated by the elastic model that was frequently used in earlier engineering calculations, so this work adopts the fractional derivative viscoelastic-plastic constitutive model to enhance the computation. Where the connecting tunnel is located, salty fine sand and silt mixed with sand make up the majority of the primary soil strata. In this study, silt with sand is used as the research object to conduct standard geotechnical tests as well as testing on the

physical and mechanical characteristics of frozen soil, such as the uniaxial compressive strength test, the triaxial shear test, and the triaxial creep test [5], [6].

DISCUSSION

The test soil samples were collected from the connecting channel's strata at a depth of 20 to 30 meters below ground. Routine geotechnical tests were carried out on the soil samples, and Table 1 lists the fundamental physical parameters needed to make the determination. The MTS 370.25 low-temperature material testing machine is used to examine the mechanical properties of artificially frozen soil. The test apparatus is depicted. The soil samples are put into cylindrical specimens measuring 50 mm by 100 mm and then put in a special incubator to cure. The MTS testing machine's loading and unloading operations are managed by a programmer. The displacement rate loading mode is used for the compression strength testing on frozen soil, and the displacement change rate is 1 mm/min. The test is over when either the peak stress or axial strain hits 20% during the test. Experiments are used to determine the compression strength of frozen soil at 5°C, 7°C, 10°C, 15°C, and 20°C. At the same time, the elastic modulus and Poisson's ratio are computed. The strain rate used in the triaxial shear testing is 1%/min, and the strain loading method is used. If the axial force reaches a peak value, shear 3% to 5% of the strain value after the peak point, and then stop the test. The test is stopped after shearing to a 20% strain value if the axial force increases. The temperature inaccuracy is kept within 0.1°C during the test, and four freezing temperatures of 5°C, 7°C, 10°C, and 15°C are adopted. The test confining pressures are, respectively, 0.5 MPa, 1.0 MPa, and 1.5 MPa. 2 Hz is the data acquisition frequency. The creep test lasts for 12 hours and has creep loading coefficients of 0.3, 0.5, and 0.7. Frozen soil differs from regular soil in terms of structure, strength, and other qualities due to the presence of ice crystals. The compressive strength of frozen soil is directly impacted by changes in temperature. The internal makeup of frozen soil gradually changes as the temperature drops, and unfrozen water turns into ice crystals, increasing the soil's compressive strength. Depicts the link between the temperature of frozen soil and uniaxial compressive strength.

It is clear that the elastic modulus of frozen soil increases as the freezing temperature decreases within the test temperature range, grows linearly, and that there is a good link between the two. The elastic modulus generally rises by 8.70 MPa for each degree of temperature decrease. The interpolation approach can be used to determine the elastic modulus of the appropriate soil layer at any temperature within the test temperature range. Three stages can be broadly distinguished in the triaxial shear process of frozen soil: elastic growth stage, plastic yield stage, and rapid failure stage. The stress-strain curve appears to be growing linearly at the beginning of loading. Since the soil is currently at the period of elastic development, its deformation is mostly caused by compression between soil particles. The soil sample starts to experience irreversible plastic deformation as a result of the constant rise in stress, and the plastic deformation keeps becoming worse. The plastic yield stage, which occurs when the maximum tension is reached, is marked by the emergence of small fissures on the soil's surface. The accelerated failure stage occurs when the sample fails as a result of the soil crack developing, spreading, and penetrating after the sample reaches its maximum stress.

The isochronal curve of stress-strain is not a straight line or broken line, which makes the creep of frozen soil a typical nonlinear rheology. Nonlinearity can result from changes in the stress level and the passage of time, and these two factors interact to affect nonlinearity. The strain will progressively get worse over time if the stress placed on the frozen soil stays constant. The frozen soil first displays instantaneous elastic and plastic deformation before entering the first stage, or the unstable creep stage. The distortion caused by the creep of frozen soil is attenuating, meaning it will eventually stabilize. Following that, the strain rate roughly stays constant as it moves into the second stage, known as the stable creep stage. The second stage

of creep lasts longer and even the third stage rapid creep does not develop when little stress is applied to frozen soil. Contrarily, the second creep stage is quite brief or even doesn't exist [7].

Del for Fractional Derivative Viscoelastic-Plastic Creep:

Fractional calculus is used to characterize the nonlinear mechanical behavior of frozen soil creep due to its advantages in nonlinear dynamic systems. An enhanced fractional-order viscoelastic-plastic creep constitutive model for frozen soil is suggested in this research. On the one hand, the ideal viscoelastic body is enhanced by substituting the fractional viscous body for the classical viscous body, and on the other, the impact of stress on the creep properties of frozen soil, particularly the accelerated creep, is taken into account. It is suggested that a fractional viscoelastic body with order larger than 1 be used, which is sensitive to changes in stress since its order might vary depending on the level of stress. The unsteady fractional-order differential integral creep model of frozen soil is then constructed and proven by connecting the classical elastic body, classical viscous body, improved fractional-order elastoplastic body, and improved fractional-order viscoelastic body in series.

Finite Element Analysis:

The displacement field and stress field of the frozen wall are simulated using ANSYS finite element analysis software and the viscoelastic-plastic constitutive equation of frozen soil proposed in this research. The three-dimensional solid element SOLID186 is used, and the PCG solver is chosen. The plastic and creep deformation of frozen soil should be taken into account in the calculation due to the lengthy connecting tunnel, the significant volume of freezing, the lengthy excavation and building times, the complicated surrounding environment, and the high needs for deformation management. As a result, the calculation is enhanced by using the fractional derivative viscoelastic-plastic model. The mechanical analysis of the frozen curtain uses a three-dimensional mechanical model. Table 7 lists the material parameters, and the values for frozen soil's mechanical characteristics are interpreted as the mechanical characteristics of frozen soil at 10°C. As illustrated in Figure 12, 1/4 of the structure is used as the calculation model in accordance with structural symmetry [8], [9].

Calculations are made to determine the overall displacement and frozen curtain displacement brought on by the connecting route excavation, respectively. The results of the calculations are displayed. The maximum ground deformation measured from the total displacement reprogram is 34.3 mm; the maximum ground deformation measured from the displacement reprogram of the frozen curtain is 21.2 mm; and the frozen soil deformation represents 61.8% of the total ground deformation. The displacement curve of the upper frozen curtain of the connecting channel at various times using the tunnel center as the origin and the distance from the center of the tunnel as the variable. The creep law of frozen soil within 24 hours following the excavation is depicted in Figure 16 using the frozen soil in the middle of the connecting route as the research object. The frozen curtain's displacement curve is simultaneously parabolic at the upper section of the connecting tunnel and that the connecting passage's midpoint is the location of the largest vertical displacement. With time, the vertical displacement increases, and the increase is higher the closer to the middle you are. The estimated maximum vertical displacement following excavation is 22.5 mm after 8 hours, 23.2 mm after 20 hours, and 23.3 mm after 24 hours. Every four hours, the vertical displacement rises by 0.74 mm, 0.58 mm, 0.31 mm, 0.20 mm, 0.16 mm, and 0.13 mm, respectively. The creep increase gradually declines, indicating an attenuation creep increase, and gradually tends to be stable. The tracking grouting was done in the real project in accordance with the monitoring value. The latter measured values are therefore less than the latter estimated values.

Stress and strain:

Figure 17 depicts the von Misses stress distribution reprogram of the frozen soil following the excavation. Figure 18 displays the von Misses stress of the frozen soil at the middle-upper of the connecting route after 24 hours. The von Misses stress distribution reprogram of frozen soil shows that the stress distribution is largely uniform, with the majority of values falling between 0.037 MPa and 0.663 MPa. At the intersection of the tunnel and the frozen soil, there is a stress concentration point with a maximum of 1.45 MPa. The von Misses stress of the frozen soil in the middle-upper part of the connecting tunnel exhibits a steady decreasing trend during the frozen soil creep, with a minor reduction, and finally tends to be stable, as can be seen in Figure 18. As illustrated in Figure 19, the entire frozen curtain is split into the elastic zone, plastic zone, and damage zone based on the strain of the frozen curtain in its final stable form.

In geotechnical engineering and permafrost-related research, artificial frozen soil models are essential tools that enable scientists and engineers to simulate the complicated behavior of frozen ground under varied environmental and load circumstances. We can better comprehend the mechanical and thermal responses of naturally frozen soils thanks to these models, which reflect their distinctive characteristics. We explore the complexities of artificial frozen soil models in this talk as well as how they can be used to analyses creep characteristics, a crucial component of permafrost behavior. When referring to frozen soil, the term "creep" describes the slow, continuous deformation and settling that takes place under pressure or tension, frequently influenced by temperature changes. Given that many constructions, including roads, pipelines, and buildings, are located in permafrost regions, it is essential to comprehend creep behavior when designing infrastructure. The stability and integrity of these constructions may be impacted by the mechanical behavior of frozen soil under sustained loads and temperature changes. For the purpose of researching creep properties, artificial frozen soil models are used as controlled laboratory conditions. These models enable for the controlled conduct of experiments by simulating the temperature, mechanical, and hydraulic characteristics of naturally frozen soils. In order to create these models, numerous important factors and concerns must be taken into account:

Soil Selection: Choosing the right soil is important. To make a realistic frozen soil specimen, scientists often combine soil, water, and additives. The mixture's ingredients should have a grain size distribution, mineral content, and ice content that resemble natural permafrost. Controlling the temperature is crucial for reaching and holding the desired freezing points. To simulate the freezing temperatures, present in permafrost zones, the specimen can be cooled to below zero using refrigeration systems or liquid nitrogen. Artificial frozen soil models must be put under loads and pressures that are a good representation of actual environmental conditions. In order to do this, the specimen must be subjected to lateral and vertical forces, frequently utilizing specialized testing apparatus [10], [11].

Measurement and monitoring:

In order to examine creep behavior, scientists use a variety of sensors and monitoring systems to keep track of variables like the specimen's temperature, strain, deformation, and pore pressure. The analysis of the temporal evolution of creep deformation is aided by these data. Boundary Conditions: The boundary conditions that are applied to the specimen should closely resemble the in-situ circumstances. These circumstances can include groundwater, lateral confinement, and temperature gradients. In the study of creep properties, artificial frozen soil models have various benefits. Controlled Environment: By accurately regulating temperature, stress, and other variables, researchers can conduct repeatable studies and gain a thorough grasp of how various elements affect creep behavior. Accelerated Testing: It may take years or even decades to discover creep processes in naturally frozen soils. Artificial models help researchers

speed up these procedures so they can gain important insights more quickly. Researchers can systematically change variables like temperature, stress levels, and soil composition to determine how they affect creep behavior. This makes it easier to comprehend the basic principles regulating creep. Model Validation: Numerical models and theories pertaining to frozen soil creep can be verified using artificial models. Thus, the precision and dependability of computational simulations are guaranteed. Structural Design: Information from artificially frozen soil models can be used to guide the planning and development of infrastructure in permafrost areas. Engineers are qualified to decide on foundation design and insulation specifications.

It's crucial to understand the limitations of artificial frozen soil models. Although they are useful for understanding creep behavior, they are merely distilled versions of intricate natural systems. Replicating the complete range of environmental factors and soil variability present in actual permafrost zones is a difficult task. In conclusion, models of artificially frozen soil are essential tools for researching the creep properties of frozen ground. Researchers can now explore the impact of temperature, stress, and other variables on creep deformation thanks to these models, which produce controlled laboratory settings that mimic the characteristics of natural permafrost. Engineers and scientists may better understand permafrost behavior under long-term stresses through experimentation and data analysis, which will lead to cold-weather infrastructure that is more durable and secure [12], [13].

CONCLUSION

Many significant physical and mechanical property parameters of the soil layer are obtained through the uniaxial compressive strength test, triaxial shear test, and triaxial creep test of frozen silt with the sand soil layer, providing the fundamental framework for the advancement of freezing engineering. A fractional-order constitutive model of frozen silt with sand is proposed through a series of triaxial creep tests for artificially frozen soil under various loads and temperatures. The results that could be drawn are as follows. The creep of frozen soil exhibits a typical nonlinear rheology; that is, the stress-strain isochronal curve is not a broken or straight line. Nonlinearity can result from changes in the stress level and the passage of time, and these two factors interact to affect nonlinearity. The second stage of creep lasts longer and even the third stage does not develop when little stress is applied to frozen soil. Contrarily, the second creep stage is quite brief or even doesn't exist. The three stages of artificial frozen soil creep, particularly the accelerated creep stage, can be described by the proposed fractional derivative viscoelastic-plastic creep model. The model parameters are produced by fitting and analyzing the creep curves under various temperature and stress settings using the particle swarm optimization technique and least squares algorithm. It is discovered that the proposed fractional-order model can very effectively replicate the properties of frozen silt with sand by comparing the calculated findings with the tested ones. The suggested model is more accurate and sensitive to stress than other models of creep in frozen soil. The effectiveness of the model was confirmed through simulation of the connecting channel construction and comparison with the actual data collected on-site. This further confirms that the model has significant guiding relevance for the freezing project.

REFERENCES:

[1] D. Li, J. Chen, and Y. Zhou, “A Study of Coupled Creep Damaged Constitutive Model of Artificial Frozen Soil,” *Adv. Mater. Sci. Eng.*, 2018, doi: 10.1155/2018/7458696.

[2] D. W. Li, J. H. Chen, and Y. Zhou, “Elastic-plastic constitutive model of artificial frozen soil based on cascade-correlation artificial neural network,” *Meitan Xuebao/Journal China Coal Soc.*, 2016, doi: 10.13225/j.cnki.jccs.2014.1347.

[3] D. Li, X. Yang, and J. Chen, "A study of Triaxial creep test and yield criterion of artificial frozen soil under unloading stress paths," *Cold Reg. Sci. Technol.*, 2017, doi: 10.1016/j.coldregions.2017.06.009.

[4] L. Zhao, P. Yang, L. C. Zhang, and J. G. Wang, "Cyclic direct shear behaviors of an artificial frozen soil-structure interface under constant normal stress and sub-zero temperature," *Cold Reg. Sci. Technol.*, 2017, doi: 10.1016/j.coldregions.2016.10.011.

[5] O. L. Liu, " Investigating the Relationship Between Test Preparation and TOEFL iBT ® Performance ," *ETS Res. Rep. Ser.*, 2014, doi: 10.1002/ets2.12016.

[6] S. O. Gbadamosi *et al.*, "A patient-held smartcard with a unique identifier and an mhealth platform to improve the availability of prenatal test results in rural Nigeria: Demonstration study," *J. Med. Internet Res.*, 2018, doi: 10.2196/jmir.8716.

[7] D. Albanese, S. Riccadonna, C. Donati, and P. Franceschi, "A practical tool for maximal information coefficient analysis," *Gigascience*, 2018, doi: 10.1093/gigascience/giy032.

[8] A. Rasheed and M. S. Anwar, "Numerical computations of fractional nonlinear Hartmann flow with revised heat flux model," *Comput. Math. with Appl.*, 2018, doi: 10.1016/j.camwa.2018.08.039.

[9] M. Sasso, G. Palmieri, and D. Amodio, "Application of fractional derivative models in linear viscoelastic problems," *Mech. Time-Dependent Mater.*, 2011, doi: 10.1007/s11043-011-9153-x.

[10] K. Wei, F. Wang, P. Niu, S. Wang, and P. Wang, "Experimental Investigation and Theoretical Model of Viscoelastic and Plastic Dynamic Properties of Rail Pads," *Tiedao Xuebao/Journal China Railw. Soc.*, 2018, doi: 10.3969/j.issn.1001-8360.2018.12.015.

[11] H. Chen, W. Xu, W. Wang, R. Wang, and C. Shi, "A nonlinear viscoelastic-plastic rheological model for rocks based on fractional derivative theory," *Int. J. Mod. Phys. B*, 2013, doi: 10.1142/S021797921350149X.

[12] A. Krasnobrizha, L. Gornet, P. Rozycki, and P. Cosson, "Rapid Determination of the Fatigue Limit by the Simulation of Self-Heating Test by the Collaborative Model Based on the Fractional Derivative Approach," in *Procedia Engineering*, 2018. doi: 10.1016/j.proeng.2018.02.021.

[13] G. Spathis and E. Kontou, "A fractional transient model for the viscoplastic response of polymers based on a micro-mechanism of free volume distribution," *Mech. Time-Dependent Mater.*, 2017, doi: 10.1007/s11043-017-9347-y.

CHAPTER 10

EFFECTS OF DIETARY POLYPHENOLS ON CELL BIOCHEMISTRY AND PATHOPHYSIOLOGY

Rohit Saini, Assistant Professor, Department of Agriculture and Environmental Sciences
Shobhit University, Gangoh, Uttar Pradesh, India
Email Id- rohit.saini@shobhituniversity.ac.in

ABSTRACT:

Dietary polyphenols, which are present in large quantities in fruits, vegetables, tea, coffee, and red wine, are receiving more attention because of their potential to have positive impacts on health. The complex interaction between dietary polyphenols and cell biochemistry is examined in this review, as well as how they affect pathophysiological processes. Within cells, polyphenols demonstrate a variety of methods of action, including antioxidant capabilities, signaling pathway modification, and epigenetic control. These bioactive substances have been demonstrated to have an impact on important biological processes such cell division, oxidative stress, apoptosis, and inflammation. Additionally, dietary polyphenols show promise in reducing a number of pathophysiological ailments, such as cancer, metabolic syndrome, neurodegenerative disorders, and cardiovascular diseases. The study gives a thorough description of the molecular processes that underlie how dietary polyphenols affect cell biochemistry and shows how they may be used as therapeutic agents to treat and prevent disease.

KEYWORDS:

Dietary, Inflammation, Polyphenols, Pathophysiological Processes.

INTRODUCTION

A wide range of disease conditions, including cancer, cardiovascular disease, and neurodegenerative disorders, have been shown to benefit from polyphenols, which are found in fruit and vegetables, wine, tea, extra virgin olive oil, chocolate, and other cocoa products. Numerous biological effects of polyphenols have been linked to their antioxidant capabilities, either directly or indirectly through potential influences on intracellular redox status or through their inherent reducing capacities. As a result, polyphenols may shield cellular components from oxidative harm and have been shown to lower the incidence of certain degenerative conditions linked to oxidative stress, including as cancer, type 2 diabetes, and cardiovascular conditions. Nevertheless, mounting evidence indicates that the traditional antioxidant activity that donates hydrogen is unlikely to be the only reason for their cellular impacts in vivo. In fact, it has lately become evident that polyphenols can display a number of new, still-unknown features in complex biological systems. It is clear that polyphenols are potent bioactive molecules, and determining their potential as chemo preventive or anticancer agents as well as inhibitors of neurodegeneration requires a clear understanding of their precise mechanisms of action as either antioxidants or modulators of cell signaling. This special issue contains 9 review papers that summarize the most recent research on the health benefits of polyphenols in addition to 14 original research pieces that deepen our understanding of the biological roles of polyphenols from various sources [1], [2].

Potential Cancer Risk from Polyphenols:

Although epidemiological research on the chemo preventive and anticancer effects of tea polyphenols has not yet produced definitive results, there is a growing trend to use these

compounds as conservative therapy for patients with less advanced prostate cancer. In an effort to better understand how tea polyphenols might be used to prevent prostate cancer, two groups S. Camino et al. and P. Ravalli et al. review the most current findings regarding tea polyphenols and human prostate cancer risk. The original study by C. Oleg et al. demonstrates that coffee acid, a single component of coffee, and polyphenol extracts both lower cycling D1 in HT29 colon cells, indicating that both compounds have chemo preventive characteristics. Data on the ant mutagenic effects of cur cumin and epigallocatechin-3-gallate in human oropharyngeal mucosa cultures exposed to cigarette smoke condensate were presented by P. Baumeister et al. and show that dietary polyphenols can stop tobacco-related nontoxicity in the upper aero digestive tract mucosa. D. Zhang et al. and C. Widen et al. report the antioxidant and growth-inhibiting activities of flavonoid extracts on erythrocyte and an erythroleukemia cell line, respectively, in relation to other cancer types.

Coffee, syringes, and protocatechuic acids are phenolic acids produced by the gut after the digestion of polyphenols or directly derived from dietary consumption. The antioxidant activity of these substances is investigated by L. Zamboni et al. in membrane model systems and in the leukemia cell line HEL. These substances contrasted the intracellular ROS rise caused by exogenous oxidative stress in both leukemia and normal cells and demonstrated a chain-breaking antioxidant in membrane models. These findings provide more evidence that the antioxidant ROS-depleting approach is an effective method for treating cancer [3], [4].

Polyphenols and the Risk of Cardiovascular Disease:

Quercetin is a flavonoid that occurs naturally and has been demonstrated to have anti-inflammatory and cardio protective effects. In their work on the preventive effect of quercetin against cardiac dysfunction in sepsis-affected rats, C. Angelina and S. Hernia show that this flavonoid is implicated in both the suppression of cell proliferation and the induction of apoptosis. These findings imply that quercetin might be an effective preventative treatment for inflammatory cardiovascular disorders. Anthocyanins are now known to have antiatherogenic and vascular protective actions. M. Akhlaghi and B. Bandy used rat embryonic ventricular H9c2 cells treated to simulated ischemia-reperfusion and tart-butyl hydro peroxide to compare the protective effect produced by various flavonoids. They also attempted to separate direct effects from indirect preconditioning effects. The findings confirmed the notion that catechism may function as preconditioning agents, with quercetin and epigallocatechin gal late being the most effective antioxidants among the flavonoids examined in acute oxidative stress settings. Our understanding of the molecular mechanisms underlying the vascular protection provided by anthocyanins in the context of preventing endothelial dysfunction and atherosclerosis is increased by the study of J. Piano et al. Data showed that malvidin-3-glucoside inhibits peroxynitrite-induced mitochondrial apoptotic signaling pathways and reduces the production of reactive substances after cell aggressiveness. Additionally, A. Kondrashov et al. determined in vivo the beneficial effects of administering red wine extracts to hypertensive rats.

Polyphenols and the Risk of Neurodegenerative Diseases:

In a review paper, C. P. Dias et al. explore some new research on the influence of various dietary polyphenols on the proliferation and differentiation of hippocampus cells as well as models of anxiety and depression. It appears that dietary polyphenols reduce anxiety and depressive symptoms, perhaps in part via regulating adult hippocampal neurogenesis. The use of diet as a treatment intervention for diseases connected to mental health may benefit from research on the effects of dietary polyphenols on behavior and AHN. The antioxidant characteristics of wine polyphenol components, such as their capacity to scavenge free radicals and also control NO activity, are well recognized. According to A. Basil et al., polyphenols may exert their neuroprotective effects by preventing the production of reactive oxygen

species, which would reduce inflammation and alter the activity of intracellular signal transduction molecules. This is one of many neuroprotective mechanisms of action that have been proposed. Recent evidence, according to a thorough review by D. Vauzour, suggests that polyphenols have protective signaling effects that reduce oxidative/inflammatory stress signaling, increase protective signaling, and have neurohormetic effects that cause the expression of genes for antioxidant enzymes, phase-2 enzymes, neurotropic factors, and cytoprotective proteins. The Nrf-2/ARE pathway, the NF-B pathway, and the Sirtuin-FoxO pathway are some examples of such pathways. Polyphenols may be able to stop the advancement of neurodegenerative diseases because these systems work together to maintain brain homeostasis and are crucial for neuronal stress adaptation. The putative neuroprotective impact of certain polyphenols has been covered in another review by S. Divinely et al. The links between the neuroprotective properties of the chosen polyphenols and their potential therapeutic efficacy in Alzheimer disease have been underlined in particular by the authors. Schisandrin greatly reduced the short-term and spatial reference memory impairments caused by A1-42 in vivo, according to D. Hu et al. Additionally, SCH therapy boosted GSH levels and the GSH/GSSG ratio in the mouse cerebral cortex and hippocampus while decreasing malondialdehyde and GSSG levels in the brain's cerebral cortex and hippocampus. These findings imply that SCH may protect against Alzheimer's disease by enhancing cognition through an ant oxidative effect. The effects of quercetin and sesame on the neuroinflammation brought on by the parkinsonian toxin 1-methyl-4-phenylpyridinium in a glial-neuronal system have been examined in the work by J. Bourneville et al. These findings show that quercetin and lignin sesame reduce MPP+-evoked microglial activation and imply that both of these molecules may be thought of as strong, naturally occurring anti-inflammatory substances [5], [6].

Polyphenols' Function in Redox Modulation:

M. Cohan et al. look into how digestion and cooking affect the ability of culinary herbs to reduce inflammation. This study demonstrates that the culinary herbs rosemary, sage, and thyme have strong anti-inflammatory activity when used in cooking, which may be because of their polyphenol content. Millions of people in South America drink mate tea every day, which is made from the aqueous extraction of Ilex paraguariensis leaves. The effects of acute and chronic mate tea consumption on those caused by acute and chronic ethanol administration are studied by B. Scalar et al. As a result of the in vivo administration of ethanol, the results demonstrated that both acute and chronic mate tea treatment reduced oxidative stress in the rat hippocampus and blood. This shows that mate tea may have a high antioxidant capacity, likely as a result of its bioactive ingredients, and that mate tea consumption may help ward off illnesses brought on by oxidative stress. The connection between apoptosis and delayed luminescence in human leukemia is discussed by J. Baron et al. The effects of two flavonoids, quercetin and epigallocatechin gal late, when applied alone or in combination with menadione or H2O2 on Junket T cells under oxidative stress. Flavone mononucleotide reacted with menadione, epigallocatechin gal late, and H2O2, but not quercetin, and changed its electronic configuration, lowering delayed luminescence emission. And jar et al. address the potential health advantages of cocoa polyphenols in review papers. With a focus on the effects on skin, P. Oyetakinwhite et al. evaluate the protective mechanisms of green tea polyphenols, while M. Cist et al. summarize the most recent research on the impact of different flavonoids on the respiratory burst of mammalian neutrophils.

DISCUSSION

In the areas of nutrition, biology, and medicine, research into how dietary polyphenols affect cell biochemistry and pathophysiology is expanding. Numerous plant-based foods and beverages, including fruits, vegetables, tea, coffee, and red wine, are rich in polyphenols, which

are being studied more and more for their possible health-promoting qualities. These naturally occurring substances include a varied set of molecules with a wide variety of biological activity and are distinguished by their polyphenol structures. Dietary polyphenols interact with cellular elements and signaling pathways within the human body, affecting cell biochemistry and, as a result, being key players in the pathophysiology of numerous disorders. It is crucial to investigate the underlying processes by which these bioactive substances exert their effects in order to fully understand the complex interactions between dietary polyphenols and cell biochemistry. The section that follows explores the various ways that dietary polyphenols affect cellular functions before illuminating their effect on pathophysiological situations. How Dietary Polyphenols Affect Cell Biochemistry: Mechanisms of Action Dietary polyphenols influence cell biochemistry through a variety of different methods. These intricate and complimentary pathways help explain the complex ways that polyphenols affect cellular functions. Key mechanisms include the following.

Antioxidant Activity: The ability of polyphenols to act as antioxidants is perhaps one of their most well-known characteristics. These substances have the ability to remove free radicals and reactive oxygen species reducing oxidative stress in cells. Numerous pathophysiological factors, such as ageing and chronic diseases, are linked to oxidative stress. Resveratrol and other polyphenol antioxidants like flavonoids protect cellular constituents including DNA, proteins, and lipids by scavenging dangerous free radicals and assisting in the maintenance of redox equilibrium. Signaling Pathways Modulation: Polyphenols have the ability to alter intracellular signaling pathways. Depending on the situation, they can either activate or inhibit certain pathways. For instance, antioxidant defenses are regulated by nuclear factor elytroid 2-related factor which can be activated by polyphenols like epigallocatechin gal late (EGCG) from green tea. On the other hand, they can block pro-inflammatory pathways including nuclear factor-kappa B and mitogen-activated protein kinases so lowering inflammation and the damaging impact it has on cells. Recent studies reveal that polyphenols may have an impact on epigenetic changes such DNA methylation and histone acetylation. These epigenetic modifications can change how genes are expressed, which affects cell behavior. For instance, histone deacetylase inhibitory action in polyphenols like cur cumin and resveratrol has been demonstrated, potentially altering gene transcription and cell differentiation [7], [8].

Polyphenols have the ability to act as enzyme inhibitors, preventing the activity of enzymes involved in a variety of cellular activities. For example, the flavonoid quercetin, which is included in many foods, has the ability to reduce the activity of enzymes like tyrosine kinases, which are essential for cell signaling and proliferation. Metal Chelation: Some polyphenols have the ability to chelate metals, which allows them to bind to transition metals like iron and copper. Polyphenols can stop metal-catalyzed processes that produce damaging ROS inside of cells by securing these metals.

Effects on Inflammation:

Cardiovascular disease, cancer, and neurological illnesses are just a few pathophysiological conditions that exhibit chronic inflammation as a defining feature. By regulating the expression of inflammatory mediators such cytokines and chemokine's and by inhibiting the activation of inflammatory signaling pathways, polyphenols can reduce inflammation.

Dietary Polyphenols Influence Cellular Processes:

Dietary polyphenols have a dramatic impact on cell biochemistry by influencing a variety of cellular functions. Among the major procedures that polyphenols have an impact on are: Strong antioxidants, polyphenols help combat oxidative stress within cells by lessening the harm done by free radicals and reactive oxygen species. The preservation of biological elements including DNA, proteins, and lipids is also made possible by this protective function. Anti-inflammatory

effects of polyphenols prevent the synthesis and release of pro-inflammatory chemicals. Polyphenols aid in the reduction of chronic inflammation by inhibiting inflammatory signaling pathways and regulating immunological responses. Apoptosis Polyphenols can affect the ratio of cells that survive to those that die. They might because cancer cells to undergo apoptosis programmed cell death which would stop the disease from spreading and growing out of control while protecting healthy cells. Cell Proliferation and Differentiation: Certain polyphenols have the capacity to control cell division and proliferation, which is essential for tissue regeneration and repair. For instance, polyphenols like epicatechin can help stem cells differentiate into particular cell types.

Cell Signaling:

Polyphenols alter intracellular signaling pathways, which have an impact on functions like cell division, growth, and metabolism. These substances have the ability to stimulate signaling pathways that support cell survival while blocking those that result in apoptosis or inflammation. Impact on Disease States from Pathophysiological Implications Understanding how dietary polyphenols affect cell biochemistry is essential to understanding how these compounds contribute to the pathophysiology of various disorders. The effects of polyphenols on particular disease states are examined in the following sections.

Cardiovascular illnesses:

The development of cardiovascular illnesses, such as atherosclerosis and hypertension, is significantly influenced by oxidative stress and inflammation. Resveratrol and flavonoids are examples of polyphenols that have been found to enhance endothelial function, lower blood pressure, and prevent the oxidation of low-density lipoprotein (LDL) cholesterol, all of which are beneficial for cardiovascular health. Cancer: Research on polyphenols has focused on their capacity to control cell growth and trigger apoptosis. These substances may prevent cancer cells from spreading and growing. For instance, the anti-inflammatory and anti-proliferative qualities of turmeric's cur cumin have showed promise in the prevention and treatment of cancer.

Neurodegenerative Disorders:

Neuroinflammation and oxidative stress play major roles in the development of neurodegenerative illnesses including Alzheimer's and Parkinson's. By minimizing oxidative damage and neuroinflammation, polyphenols, particularly those contained in berries, green tea, and dark chocolate, have neuroprotective effects. Diabetes and Metabolic Syndrome: Polyphenols can improve insulin sensitivity and control glucose metabolism, making them potential friends in the treatment of type 2 diabetes and metabolic syndrome. Red wine's resveratrol, which has positive effects on glucose homeostasis, has drawn attention. Obesity: Obesity is frequently linked to oxidative stress and chronic inflammation. Polyphenols, like those found in berries and green tea, may aid in the fight against obesity by lowering inflammation, boosting fat metabolism, and encouraging weight loss. Ageing: Oxidative stress and inflammation have cumulative effects that speed up ageing. By lowering cellular damage and encouraging cellular repair mechanisms, dietary polyphenols with antioxidant characteristics may be able to delay the ageing process [9], [10].

CONCLUSION

A fascinating topic of study in the fields of cell biochemistry and pathophysiology is dietary polyphenols. The various functions of polyphenols within cells have been highlighted in this study, demonstrating their capacity to regulate crucial processes via a variety of ways. Polyphenols have a substantial impact on cell biochemistry through a variety of mechanisms, including their antioxidant qualities that combat oxidative stress and their modulation of

complex signaling cascades and epigenetic alterations. The wide range of pathophysiological disorders that dietary polyphenols have an impact on highlights their potential as therapeutic agents. They represent prospective prospects for the prevention and treatment of a wide range of illnesses, including as cardiovascular diseases, neurological disorders, cancer, and metabolic syndrome because of their capacity to reduce inflammation, oxidative stress, apoptosis, and aberrant cell proliferation. Dietary polyphenols have become bioactive substances that have the power to significantly impact pathophysiological processes as well as cell biochemistry. Our understanding of human health will likely be improved by further study into the mechanisms of action and therapeutic applications of these substances, which may also lead to the development of novel ways to disease treatment and prevention.

REFERENCES:

[1] T. Maraldi, D. Vauzour, and C. Angeloni, "Dietary polyphenols and their effects on cell biochemistry and pathophysiology 2013," *Oxidative Medicine and Cellular Longevity*. 2014. doi: 10.1155/2014/576363.

[2] C. Angeloni, T. Maraldi, D. Milenkovic, and D. Vauzour, "Dietary polyphenols and their effects on cell biochemistry and pathophysiology 2014," *Oxidative Medicine and Cellular Longevity*. 2015. doi: 10.1155/2015/782424.

[3] C. Angeloni, L. Pirola, D. Vauzour, and T. Maraldi, "Dietary polyphenols and their effects on cell biochemistry and pathophysiology," *Oxidative Medicine and Cellular Longevity*. 2012. doi: 10.1155/2012/583901.

[4] S. Balasubramanian, S. Kanade, B. Han, and R. L. Eckert, "A proteasome inhibitor-stimulated Nrf1 protein-dependent compensatory increase in proteasome subunit gene expression reduces polycomb group protein level," *J. Biol. Chem.*, 2012, doi: 10.1074/jbc.M112.359281.

[5] A. R. M. Ruhul Amin *et al.*, "Enhanced anti-tumor activity by the combination of the natural compounds (-)-epigallocatechin-3-gallate and luteolin: Potential role of p53," *J. Biol. Chem.*, 2010, doi: 10.1074/jbc.M110.141135.

[6] J. M. Bourre, "Effects of nutrients (in food) on the structure and function of the nervous system: Update on dietary requirements for brain. Part 1: Micronutrients," *Journal of Nutrition, Health and Aging*. 2006.

[7] O. I. Aruoma *et al.*, "Low molecular proanthocyanidin dietary biofactor Oligonol: Its modulation of oxidative stress, bioefficacy, neuroprotection, food application and chemoprevention potentials," *BioFactors*. 2006. doi: 10.1002/biof.5520270121.

[8] N. T., F. E., and A. S., "Food ingredients and lipid mediators," *Curr. Nutr. Food Sci.*, 2007.

[9] R. L. Prior *et al.*, "Antioxidant Capacity As Influenced by Total Phenolic and Anthocyanin Content, Maturity, and Variety of Vaccinium Species," *J. Agric. Food Chem.*, 2009.

[10] A. F. Zeina *et al.*, "Enfoque De Los Trastornos Del Equilibrio Acido-Base," *Biol. Eng. Trans.*, 2016.

CHAPTER 11

CHARACTERISTICS OF GRAVEL SOIL FOR FROST HEAVE AND MULTIFACTOR REGRESSION PREDICTION

Rohit Saini, Assistant Professor, Department of Agriculture and Environmental Sciences
Shobhit University, Gangoh, Uttar Pradesh, India
Email Id- rohit.saini@shobhituniversity.ac.in

ABSTRACT:

Typically, gravel soil is thought to be resistant to frost heave. Gravel soil, however, may also induce frost heave under specific circumstances, as evidenced by the numerous frost heave deformations of foundations in seasonal cold regions. A series of laboratory tests on one-dimensional frost heave were carried out utilizing an improved experiment equipment under the open- and closed-water replenishment conditions in order to get a thorough understanding of the frost heave features of gravel soil. On the frost-heaving ratio of gravel soil, the effects of various parameters including initial moisture content, clay content, compactness, overlying load, and water replenishing were examined. Additionally, the fundamental frost heave features of a gravel soil sample, such as the amount of frost heave, the speed of frost heave, the depth at which it freezes, the rate at which it freezes, and the distribution of moisture content after freezing, were examined. Additionally, the appropriate mechanisms were covered. Results revealed a linear link between initial moisture content, overlying load, and frost-heaving ratio in the open water replenishment condition as well as a quadratic polynomial association between clay content, compactness, and frost-heaving ratio.

KEYWORDS:

Appropriate Mechanisms, Cold Regions, Gravel Soil, Replenishment.

INTRODUCTION

Coarse-grained soils are frequently used as natural foundation materials in foundation engineering construction, including highways, railways, airports, dams, and excavations. They can demonstrate outstanding performance in compaction, shearing intensity, water permeability, and liquefaction under dynamic load, and have the advantages of rich reserves, easy access, and economics. Due to their large grain size, low grain surface energy, weak hydrophilic performance, little film water, large porosity, undetectable capillarity, and weak water migration, coarse-grained soils are typically classified as frost heave insensitive materials. Additionally, water readily turns to ice in situ. However, Liu et al. Zhang and Liu et al. Found that the coarse-grained soils can also produce obvious frost heave phenomenon under the combination of certain clay content the mass fraction of the particle with a diameter less than 0.075 mm initial moisture content, and freezing temperatures. These findings were based on the observation of frost heave of subgrade of Harbin-Dalian high-speed railway in Northeast In order to effectively minimize frost heave deformations of coarse-grained soil foundation, it is important to thoroughly investigate the frost heave characteristics of coarse-grained soil. The study of soil frost heave features has long been a focus and hot topic.

Numerous studies on the process of frost-heaving have been conducted since Everett and Miller put forward the first and second frost theories, respectively [1], [2]. These studies have produced some conclusive findings. Frost-heaving fillers, particularly the frost heave features of the coarse-grained soil, are also examined as our understanding of the mechanism causing frost heaving in permafrost grows. The experimental research of Chen et al. After that demonstrated that the frost-heaving ratio of sand gravel increases with the decreasing freezing

rate as a power function in the open water replenishing situation because it promotes cry suction.

Additionally, the addition of a little amount of powdered clay to the sand gravel enhances the particle viscosity, which in turn increases the gravel's susceptibility to frost heave under conditions of open water replenishment. According to Vinson et al. and Chen and Wang the presence of more fine-grained soil and clay minerals will make coarse-grained soil more susceptible to frost heave. Vinson et al. conducted additional research on the impact of fine particle size on the susceptibility of coarse-grained soil to frost-heaving, established a correlation between the frost-heaving ratio and segregation potential, and then noted that the correlation coefficient increases with decreasing particle size. Through laboratory testing, Xu demonstrated that even under conditions of complete water saturation, the frost-heaving ratio is no more than 2% when the proportion of powder and clay in granular soil is less than 12%. The frost-heaving ratio clearly rises as the concentration of powder and clay exceeds 12%. When examining the properties of frost heave in rocks during the freeze-thaw cycle, Islander discovered that porosity is a significant role.

The frost-heaving ratio of 1% is the standard to distinguish the frost heave sensitivity of coarse-grained soil by laboratory freezing tests, according to Konrad and Lemieux. They believe that when the content of fine-grained soil in coarse-grained soil is less than 7%, the frost heaving of coarse-grained soil is relatively small, but the amount of water supplement is very obvious. Using the fluorimetric tracing method, Aaronson and Sego identified the location of the unfrozen water film during the freezing of coarse-grained soil. Ye et al. Pointed out that gravel with fine grain content less than 15% belong to frost heave insensitive materials and can be used to build the ant freezing layer of subgrade. This is in accordance with the classification characteristics of railway subgrade filling material and the criterion of maintenance for railway track. The properties of a novel type embankment and coarse-grained embankment with regard to frost heave and thawing were examined by Lai et al. used an indoor frost heave experiment to show that the moisture content, porosity, and fine particle content all had an impact on the frost heave characteristics of graded crushed stone used as filler on the surface of the foundation bed. The moisture content was found to be the main influencing factor. Zhao et al. and Wang et al. highlighted that the main factor affecting the frost-heaving ratio of graded crushed stones was moisture content, followed by fine particle content, compactness, and cold end temperature, and that the correlation degree between them was not significant. This was done through the orthogonal experiment and grey correlation analysis of gradation crushed stone in the cold region.

To summarize, certain frost heave is also produced by the interaction of a few variables and levels of coarse-grained soil. The following elements of the gradation of soil particles, the number of fine particles and their mineral composition, the water content, density, permeability coefficient, capillary action, and external load are among the factors influencing the frost heave of coarse-grained soil. However, there are significant differences between the research findings and interpretation of the impact laws of several factors on coarse-grained soil frost heaving. In particular, it is unclear how to comprehend how different elements affect the characteristics of frost heave. The interaction and association between several parameters and the frost-heaving ratio of coarse-grained soil require more investigation. It is necessary to increase the connections between the findings of the research and the engineering itself [3], [4]. Therefore, a thorough investigation into the frost heave properties of coarse-grained soil is required. For many years, the research team has focused on the study of frost damage in the seasonally frozen region of the Qinghai-Tibet Plateau, particularly the systematic and ongoing observation of frost heave in the gravel soil foundation of the pavement construction at Ghoul Airport. In order to study the properties of frost heave in coarse-grained soil, the gravel soil in the

seasonally frozen area of the Qinghai-Tibet Plateau was chosen as the representative research object. In order to conduct a systematic investigation into the frost heave characteristics, a number of laboratory experiments on the frost-heaving ratio of gravel soil were conducted using an improved experiment apparatus under open- and closed-water replenishing conditions. For more information, see the 2.1 section. On the frost-heaving ratio, the effects of several parameters, such as initial moisture content, clay content, compactness, overlying load, and water replenishing, were compiled and addressed. A gravel soil sample's basic frost heave property, such as the amount, speed, depth at which it freezes, and the distribution of its moisture content after freezing, were also examined. The multifactor regression empirical formula was established by multiple regression analysis in order to forecast the frost-heaving ratio of gravel soil under certain collocations of variables and levels under the closed water replenishing condition. Finally, practical recommendations for controlling coarse-grained soil in seasonal frozen areas and preventing frost heave were made.

Prepared Soil Sample:

Ghoul Airport, which is situated in the seasonal frozen soil region of the Qinghai-Tibetan Plateau, was selected as the research background and prototype in this paper. Ghoul Airport has a climate that is characterized by low air temperatures the annual average temperature is about 4°C abundant rainfall snow long negative temperature periods even more than 8 months large frozen depths the maximum frozen depth is about 2.5 m small cooling rates, and long retention times of freezing fronts in soil. Because of this, moisture migration and frost heave are likely to be intensified under certain regional climatic conditions. All soil samples were taken from the Qinghai Ghoul Airport's field experiment area. Ghoul Airport's infill portion was primarily filled with natural gravel soil, but as is customary during construction, some surface silt could have been added, causing an uneven distribution of clay content. Due to the challenges associated with collecting, transporting, and preserving samples of undisturbed soil, this study adopted the reshaping of disturbed dirt using bagging, packing, impurities filtration, and air drying. The surface silt was chosen as the reference item, and the natural gravel soil was chosen as the main experiment topic. The screening test revealed that the native gravel soil has a clay concentration of 6.9% and that the surface silt has a 50% clay content. The soil base of the pavement at Ghoul Airport had an average clay percentage of 9.7%; at some measurement places, it even exceeded 20%. Therefore, we selected 45% as a comparison group and four kinds of clay content 10%, 15%, 20%, and 25% to research the impact of clay content on gravel soil's frost heave features. By evenly combining the two soil samples natural gravel soil and surface silt) in accordance with the various proportions, five different types of soil samples with clay contents of 10%, 15%, 20%, 25%, and 45% were produced [5], [6].

DISCUSSION

The grading curve of the aforementioned two soil samples was acquired by the grain size analysis test, which is displayed in Figure 1, in accordance with the test requirement Test Methods of Soils for Highway Engineering. Figure 1 shows that surface silt has a higher concentration of fine particles than natural gravel soil, which has a lower concentration. Furthermore, it was discovered that the curvature and coefficient of no uniformity of natural gravel soil 47 and 2.1, respectively are all higher than those of surface silt. Surface silt has a decent gradation since its coefficient of no uniformity is not less than 5 and its curvature is between 1 and 3. However, the natural gravel soil's coefficient of no uniformity is excessive, suggesting the lack of intermediate particles and poor gradation. In the actual building process, the surface silt has a tendency to be mixed with natural gravel soil, which not only raises the clay content of the soil foundation but also partially fills the middle diameter of the missing natural gravel soil. The frost-heaving phenomena of grit soil foundation is made worse by this effect. Five different types of soil samples comprising 10%, 15%, 20%, 25%, and 45% silt,

respectively, were prepared using the techniques outlined in "Soil Samples Preparation," and the results are displayed. It can be seen that while the standard maximum dry density dropped with clay concentration, the ideal beginning moisture content increased. The two types of soil samples had a relative density of 2.71, showing that there was very little effect of grain composition on relative density of soil grain and that all types of clay content in gravel soil may be calculated using the same number. A jar was used to test the relative density of the soil sample with 10% clay content, and a pycnometer was used to assess the relative density of the soil sample with 45% clay content.

Experimentation Principle:

The two primary indicators used to assess the frost heave characteristics of soil are frost heave amount and frost-heaving ratio. The quantity of frost heave is the soil's vertical displacement as a result of soil freezing. The former, also referred to as the frost heave coefficient, is the ratio of the increase in longitudinal height to the specimen's initial height under nonliteral deformation and one-dimensional freeze. The standard rule, however, is only relevant to small-sized soils like cohesive soil and sandy soil due to the small size of the equipment, and it is not suited for determining the frost-heaving ratio of gravel soil with greater particle size. The conventional frost-heaving ratio experiment setup also has a few flaws, hence

The following enhancements have been created:

(1) The soil sample box was made larger. The interior diameter was expanded from 10 cm to 15 cm, the height from 10 cm to 16 cm, and the distance between temperature sensors was increased from 1 cm to 2 cm in accordance with the principle of similarity.

(2) The experiment used a modified pressure system. To make the adjustment more practical, the weight pressure was switched out for air cylinder pressure, and the pressure range was expanded. An air compressor, pressure control valves, an air cylinder, and a connecting pipe make up the new pressure system.

(3) The mechanism for acquiring data has been enhanced. All sensors could automatically collect the signals of displacement and temperature, and the signals were recorded and saved by computer. The dial indicator with an accuracy of 0.05 mm was replaced by a displacement sensor with an accuracy of 0.001 mm for observing the changes in the frost heave amount.

(4) The system for cold baths has been upgraded. The cold bath method only set a preset freezing temperature in the typical frost-heaving ratio experiment setup, which was at odds with the true law of air cooling. Therefore, to make the freezing temperature more accurate to the scenario, a cold bath system with an automatic cooling function was employed. Additionally, the usual frost-heaving ratio experiment apparatus had the cold side placed at the bottom, which did not correspond to the foundation's true top-down cooling. The chilly side was positioned at the top of the improved frost-heaving ratio experiment apparatus to reflect the actual condition [7], [8].

The method for replenishing water has been enhanced. In order to accommodate the actual groundwater refilling, the water import was charged from top to bottom of the Maddox water replenishing bottle, which was employed to maintain a steady water level. The displacement sensor was used to track changes in the water level in the water replenishing system while automatically collecting and storing data. A soil sample box, a constant temperature environment of the box and temperature control system, a temperature monitoring system, a displacement acquisition unit monitoring system, a data acquisition unit, a pressure system, and a water replenishing system make up the improved frost heave experiment apparatus. The experiment included high-precision hardware, including the temperature sensor, displacement sensor, and data collecting terminal. The accuracy of the experimental results was guaranteed

by the calibration of every experiment unit prior to the start of the experiment. To lessen the mistake brought on by the sample cylinder's own distortion, the upper and lower sides of the cylinder wall were simultaneously tightened. Thermal insulating material was used to enclose the soil sample container in order to maintain temperature. For the duration of the experiment, two filter sheets were placed on top and bottom of the soil sample to stop moisture loss. Additionally, numerous sets of experiments were conducted in contrast to the conventional frost heave experiment equipment in order to confirm the dependability of the enhanced frost heave experiment apparatus.

In particular, the same soil sample 45% clay content the same test factor index compactness 95%, overlying load 20 kPa and the same cooling environment were used in the laboratory tests on one-dimensional frost heave conducted by the traditional experiment apparatus and the improved experiment apparatus, respectively. Figure 6 displays the results of the contrast testing. The nearly identical findings of the two groups of tests could be seen, demonstrating the dependability of the upgraded frost heave experiment setup. So, the frost-heaving ratio of coarse-grained soils may be tested using the enhanced frost heave experiment apparatus.

Experiment Programmed and Procedures:

Four criteria the starting water content, clay content, compactness, and overlying load were chosen, and an experimental design with multiple components was carried out. The beginning moisture content was created using the best initial moisture content for the 3-5 levels of clay in the aforementioned 5 types of soil. This ranges from 3% to 18%. We chose 85%, 90%, 95%, and 100% as the compaction indexes since the actual airport foundation's compactness was often managed at between 90% and 98%. The four levels of the overlying load 10 kPa, 20 kPa, 30 kPa, and 40 kPa were chosen. The multifactor analysis was carried out on the basis of the results of the single factor test in order to investigate the order in which different factors have an impact on frost-heaving ratio and to obtain the empirical formula for multifactor regression for predicting the frost-heaving ratio of gravel soil under specific collocations of factors and levels. In order to ensure that the sample's internal temperature reached 1°C, at which time the freezing process was started, the temperature of the cold bath and the calorstat were set at 1°C for 6 hours. To mimic the rule of atmospheric cooling, the cold bath's temperature dropped from 1°C at a rate of 0.2°C/h during the freezing phase, lasting roughly 72 hours until stability of deformation. The sample was immediately taken out of the soil sample box after freezing, and was then evenly divided into 7 pieces by slicing. The sample's moisture distribution was quantified using the drying method [9], [10].

Findings and Evaluation:

Table 2 illustrates how different beginning moisture contents affect the frost-heaving ratio. When clay percentage is constant, the frost-heaving ratio increases with starting moisture content. The following is thought to be the cause: The soil sample's water bonding becomes tighter as its moisture level rises, and the ongoing movement of water becomes more noticeable. The fitting curves show a unary linear relationship between the frost-heaving ratio and the starting moisture content. The fitting curve's size order of slope is 25% > 45% > 15%. This may be explained by the fact that the soil sample with the lowest dry density among the three had a 45% clay content (see the outcomes of the standard compaction test). The bigger the soil pore, the more ice it can hold, and the lower the frost-heaving ratio, the looser the soil structure is. The soil sample with a clay concentration of 25% has a higher dry density than the one with a clay content of 45%, and the moisture migration was more noticeable due to the smaller soil pores. The soil samples with a 15% clay content have the highest dry density and cohesive force between soil particles of the three. As a result, it is most likely to result in a

combined water film that overlaps and thickens, which reduces soil permeability and narrows the channel of water migration.

Clay content:

Illustrates how different clay concentrations affect frost-heaving ratio. The frost-heaving ratio rises with clay concentration in accordance with a polynomial function when the saturation level is held constant, as shown by the fitting curves. The following is thought to be the cause: An increase in clay content causes soil particles' total surface area and surface energy to increase. Higher surface energy causes soil particles to absorb more water film. A thin film channel that is ideal for ongoing moisture transport is formed by the water film that connects soil particles. Since the clay content is fixed, the frost-heaving ratio rises as saturation levels do. The cause is thought to be as follows: in addition to the fact that the initial moisture content rises as saturation levels rise, decreasing soil pore volume and easier filling of the pore with frozen ice both increase the likelihood of soil particle displacement due to frost heave. By comparing the coefficients of the three fitting curves in Table 3, it can be seen that the growth rate gradually slows down and that the frost-heaving ratio and the clay content have a nonlinear rising relationship. When there is little clay present, the frost-heaving ratio rises quickly. The growing rate of the frost-heaving ratio gradually slows down when the clay content is high. There are about four phases in the gravel soil frost heave process, as may be observed.

(i) During the frozen-shrink phase, the amount and rate of frost heave development were extremely modest, developed slowly, and even displayed a negative value. Due to the contraction of soil particles at low temperatures, the quantity of frost heave not only did not rise, but it actually decreased.

(ii) The quickly growing phase: As the freezing process continued, the amount of frost heave increased. Due to the severe ice segregation that occurred during this time, the frost heave speed surged quickly and peaked, suggesting that the rate of soil frost heave deformation increased quickly.

(iii) The slow-increasing phase: Over time, the pace of the frost heave slowed and the volume of frost heave grew slowly. This might be explained by the limited permeability of the frozen fringe and the insufficient moisture supply under the closed water replenishing situation, both of which would reduce moisture migration to the ice lens. The sluggish growth of the thickness of ice lens and degree of succession lead to the lowering of growth speed of frost heave amount.

(iv) The comparatively steady phase, in which the frost heave speed remained constant until the experiment's conclusion. The frost heave speed fluctuated within much tighter bounds than in phases (2) and (3), despite oscillations that may have been brought on by unstable voltage. The quantity of unfrozen moisture reduced, which led to a reduction in moisture migration and the cessation of ice lens growth. Under a closed water replenishment environment, the differential in soil moisture potential along the frost front is what essentially drives the moisture migration. In turn, the amount of frost heave decreased until it nearly reached a constant number.

Freeze Depth and Speed of Freezing:

Figure 10 depicts the link between the depth of the frozen layer and the duration of the freezing. At the start of the freezing process when cooling was provided, the frozen depth was shown to gradually shift lower from the top of the sample initial moisture content 9%, clay content 15%, compactness 95%, and overlying load 20 kPa. The variable gradient of frozen depth gets less and smaller as freezing time goes on. The soil sample eventually entered a stabilization phase with minimal changes in frozen depth. Initial moisture content, thermal conductivity, and

cooling temperature were found to be related to the velocity of frost front progress and maximum frozen depth [11], [12].

CONCLUSION

Under the closed water replenishing condition, the frost-heaving ratio rose linearly with initial moisture content, rose with clay content in accordance with a polynomial function, decreased gently linearly with an increase in overlying load, increased first and then decreased with an increase in compactness in the form of a polynomial function, and approached its maximum at a compactness of 95%. The frost-heaving ratio of gravel soil can be observed to increase many times higher under the open water replenishing condition than under the closed water replenishing condition. It can be seen that there are about four phases in the process of frost heave of gravel soil: the frozen-shrink phase, the fast-increasing phase, the slow-increasing phase, and the generally stable phase. Each phase's freezing speed and frost heave speed are closely connected. The distributions of moisture content after freezing showed that the gravel soil sample experienced moisture migration during freezing. The fact that the frozen front section's moisture level was much higher than the original moisture content suggests that moisture moved to the freezing front during freezing. The multifactor regression study produced the multifactor regression forecast formula. As can be observed, under closed water replenishing conditions, the initial water content and clay content have a significant impact on the frost-heaving ratio of gravel soil. This regression model's application, which has definite engineering application value, can forecast the frost-heaving ratio under the comprehensive influence of several various elements.

REFERENCES:

[1] X. Long, G. Cen, L. Cai, and Y. Chen, “Experimental Research on Frost Heave Characteristics of Gravel Soil and Multifactor Regression Prediction,” *Adv. Mater. Sci. Eng.*, 2018, doi: 10.1155/2018/5682619.

[2] J. Liu, G. Cen, and Y. Chen, “Study on frost heaving characteristics of gravel soil pavement structures of airports in Alpine regions,” *RSC Adv.*, 2017, doi: 10.1039/c7ra02151h.

[3] L. B. Wu, F. J. Niu, Z. J. Lin, W. Qi, and W. J. Feng, “Effect of replacing-filling and dewatering-draining measures on frozen characteristics of weak subgrade in cold valley region,” *Jiaotong Yunshu Gongcheng Xuebao/Journal Traffic Transp. Eng.*, 2018.

[4] Y. Ye, Z. Wang, A. Cheng, and M. Luo, “Frost heave classification of railway subgrade filling material and the design of anti-freezing layer,” *Zhongguo Tiedao Kexue/China Railw. Sci.*, 2007.

[5] G. Cen, X. Long, G. Hong, J. Liu, X. Wang, and Y. Jia, “Frost heaving properties of gravel soil in seasonal frozen region of Qinghai-Tibet Plateau,” *Harbin Gongye Daxue Xuebao/Journal Harbin Inst. Technol.*, 2016, doi: 10.11918/j.issn.0367-6234.2016.03.009.

[6] L. A. Soltis, “Compacted Fill For Plant Foundations.,” *Plant Eng. (Barrington, Illinois)*, 1977.

[7] V. R. Voller *Et Al.*, “Rodio Geotechnik Ag,” *Sol. Energy*, 2011.

[8] Chen Xiabai, Jiang Pin, And Wang Yaqing, “Some Characteristics Of Water Saturated Gravel During Freezing And Its Applications.,” In *Computers & Chemical Engineering*, 1980.

[9] A. L. Samuel, “Some studies in machine learning using the game of checkers,” *IBM J. Res. Dev.*, 2000, doi: 10.1147/rd.441.0206.

[10] K. Pan, D. N. Kim, F. Zhang, M. R. Adendorff, H. Yan, and M. Bathe, “Lattice-free prediction of three-dimensional structure of programmed DNA assemblies,” *Nat. Commun.*, 2014, doi: 10.1038/ncomms6578.

[11] W. D. Hairston and J. A. Maldjian, “An adaptive staircase procedure for the E-Prime programming environment,” *Comput. Methods Programs Biomed.*, 2009, doi: 10.1016/j.cmpb.2008.08.003.

[12] A. L. Samuel, “Eight-move opening utilizing generalization learning. (See Appendix B, Game G-43.1 Some Studies in Machine Learning Using the Game of Checkers,” *IBM J.*, 1959.

CHAPTER 12

TEMPERATURE EFFECTS ON THE ADHESION PROPERTIES OF THE SOIL-STRUCTURE INTERFACE

ABSTRACT

Under mud cake working conditions, the constant contact between the shield cutter head and the soil on the excavation surface can result in high temperatures during the shield tunneling and excavation process, which alters the characteristic of the soil and cutter head adhesion and intensifies the phenomenon of making a mud cake on cutter, ultimately creating a vicious cycle. A home-made experiment apparatus was used to test the soil adhesive situation and adhesion force at various interface temperatures in order to explore the impact of temperature on the features of the adhesion of the soil on the surface of the structure. The results showed that the moisture content has a significant impact on the soil's adhesion force. The adhesion force initially increased and then decreased as the moisture content increased, reaching its peak value close to the moisture content of the plastic limit. When the contact temperature is low, the adhesion force varies very gradually. Except for soils with high moisture content, adhesion force increases as the interface temperature rises beyond 50°C; in addition, the amount of soil attached to the surface of a structure is significantly influenced by the interface temperature.

KEYWORDS:

Excavation Surface, Intensifies, Interface Temperature, Shield Cutter.

INTRODUCTION

China is now seeing a significant uptick in subway construction. Shield technique has been extensively used as the primary method for building subways because to its benefits of minimal impact, high mechanization, excellent safety, low labor intensity, and quick development. Shield tunneling often runs into the challenging issue of building mud cake with cutter head while operating in complicated strata, particularly in clay strata, mudstone strata, and other strata rich in clay mineral particles. When the shield cutter head penetrates the clay layer and forms solid or semisolid masses by compacting the cutter head, the clay debris cutoff will stick to the cutter head's surface and prevent it from penetrating, decreasing the penetration so that the efficiency of shield excavation decreases. One of the key factors in the development of mud cake on the cutter head surface is the adherence of soil. The presence of mud cake will not only raise the shield cutter's torque but will also obstruct the slurry discharge pipe's suction aperture, which will negatively impact shield construction technology and construction safety. The cost of construction will significantly rise owing to the treatment and repair of a number of construction issues, including risk mitigation, mud cake removal, shield system rebuilding, stop and open tank operation, and residue improvement [1], [2].

The temperature of the shield cutter head is typically 40–50°C under normal working conditions, but during tunneling, particularly for the composite stratum, the torque and total thrust of the cutter head significantly increase as the advance speed slows down due to the formation and growth of the mud cake, resulting in a temperature of 400–500°C or even higher. A kind of vicious circle develops as a result of the high temperature, which can raise the temperature of the soil in contact with the excavation surface and improve the clay's adhesion, causing the soil moisture to migrate and intensify the formation of mud cakes. This phenomenon of mud cakes on the cutter head is further aggravated as a result. Numerous studies suggest that the soil's temperature and moisture content significantly affect its properties. To determine the formation mechanism and development law of shield mud cake

and resolve the prevalent engineering issue of mud cake formation on the cutter head, it is necessary to comprehend the law of the influence of the increasing interface temperature on the adhesion properties of the soil. This effect of temperature occurs primarily at the interface of the cutter head and the excavation surface during shield tunneling. In order to determine the law of the influence of temperature on soil adhesion, the amount of adhered soil and the force of adhesion between soil and the metal structure surface at various interface temperatures were tested in this study. This allowed researchers to better understand the law governing the formation and development of mud cakes and offered a solution to the issue of mud cake on the cutter head [3], [4].

Experimentation Equipment:

To evaluate the soil's adherence to the metal surface at various temperatures, a specially developed adhesive test apparatus was created, as shown in Figure 2. By drawing on the work of other researchers, this experiment created a metal cone as the test specimen in order to limit the impact of the interface's lateral friction on the determination of adhesion and to ensure that the soil thoroughly connects with the interface. The test cone had an apex angle of 50° and was constructed of 304 stainless steels. The bottom cone was in touch with the test soil and stood 32 mm tall. To heat the test cone, the top portion of the cone was covered with a polyimide heating film. The temperature controller powered the heating film and measured the cone's temperature using an incorporated negative temperature coefficient temperature sensor. The space between the NTC temperature sensor and the cone was filled with silicone grease to transfer heat for improved temperature measurement. The electric traction test equipment was used to drive the test cone in order to draw the top sling and remove the test cone's surface from the test soil.

Depicts the experiment's traction test apparatus. In accordance with the predetermined rotational criteria, the pulse signal generator generated a pulse signal. The driver first received the pulse signal and then turned it into an angular displacement before sending it to the stepping motor, which rotated and produced a rotational torque. The rod was attached to the stepping motor, and a sliding block was fastened to the screw rod so that the stepping motor's rotation translated into the sliding block's vertical displacement. The electronic tension meter was fixed to the sliding block through the connecting piece, causing its vertical displacement to occur simultaneously with the sliding block. The connecting rope's force measuring hook was attached to one end of the device while the other end was fastened to the test cone sling so that the electronic tension meter could measure the cohesive force.

Soil Sample Preparation:

The undisturbed soil was dried and crushed, then sieved to retain the soil with particle diameters of 0.5 mm or less. This soil was then mixed evenly with water to the design moisture content, applied using the paste method to fill the mixed soil into the soil box by several layers, and scraped until the soil surface was flat. Finally, a soil sample was taken by standing for 24 hours while being covered in plastic film. It may be said that the soil sample is effective and suitable for testing if there is an error of less than 0.5% between the measured moisture content and the planned value.

Experiment Design:

In this experiment, soil samples were taken with varying moisture contents: 19%, 21.21% 23%, 27%, 31%, and 35%. For soil samples with temperatures of 26.5°C (room temperature), 40°C, 50°C, 60°C, and 70°C, respectively, the needed pulling force with a velocity of 5 mm/min and the adherent dirt on the cone surface were recorded for each specified value of moisture content. These were the precise techniques:

(1) Place the upper sling on the connecting rope of the tension meter in the electric traction test equipment, press the bottom portion of the test cone vertically and gently into the ground, and stand for two minutes.

(2) Activate the NTC temperature sensor, check the temperature controller's collection status, set the controller's temperature to control the interface's temperature, and activate the polyimide heating film. When the interface reaches the preset temperature, the temperature controller automatically shuts off and the heating stops.

(3) Start the electric traction test device, provide higher tension to the test cone to remove it from the test soil, check the tension that was applied when the cone surface was being separated from the soil, and record the condition of the soil that was stuck to the test cone's surface [5], [6].

DISCUSSION

The soil body started to rheology at the start of the test after coming into contact with the test cone's tip while being compressed. The dirt surrounding the spinal tip started to stretch to the top end of the test cone as it sank into the ground, creating a contact surface with the test piece. An adhesion interface eventually developed as a result of the redistribution of soil particles and soil moisture, which caused the contact area to progressively grow and start to show signs of a water ring and finally a continuous water film. The adhesion contact was disrupted along the weakest ant stripping plane by exerting force against the test cone. These fragmented soil layers adhered to the cone's surface and moved when the weakest ant stripping plane developed within the soil body. The Changes in Soil Sample Adhesion Force with Changes in Moisture Content. The interface separation tensile test was performed on six sets of materials with varying moisture concentrations. This research will use the applied tensile force during the separation of the soil from per unit area of the test cone surface as the measured adhesion force for analysis by referring to the prior research. This is because there are two adhesion forces in the direction of normal and tangent and they primarily act on the contact surface between the metal cone and the soil.

Depicts how variations in moisture content affect the soil samples' ability to adhere to one another. It was demonstrated that the adhesion force of the five groups with five different values of interface temperatures increased quickly with the increase in moisture content before the plastic limit, with the maximum value appearing close to the plastic limit. Ultimately, this force decreased with the increase in moisture content. The adhesion force eventually stabilized at somewhat high moisture content levels. This legislation generally matched the findings of other researchers' studies. The fluctuation trend shows that, regardless of the moisture level, there was very little adhesive force. When the moisture content was between the liquid and plastic limits, it had a noticeable impact on the adhesion force; the adhesion force increased as it got closer to the plastic limit. The contours of the adhesion force variation with moisture content at lower interface temperatures (26.5°C and 40°C) almost coincided.

The Adhesion Force of Soil Samples Varies with Changes in Interface Temperature. At five distinct contact temperatures ranging from 26.5 to 70°C, the adhesion force on the per unit area of six sets of samples with varying moisture levels was assessed. Demonstrates that given the low contact temperature, the adhesion force of each group changed slightly with temperature. Except for the soil with higher moisture content (31% and 35%), the adhesion force decreased somewhat when the interface temperature reached 50°C. As the interface temperature continued to rise, the adhesion force of each moisture content group increased when the temperature exceeded 50°C. In the case of higher moisture content (%), the adhesion force slightly increased with the rise in interface temperature. When the interface temperature was low (40°C), the amount of adhered soil after the interface separation was extremely small;

when the soil moisture content was between 21.21% and 31%, the amount of adhered soil increased with the increase of the interface temperature; and when the interface temperature was greater than 40°C, the growth rate gradually increased while the adhesion amount increasing exponentially with temperature. When the sample was at a lower degree of moisture content (%), there was almost no soil adhered on the cone and there was no effect of the interface temperature on the adhesion as the interface temperature increased continuously. The amount of adhered soil slowly increased when the interface temperature was greater than 50°C [7], [8].

As when the test cone surface was separated from the soil body under conditions of low interface temperature and moderate soil moisture content, the amount of adhered soil was very small and had only a small amount of flake-like soil mass adhesion. When the interface temperature rose, the adhered soil started to adhere in the shape of blocks and gradually developed after the interface was separated. When the interface temperature reached higher values, the amount of a soil mass adhesion increased. Since the soil was dry and loose when the sample's moisture content was low the quantity of adhering dirt was mostly unaffected by the temperature of the contact. The adhered soil can adhere to the cone surface in a paste form after the interface was separated when the interface temperature was low; as the interface temperature rose, the adhered soil decreased and paste adhered soil disappeared; when the interface temperature was high, a large number of flake-like soil masses gradually adhered to the surface of the cone. When the soil was at the state of high moisture content, the soil was soft and flow plastic.

Discourse:

The soil exhibited both cohesion and adhesion properties at once as a complex physical system. Adhesion is the mechanical behavior of soil clinging to the surface of other structures, while cohesion is the attraction between soil particles. A particular depth of soil under the interface layer was necessary for soil to adhere to the interface. The strength and location of the weakest ant stripping plane determine the energy needed for separation and the position of the separation plane when the interface separates. The adhesion to the surface of the structure thus relies on the dynamic fluctuation of the cohesion and external adhesion of the soil at a certain depth within the effect range of the interface. Additionally, the interaction between solid soil particles, water, and structural surfaces leads to the cohesion and adhesion of soil. When liquid water comes into contact with a solid surface, the structure of the water adjacent to the solid surface will become stable from a thermodynamic perspective because of the interaction between the force fields of the solid surface and water molecules. This means that the water's bonding structure will increase and its energy will decrease. A certain force had to be applied to the adhesion interface to increase the interface energy in order to achieve tensile failure because the water film between clay particles and the water film between the particles and the structure's interface had a low energy level. The size, thickness, and energy state of the interface water film are often correlated with the tensile failure force. Soil moisture content at a certain depth and interface energy state have an impact on the properties of the adhesion of the soil-structure interface within the influence range of the interface.

Moisture content's effects on adhesion characteristics:

The soil's ability to adhere is most obviously influenced by its moisture level. When the soil moisture content falls below the plastic limit, the soil becomes dry and brittle, an annular water film forms at the place where the soil particles come into contact with one another but the water films are not linked, and structured water occurs. The internal cohesion of the soil is greater than the external adhesion force between the soil and the outer surface due to the large specific surface area of clay particles and its greater binding capacity with moisture than that between

moisture and metal surface, which causes the interface failure to primarily occur at the interface between the soil and the structure surface, and the external adhesion force of the soil controls the adhesion. The external adhesion force is relatively minimal since the water layer between the soil and the surface of the structure is currently independent and discontinuous, which results in a low adhesion force and a little quantity of attached soil on the macroscopic aspect.

As the moisture content rose, the water ring formed. The water films between soil voids connected and formed a network when the moisture content reached the plastic limit; as a result, the water films between soil and the surface of the structure started to become continuous, increasing the soil's external adhesion force, which was seen as a large adhesion and a very low amount of adhered soil. The water film thickened as the moisture content continued to rise, the effect of the solid surface on the middle portion of the water film decreased, the energy was the same as that of the free water, and the external adhesion force gradually decreased, which was demonstrated by the gradual reduction in adhesion force and the small amount of adhered soil. When the moisture content was extremely high, the spaces in the soil body were nearly completely filled with water. If the moisture content is raised further, the rate at which the adhesion force decreases will slow down.

Temperature Effects on the Adhesion Characteristic:

The adhesion qualities are also rather obviously influenced by the contact temperature, which is mostly seen in two areas:

(1) The variable in moisture content under the effect of the interface with moisture and heat migration brought on by local heating.

(2) As the temperature of the interface rises within the influence range of the interface, the energy of the soil water increases and the energy needed to destroy the adhesion interface decreases.

When the interface temperature was low for soil with low moisture content, the temperature gradient between the soil at the interface and the internal soil was low, and the soil moisture and interface energy within the influence range of the interface did not change much with limited influence on the adhesion force and the amount of adhered soil. However, when the interface temperature increased to about 50°C, the moisture migration caused by the temperature gradient force was slowed down. The external adhesion force is lower than the internal cohesion of the soil under the same moisture conditions because the interface adhesion is primarily affected by the interface energy and the high energy at the interface. As a result, it behaves as broken at the interface, has less adhered soil, and has decreased adhesion force compared to low interface temperature. The moisture migration produced by the temperature differential became more apparent as the interface temperature rose and the pore water in soil voids within the effect range of the interface moved to the interior of the soil (Figure 8). While the cohesion force and external adhesion force rose, the moisture at the contact dropped. At this point, the soil moisture content at the interface had a major impact on the characteristic of interface adhesion, and the adhesion force rose. Simultaneously, a high energy plane with a moderate temperature and moisture content emerged within the soil as a result of the interface temperature's conduction to the soil's interior. Because this plane has a low harm energy, it is the least effective ant stripping plane. The weakest ant stripping plane formed from the interface to the interior of the soil as the interface temperature rose and because the internal cohesion force on this plane was lower than the external adhesion force, damage gradually developed from the interior of the soil during separation as the amount of adhered soil rapidly increased.

The increase in interface energy brought on by a rise in temperature had little impact on the adhesion of soil, but the impact of a change in soil moisture was clear for soil with a higher moisture content due to the thicker water film and the low value of energy required for tensile failure. The soil moisture dropped and the adhesion force rose for the soil at the contact as a result of the interface temperature. When the adhesion force was stronger than the cohesion force, the damage came from inside the soil, and the attached soil grew. When the soil's moisture content was high, it was in a flow plastic condition and the cohesive force was extremely weak. The soil was easily damaged from the inside when paste soil was adhered to the contact surface when the interface temperature was low. As the interface temperature rose, the soil's moisture content decreased, its cohesion increased quickly, its integrity at the interface increased, and the amount of attached soil decreased. The failure mode changed from interface failure to the failure of the weakest ant stripping plane with higher moisture content inside the soil as the interface temperature continued to rise. As a result, the soil moisture content at the interface continued to decline and the external adhesion force of the interface increased [9], [10].

CONCLUSION

By examining the test results and the aforementioned occurrences, it can be deduced that the moisture content and interface temperature both significantly affect the soil-structure interface's adhesion properties. The most evident factor affecting the soil's ability to adhere is its moisture level. The adhesion force is relatively low while the moisture content is below the plastic limit, but it increases quickly and peaks just around the plastic limit when the moisture content progressively approaches to that level. When the moisture content rises to the liquid limit, the adhesion force steadily declines. The moisture content of the soil within the interface's influence range will be impacted by its temperature, resulting in a decrease in the moisture content of the soil at the interface and a change in the adhesive force. With the exception of the sample with a high moisture content the adhesion force varies little with temperature when the interface temperature is low; however, as the interface temperature approaches 50°C, the adhesion force drops. The adhesive force of each group grows as the interface temperature rises constantly; when the moisture content is larger, the adhesion force somewhat rises as the interface temperature rises. The location of the weakest ant stripping plane within the interface's influence range will be impacted by the interface's temperature, which also alters the composition of soil that has adhered. When the soil moisture content is modest, the quantity of attached soil rises exponentially with the interface temperature; however, when the soil moisture content is larger, the amount of adherent soil initially rises with the interface temperature before falling. After the interface has been separated, there is essentially no dirt adhering to the metal surface when it is reasonably dry, and the temperature of the interface has little effect on the adhesion.

REFERENCES:

[1] K. D. Ziegel, “Literature Abstracts,” *J. Texture Stud.*, 1972, doi: 10.1111/j.1745-4603.1972.tb00642.x.

[2] R. Chemicals, A. Chemical, S. Specifications, C. Society, N. Formulary, and U. S. P. Convention, “Standard Test Method for Hydroquinone in Vinyl Acetate 1,” *Polymer (Guildf).*, 2001.

[3] J. S. Aguilar, “Alternativas De Aprovechamiento De La Cascarilla De Arroz En Colombia.,” *J. Agric. Food Chem.*, 2009.

[4] Minam, “Ley Nº 27446, Ley del Sistema Nacional de Evaluación de Impacto Ambiental,” *J. Agric. Food Chem.*, 2001.

[5] H. Chelabi, L. Khiari, J. Gallichand, and C. A. Joseph, "Soil sample preparation techniques on routine analyses in Quebec affect lime and fertilizer recommendations," *Can. J. Soil Sci.*, 2016, doi: 10.1139/cjss-2015-0062.

[6] R. J. VanCott, B. J. McDonald, and A. G. Seelos, "Standard soil sample preparation error and comparison of portable XRF to laboratory AA analytical results," *Nucl. Instruments Methods Phys. Res. Sect. A Accel. Spectrometers, Detect. Assoc. Equip.*, 1999, doi: 10.1016/S0168-9002(98)01000-6.

[7] J. S. Nikolić *et al.*, "Novel Sorbent and Solvent Combination for QuEChERS Soil Sample Preparation for the Determination of Polycyclic Aromatic Hydrocarbons by Gas Chromatography–Mass Spectrometry," *Anal. Lett.*, 2018, doi: 10.1080/00032719.2017.1367007.

[8] S. Goto, T. Hosokawa, Y. Saitoh, and K. Sera, "Soil sample preparation for PIXE analysis," *Int. J. PIXE*, 2014, doi: 10.1142/s0129083514400014.

[9] S. S. Albaseer, R. Nageswara Rao, Y. V. Swamy, and K. Mukkanti, "An overview of sample preparation and extraction of synthetic pyrethroids from water, sediment and soil," *Journal of Chromatography A*. 2010. doi: 10.1016/j.chroma.2010.06.058.

[10] D. S. Bol'Shakov, V. G. Amelin, and A. V. Tret'Yakov, "Determination of polar pesticides in soil by micellar electrokinetic chromatography using QuEChERS sample preparation," *J. Anal. Chem.*, 2014, doi: 10.1134/S1061934814010055.

CHAPTER 13

EXPLORING THE EXPANSIVE SOIL IMPORTANCE: DYNAMIC MECHANICAL PROPERTIES AND ENERGY DISSIPATION

Rohit Saini, Assistant Professor, Department of Agriculture and Environmental Sciences
Shobhit University, Gangoh, Uttar Pradesh, India
Email Id- rohit.saini@shobhituniversity.ac.in

ABSTRACT:

The split-Hopkinson pressure bar test was used in this study to examine the dynamic mechanical properties of expansive soil stabilized by fly ash and lime under impact stress. The dynamic mechanical characteristics and final fracture morphology of stabilized soil were examined, and the failure mechanism was looked at from the angle of energy dissipation. The test findings show that plain soil and pure fly ash-stabilized soil both display high flexibility under an impact pressure of 0.2 MPa. The stabilized soil exhibits apparent brittle failure after lime addition. With the change in mix proportions, the dynamic compressive strength and absorbed energy of stabilized soil first rise and then fall. At 20% fly ash and 5% lime (20% F + 5% L the dynamic compressive strength and the absorbed energy both reach their maximum values. Most of the incident energy is reflected back to the incident bar during the test. While the absorbed energy is inversely associated with the fractal dimension, the absorbed energy of stabilized soil increases linearly with the growth in dynamic compressive strength. Regarding the two distinct magnification ratios, the fly ash-lime combination stabilized soil has a lower fractal dimension of pore morphology than the plain soil.

KEYWORDS:

Compressive Strength, Incident Energy, Morphology, Split-Hopkinson.

INTRODUCTION

In terms of moisture fluctuations, expansive soil is a form of clay that frequently expands and contracts. Iolite and montmorillonite are two of its primary mineral constituents. The issue brought on by expansive soil was not initially identified by the United States Reclamation Bureau until 1938, during a foundation engineering project in Oregon. Engineers are well aware of the harm that expanding soil may do to engineering. Many academics have been researching different techniques to stabilize expanding soil in recent years. According to the research findings, fly ash cement and lime and other ingredients all work well to lessen the expansion potential of expansive soil. In addition to researching ingredients like fly ash and lime to lessen expansive soil's expansion potential, stabilized soil's static mechanical properties have also undergone extensive research. In order to determine the ideal mix proportion of the modifier, pertinent research have determined the change laws of unconfined compressive strength split tensile strength and shear strength as well as other characteristics of stabilized soil with varied mix proportions. In addition, several researchers have microscopically depicted the mechanism for the stabilization of expansive soil with fly ash and lime. Based on the aforementioned works, a wealth of knowledge has been gathered on the study and use of stabilized expansive soil [1], [2].

However, there are very few investigations on the dynamic mechanical properties of stabilized soil under impact load, and the majority of research papers primarily concentrate on the quasi-static state. In actual engineering, the stabilized expansive soil carries both static and dynamic impact loads. The subgrade of the airport is often constructed using stabilized expansive soil. The runway roadbed is severely damaged when an aircraft is swept to the ground quickly.

Additionally, the reinforced expanding soil foundation is dynamically impacted by mechanical excavation or blasting surrounding it. Additionally, the stability of the composite foundation may be impacted by impact loads such earthquakes and vehicle vibration.

The dynamic mechanical properties of soil materials differ substantially from their static mechanical counterparts in all of the aforementioned scenarios where the dynamic mechanical response of soil materials is at issue. Research on the dynamic mechanical characteristics of stabilized soil under impact load is therefore crucial. The dynamic and static mechanical characteristics of materials or structures differ significantly, which is primarily expressed in two aspects: First, the solid medium is in a condition of static equilibrium under the influence of static loads, allowing the inertial action of the medium element to be disregarded. The motion parameters change substantially over a brief time scale of milliseconds, microseconds, or even nanoseconds, which is a characteristic of impact loads. The inertial characteristics of the medium micro body must be taken into account under the circumstances of such dynamic stresses. Second, the motion parameters fluctuate rapidly on a short time scale due to the nature of the heavy impact loads, which is certain to result in a high strain rate. The strain rate in a traditional static test is often in the range of 105s1–101s1, whereas in an impact test, it is typically in the range of 101s1–104s1 and even as high as 107s1, which is many orders of magnitude higher. Numerous experiments have shown that materials' mechanical behavior frequently varies as strain rates alter. Other types of inelastic deformations and fractures, such as the diffusion process brought on by stress, the evolution of damage, and the expansion of cracks, are no transient responses that are developed at a finite strain rate, in addition to the fact that the ideal elastic deformation can be seen as a transient response. Therefore, the relationship between the strain rate and the mechanical properties of the materials is fundamental. The yield limit and ultimate strength of materials grow as the strain rate rises, but elongation decreases. On the other hand, the yield lag and fracture lag become evident. The relationship between the material constitutive equation and strain rate is another reason why materials respond mechanically differently to impact loads than they do to static loads. For materials with a strain rate range of 102 s-1 to 104 s-1, the split-Hopkinson pressure bar test is frequently used as a standard technique to determine the dynamic mechanical properties. The SHPB test was used in this work to examine the dynamic mechanical characteristics of expansive soil stabilized with lime and fly ash [3].

Test Techniques:

The test's soil sample came from a building site in Huainan City's Shannon New District. Based on the measurements of the soil samples' physical characteristics, which are displayed in Table 1, it can be concluded that the soil is a weak expanding soil. According to X-ray diffraction analyses of fly ash and lime, portlandite and vanadium selenite make up the majority of the fly ash's composition, with mullet and quartz making up the remainder. To prepare the samples, the soil was first ground up and passed through a 0.5 mm sieve. A 50 mm SHPB test apparatus, as illustrated in Figure 1, was employed for the impact test. It consists of a loading system, a striker bar, an incidence bar, a transmitted bar, and a signal acquisition system.

DISCUSSION

Figure 3 displays the dynamic compressive stress-strain curves of the stabilized expansive soil with various mix amounts. As demonstrated, the expansive soil stabilized by lime and fly ash has a much higher strength than soil stabilized by fly ash alone. Plain soil's and pure fly ash-stabilized soil's strengths increase initially before progressively declining after reaching their highest values. Then a yield platform with clear signs of plastic failure arises. The strength of the stabilized soil peaks after lime is introduced and then rapidly declines, indicating a typical brittle failure. The relevant dynamic compressive strength. When fly ash is applied

individually, the stabilized soil's strength first rises and then falls as the fly ash content is increased. When 20% F is applied, the stabilized soil's peak strength increases by 47.9% to 713.58 kPa, which is higher than the strength of unsterilized soil (480.02 kPa). This is due to the fact that, within a range of fly ash contents (0%–20% F), the pozzolanic reaction of fly ash tends to produce certain hydration products that help to improve the strength of the stabilized soil. But because fly ash is a sort of fine spherical particle with a low strength, too much of it will unavoidably result in uneven mixing and agglomeration in the soil, which would weaken the surface where fly ash particles come into direct touch with one another. The surface that breaks first when exposed to an external load diminishes the strength of the soil samples. With the addition of lime, the stabilized soil strength change law displays the same regularity, peaking at 1668.75 kPa at 20% F + 5% F content, an increase of 247.9% above plain soil. The findings demonstrate that lime has a large hydrating effect on stabilized soil, greatly enhancing dynamic compressive strength.

Energy Dissipation Analysis:

The process of converting energy is what ultimately causes failure from the standpoint of thermodynamics. Materials always exchange energy with the outer environment during their failure process. The result of internal micro cracks continuously accumulating and growing is macroscopically large fracture. Thus, energy is dissipated when the process from microscopic damage to macroscopic failure occurs. In the end, material failure refers to an energy-driven state instability phenomenon. Therefore, it is crucial to examine energy dissipation in order to understand the failure process of rock and soil. Energy is the main force that drives soil deformation and failure under the influence of a dynamic impact load. The soil is a typical heterogeneous substance with lots of internal pores and fissures. The soil sample experiences stress concentration at these faults when subjected to the static load, which causes the fracture to propagate and cause failure. Due to the dynamic impact load's quick action time, the strain rate appears to be significant, and the internal soil fractures are expanding too quickly for them to do so normally. As a result, at the macroscopic level, the soil sample shows uneven and comminuted failure. As a result, its failure mode, failure process, and energy dissipation laws all appear to differ significantly from those under static stress. Thus, understanding the energy dissipation process of the stabilized soil is helpful in identifying the soil sample's failure mechanism [4], [5].

Fracture Morphology Analysis:

Figure 9 depicts the fracture morphology of stabilized soil during the SHPB test for various mix amounts. It can be noted that the soil samples under the impact load demonstrate good integrity, with the exception of a few cracks and a negligible number of fracture gaps, due to the strong plasticity of plain soil and pure fly ash-stabilized soil. Following the addition of lime, the soil samples' periphery consists primarily of minute fragments, and even pulverization takes place; the samples are clearly fractured. A fractal mechanism causes soil samples to progress from tiny degradation to macroscopic fractures. Both the numerical parameters of physical-mechanical properties and the geometrical aspects of structural evolution exhibit strong statistical self-similarity. Due to the significant degree of fragment distribution and the wide range of varied fragment sizes, a standard sieve was employed to filter the broken fragments in order to provide a visual representation of the distribution for the shattered pieces of stabilized soil after failure. The average size of the fragmented pieces was used to calculate how severely the stabilized soil had been damaged. Table 3 displays the screening findings that are consistent with formula. Given the strong integrity of plain soil and pure fly ash-stabilized soil, it is not particularly important to investigate the fracture morphology from a fractal theory perspective [6], [7].

Analysis of Microstructures:

SEM can be used to visually represent the properties of microspore morphology. SEM is one of the most essential techniques for examining the microstructures of soil and rock samples. Many academics have studied and analyzed the microscopic pore structures of soil and rock samples using SEM images up to this point but the majority of them have remained at the level of qualitative identification or morphological description of microstructure, ignoring a lot of the quantitative data contained in SEM images. The pore diameter distribution as well as the particle morphology of rocks and soil mass are both quantitatively characterized using fractal theory, in addition to the morphology and distribution aspects of complex objects. SEM pictures may clearly display the pore properties of both unsterilized and stabilized soil. If the pore morphology exhibits fractal properties, the connection between pore perimeter and area is as follows.

Under the condition of 100 times magnification (100), it can be shown that the fractal dimension of the pores in plain soil is 2.544-2.550, which is less than that of 10% F + 5% L stabilized soil. The fractal dimension of the pores in plain soil at 1000 times magnification is 1.314, and this is because the soil surface has a more flake-like thin layer structure and there are significant overlaps in the SEM images, which partially shield the pores on the soil sample's surface. Therefore, the entire pores are separated into complicated and irregular forms, which are not taken into account here, and are therefore less than that of stabilized soil made up of 10% F and 5% L. This phenomenon suggests that the internal pore architecture of plain soil is quite straightforward and roughly round. The hydration byproducts of the modifier, however, partially fill this pore structure, changing the pore morphology of stabilized soil into irregular and tiny fractures. As a result, the soil's integrity and compactness are both enhanced [8]–[10].

CONCLUSION

Based on the SHPB test, an examination of the dynamic mechanical characteristics and energy dissipation law of expansive soil stabilized with lime and fly ash was conducted in this work. Both the association between fractal dimension and absorbed energy as well as the relationship between dynamic compressive strength and absorbed energy were discovered. SEM images were used to examine the microstructures of both unsterilized and stabilized soil. These are pertinent study findings. The stabilized soil's dynamic compressive strength and absorbed energy initially rise and then fall as fly ash and lime content increases, until reaching their maximum values at 20% F + 5% L, or 1670 kPa and 1.67 J, respectively. The presence of the weak fly ash-fly ash particle surface reduces the dynamic compressive strength and absorbed energy more than the addition of 20% F + 5% L. In the test, only a very small fraction of the incoming energy was absorbed due to the low wave impedance of the soil. There is a good linear relationship between the absorbed energy and the stabilized soil's dynamic compressive strength. The amount of energy absorbed following soil failure increased with strength. From the standpoint of energy dissipation, the failure mechanism of the soil samples under impact stress is thoroughly examined. Compared to plain soil and pure fly ash-stabilized soil, fly ash-lime combination stabilized soil exhibits substantial changes in the fracture morphology. Plain soil and soil stabilized solely with fly ash have relatively high integrity under an impact stress of 0.2 MPa, whereas soil stabilized with both fly ash and lime fails with comminuted failure. In the 2.30 to 2.50 fractal dimension range, the absorbed energy gradually decreases. It demonstrates that a suitable amount of modifier has some favorable effects on the failure fracture properties of soil. The test findings show that the 20% F + 5% L modifier content is the ideal mix percentage.

REFERENCES:

[1] H. Yu, X. Huang, J. Ning, B. Zhu, and Y. Cheng, "Effect of cation exchange capacity of soil on stabilized soil strength," *Soils Found.*, 2014, doi: 10.1016/j.sandf.2014.11.016.

[2] Y. J. Du, N. J. Jiang, S. Y. Liu, S. Horpibulsuk, and A. Arulrajah, "Field evaluation of soft highway subgrade soil stabilized with calcium carbide residue," *Soils Found.*, 2016, doi: 10.1016/j.sandf.2016.02.012.

[3] P. J. Venda Oliveira, A. A. S. Correia, and J. C. A. Cajada, "Effect of the type of soil on the cyclic behaviour of chemically stabilised soils unreinforced and reinforced with polypropylene fibres," *Soil Dyn. Earthq. Eng.*, 2018, doi: 10.1016/j.soildyn.2018.09.005.

[4] H. Yang, S. K. Sinha, Y. Feng, D. B. McCallen, and B. Jeremić, "Energy dissipation analysis of elastic–plastic materials," *Comput. Methods Appl. Mech. Eng.*, 2018, doi: 10.1016/j.cma.2017.11.009.

[5] M. Abdullah-Al-Shafi *et al.*, "Designing single layer counter in quantum-dot cellular automata with energy dissipation analysis," *Ain Shams Eng. J.*, 2018, doi: 10.1016/j.asej.2017.05.010.

[6] A. Tandiroglu and T. Ayhan, "Energy dissipation analysis of transient heat transfer for turbulent flow in a circular tube with baffle inserts," *Appl. Therm. Eng.*, 2006, doi: 10.1016/j.applthermaleng.2005.05.018.

[7] S. R. Heikalabad, M. N. Asfestani, and M. Hosseinzadeh, "A full adder structure without cross-wiring in quantum-dot cellular automata with energy dissipation analysis," *J. Supercomput.*, 2018, doi: 10.1007/s11227-017-2206-4.

[8] A. Louhghalam, M. Tootkaboni, and F.-J. Ulm, "Roughness-Induced Vehicle Energy Dissipation: Statistical Analysis and Scaling," *J. Eng. Mech.*, 2015, doi: 10.1061/(asce)em.1943-7889.0000944.

[9] M. Shariati, A. Shariati, N. H. Ramli Sulong, M. Suhatril, and M. M. Arabnejad Khanouki, "Fatigue energy dissipation and failure analysis of angle shear connectors embedded in high strength concrete," *Eng. Fail. Anal.*, 2014, doi: 10.1016/j.engfailanal.2014.02.017.

[10] L. R. Corr and W. W. Clark, "Energy dissipation analysis of piezoceramic semi-active vibration control," *J. Intell. Mater. Syst. Struct.*, 2001, doi: 10.1177/104538901400438028.